November 2017

Construction Effects on the Side Shear of Drilled Shafts

Lucas Caliari De Lima
University of South Florida, lucascaliari@engineer.com

Construction Effects on the Side Shear of Drilled Shafts

by

Lucas Caliari de Lima

A dissertation submitted in partial fulfillment
of the requirements for the degree of
Doctor of Philosophy in Civil Engineering
Department of Civil and Environmental Engineering
College of Engineering
University of South Florida

Major Professor: Austin G. Mullins, Ph.D.
Rajan Sen, Ph.D.
Michael Stokes, Ph.D.
Ryan Toomey, Ph.D.
Sarah Kruse, Ph.D.

Date of Approval:
November 30, 2017

Keywords: Drilling Slurry, Exposure Time, Rock Socket,
Temporary Casing, Pullout Strength

DEDICATION

This dissertation is dedicated to my wife, Mariana, and son, Isaac. Without their support, encouragement, understanding and love, this accomplishment and all it means would never be possible. The dedication is extended to my father-in-law, Leonardo, his wife Socorro, my uncle, Canario, my sister Debora and my father, Amos, for having provided conditions to achieve the finish line of this journey.

ACKNOWLEDGEMENTS

I would like to express my eternal gratitude to Dr. Gray Mullins for his guidance, support, time, advice, knowledge exchange and patience. My acknowledgements are also extended to Dr. Rajan Sen and Dr. Michael Stokes for all the orientation, availability and guidance. Dr. Sarah Kruse and Dr. Toomey for their availability, insights and encouragement. The knowledge that was gained throughout this research is one of the most important things in my life.

Special thanks to the members of Structural Research Group at the University of South Florida, specifically Jeff Vomacka, Warren Allen, Daniel Hagerman, Kevin Johnson, Kelly Costello, Miles Mullins, Philip Hopkins, Anhar Sarsour, Sarah Mobley, Joseph Scott, Spencer Baker, Zuly Garcia and Elizabeth Mitchell. Their participation was fundamental to perform the experiments and to succeed in the beginning of the program. I am also especially thankful to the office staff in the Department of Civil and Environmental Engineering at the University of South Florida.

Thanks also to Cetco®, KB International and Matrix Construction Products for donating their products and participating during testing setup.

Most importantly, special thanks to the Florida Department of Transportation for funding this research program.

TABLE OF CONTENTS

LIST OF TABLES

LIST OF FIGURES

ABSTRACT

Design methods for side shear of drilled shafts, including the resistance factors that should be applied, do not account for any specific construction procedure. Instead, design often relies on analysis of case studies which include all construction methods used in each geomaterial type (e.g. clays, sands and rocks), or on parametric analysis. Nonetheless, literature suggests that different construction procedures result in varying side shear.

This research investigated 2 types of construction: (1) slurry stabilization in sandy soils using bentonite and polymer products that are commonly used on the field, with exposure times from near 0h to 96h, and (2) temporary casing stabilization in simulated limestone using 3 different methods for installation and extraction of the casings which included: driven, coarse-tooth rotated and fine-tooth rotated. All specimens were $1/10^{th}$ scale in relation to the most common shafts sizes constructed in the field.

The results showed that bentonite slurry causes a significant reduction on the side shear within relatively short periods of time (between 2h and 4h of open excavation), whereas polymer slurry did not show appreciable variations up to 96h.

The driven and coarse-tooth rotated temporary casing exhibited lower side shear resistance than the fine-tooth rotated casings, which can be attributed to the larger annulus outside the casing and the additional crumbled pieces of rock that degrades the contact interface with the socket concrete.

Construction-based resistance factors are suggested for each construction procedure investigated in this study and clearly show the effects from different methods.

CHAPTER 1: INTRODUCTION

Foundations are below ground structural elements responsible for distributing loads that come from above ground structures. The loads can be due to the structure self-weight, occupants, wind, rain / snow, earthquakes, vessel or vehicle impacts, machinery induced vibration and other sources. Foundation elements can be shallow (footings), which have a large area of contact with the soil but are relatively close to the ground surface, or deep, with high length to cross sectional area ratios.

Deep foundation elements resist axial loads by side shear, end bearing or a combination thereof; lateral and overturning loads depend on the ability of the adjacent geomaterial to provide sufficient passive soil resistance (Figure 1.1). The two most common deep foundation types are driven (piles) and cast-in place elements. Driven piles are commonly made of wood, steel, or concrete; cast in place elements are made from concrete (or grout).

Cast-in-place elements are broken into two categories: augered-cast-in-place (ACIP) piles and drilled shafts. ACIP piles differ from shafts in that a full depth continuous flight auger is used to pierce the ground and as the auger is extracted, grout is pumped to replace the cylindrical volume of the auger. Reinforcing steel is then placed in the fluid grout. Drilled shafts, (also known as shafts, bored piles, drilled caissons, drilled piers and cast-in-drilled-hole piles) are cylindrical, large diameter column-like reinforced concrete members. Shafts are typically between 2.5ft and 12ft in diameter (up to 30ft) and can have lengths that exceed 300ft. Shafts differ from ACIP piles in that an open excavation is formed by the successive removal of soil or rock in relatively short length increments (e.g. 1-2ft).

Shafts can be installed in soils and rock (in which it is called rock socket) where ACIP are limited in the ability to penetrate competent rock. Drilled shafts can be an economical alternative to other types of foundation given a single drilled shaft can replace several piles and significantly reduce the concrete cap size and cost.

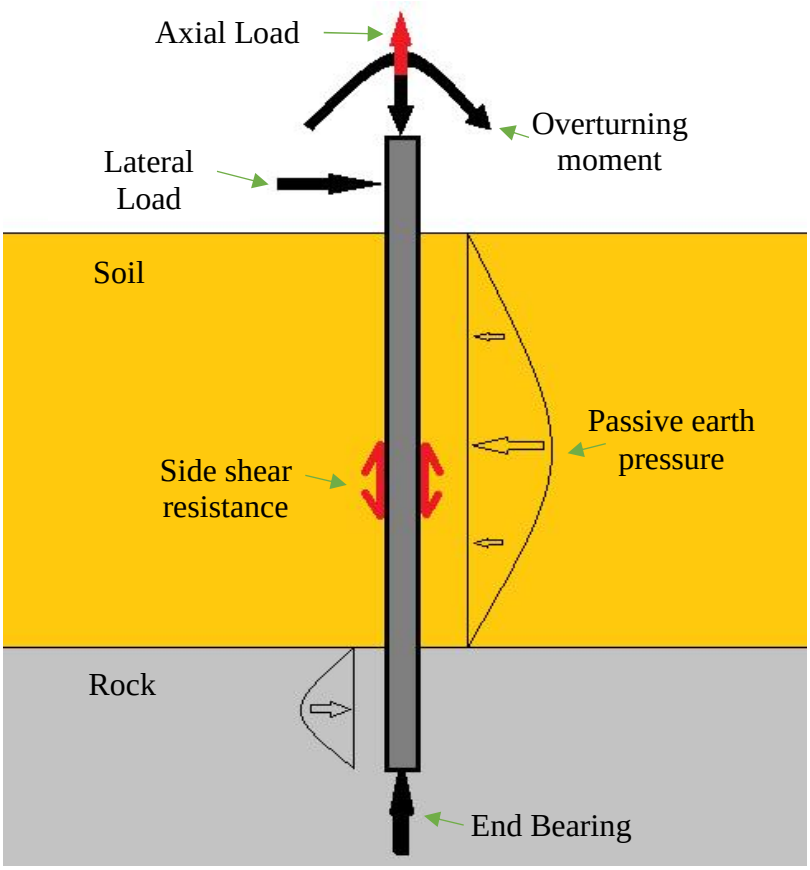

Figure 1.1. Load combinations and resistance mechanisms in deep foundations.

1.1 Problem Statement

Each type of deep foundation interacts differently with the surrounding geomaterial, resulting in particular load versus displacement behavior. The installation of drilled shafts requires soil and/or rock excavation, that can cause unpredictable changes in the K/K_0 ratio where K is the resulting lateral earth pressure coefficient after construction, and K_0 is the lateral earth pressure prior to excavation.

The excavation for drilled shaft construction requires stabilization methods to prevent collapse of the sidewalls. Typically, the stability of a drilled shaft excavation can be maintained hydrostatically (drilling slurry), mechanically (permanent or temporary casing), or by a combination of both. Each particular type of stabilization (drilling slurry, or temporary casing for instance), can affect the resulting behavior of the shafts. These effects are not currently addressed in present design methods. Upon closer review of current design methods, it becomes evident that further refinements for side shear of drilled shafts could be implemented that address the different types of excavation stabilization. The major objectives of this research program were:

- Identify the effect of slurry type on side shear (e.g. mineral or polymer).
- Identify if there is a time limit after which effects from drilling slurry (mineral and polymer) exposure may exist, and quantify how the unit side shear changes due to the effects from prolonged open excavation times.
- Identify the magnitude of side shear variations that accompany the crumbling / degradation of limestone around the temporary casing due to different casing types and installation / extraction methods.

1.2 Organization of this Dissertation

This dissertation is divided into four ensuing chapters. Chapter two presents a literature review of available publications regarding design methods and case studies pertaining to side shear of drilled shafts in soils and rocks, primarily in sand and limestone. This chapter includes the history of the development of the design methods as well as several case studies pertaining to drilled shafts excavated under drilling slurry stabilization in sandy soils and the use of temporary casings in limestone.

Chapters 3 and 4 present the research approach and results for both the influence of time exposure to bentonite and polymer slurries on the side shear of drilled shafts over time, and the effects of different types / methods of casing installation / extraction procedures on the side shear of rock sockets in limestone, respectively. Chapter 3 also includes results of slurry fluid loss experiments performed with polymer slurry at various viscosities.

Chapter 5 presents more in-depth analyses of the results presented in Chapters 3 and 4. Discussions regarding the different observed side shear behavior due to each construction procedure are included. The findings are extended to Load and Resistance Factor Design (LRFD) concepts where the measured capacity is compared to predicted design capacity (bias). LRFD resistance factors are suggested for each construction procedure that stem from the test program results.

CHAPTER 2: REVIEW OF SIDE SHEAR BEHAVIOR OF DRILLED SHAFTS

Design methods used today to determine the side shear resistance of drilled shafts in soil and rock were developed, mostly, using case studies and parametric evaluations to develop design equations. However, despite the close link to actual field conditions (e.g. O'Neill and Reese 1999) present design methods do not account for the unique features associated with each construction procedure. Instead, a lower bound envelope that encompasses the majority of the observed performance through analysis of load tests was proposed (both soils and rocks). On the other hand, the FHWA 2010 Drilled Shaft Construction Manual proposed that a more theoretical approach, based on geotechnical investigation results, is more suitable for defining the design side shear of drilled shafts in sandy soils (Brown et al. 2010).

Both the FHWA (2010) and (AASHTO 2014) design manuals present similar equations for computing the anticipated side shear of rock sockets. FDOT (2017a) requires the use of a different method developed by McVay et al. (1992), which is also based on load test results, but with relationships specifically to Florida limestone. Although the McVay method was supported by results of laboratory unconfined compression and split tensile strengths on limestone specimens taken from 14 load test sites in the field, it is theoretically linked to the Mohr-Coulomb failure criteria. Again, methods to determine rock socket resistance while based on empirical field load test results, still do not take into account the wide range of construction techniques (i.e. temporary casing versus no casing) that can lead to varied side wall roughness and/or states of cleanliness.

According to O'Neill (1981), the factors that mostly influence the behavior of drilled shafts include in-situ soil conditions, type and direction of loading, shaft geometry and, "very importantly," construction procedure. This chapter presents an overview of some of the most commonly used design methods for side shear of drilled shafts in sandy soils and rocks, including limitations. Case studies available in literature are included to illustrate, where possible, the differences in side shear behavior from varied construction methods.

This dissertation focuses on how construction and excavation stabilization methods affect the side shear resistance of a drilled shaft. The effects of concrete flow properties are not addressed.

2.1 Background

Drilled shafts are cylindrical, large diameter (sometimes exceeding 12ft), column-like reinforced concrete members, with lengths that can be in excess of 300ft. In general, drilled shaft construction is performed in three basic steps: (1) excavation, (2) placement of reinforcing cage, and (3) concreting (Figure 2.1).

Figure 2.1. Shaft construction steps: (left to right) excavation, cage placement and concreting.

The excavation requires a drill rig capable of drilling soils and/or rocks to the required depth and diameters needed to achieve the design capacity, thereby forming a deep cylindrical

void space. Drill rigs are typically mechanically or hydraulically driven with telescopic Kelley bars that are adjustable in length and attached to a single or multi-flight auger (Mullins and Winters 2014). Manuals that include construction procedures of drilled shafts, such as such as the FHWA Drilled Shaft Construction Manual (O'Neill and Reese 1999; Brown et al. 2010) and state specifications, present details for each type of construction procedure and its particularities.

On drilled shaft construction, the auger is not continuous-flight, but rather 2 or 3 flights. Once the proper tip elevation is reached, the auger is replaced with a clean out bucket in order to remove any loose material from the bottom of the excavation. The reinforcing cage is placed within the excavation, followed by concrete. This process requires the in-situ soils/rocks to act as the formwork and define the shape of the concrete (Mullins and Winters 2014).

2.2 Excavation Stabilization Techniques

Excavation stability and concreting are the two most important and yet difficult steps in shaft construction. The side walls are held in place either by fluid slurry pressure inside the excavation pressing outward on the excavated walls or by mechanical means afforded by the strength of a casing (large diameter steel pipe). In the early 1900's shaft excavations were stabilized with vertical boards and lateral bracing; excavation was carried out via men in the hole, but this method was only plausible in dry conditions.

2.2.1 Slurry Stabilization of Drilled Shafts

In cases where the ground water table is encountered within the design shaft depths, some form of fluid must be maintained within the excavation to prevent intrusion of ground water. Use of slurry stabilization is most commonly performed using mineral products (i.e. bentonite or attapulgite) or synthetic polymeric compounds mixed with water. Using water alone is not a common practice when there are no full length casings due to the enormous refill rates that would

be necessary to prevent borehole collapse (Mullins and Winters 2014). Support is provided by the radially applied hydrostatic slurry pressure to the excavated walls, which requires the slurry level to be maintained above the ground water table throughout the entire construction. The slurry inside the excavation is typically mantained between 4 and 8 feet above the water table, depending on the type of slurry (Mullins and Winters 2014).

Figure 2.2 illustrates the drilled shaft construction diagram when slurry (either mineral or polymer) is used (Brown et al. 2010). A permanent or temporary surface (starting) casing is often used to raise the slurry level, increase the hydrostatic pressure on the excavation walls (Figure 2.2a and 2.2b) and stabilize near surface soils from construction activities (Mullins and Winters 2014). This surface casing is then filled with the drilling slurry (b) and excavation is performed through the specified depth; slurry is continuously added to replace the removed soil volume. The reinforcing cage is introduced while slurry is still inside the open excavation (c). Concrete is then placed by tremie from bottom up (d). The rising heavier concrete must be able to flow through the cage, expel the slurry and create an intimate contact with the excavated walls I.

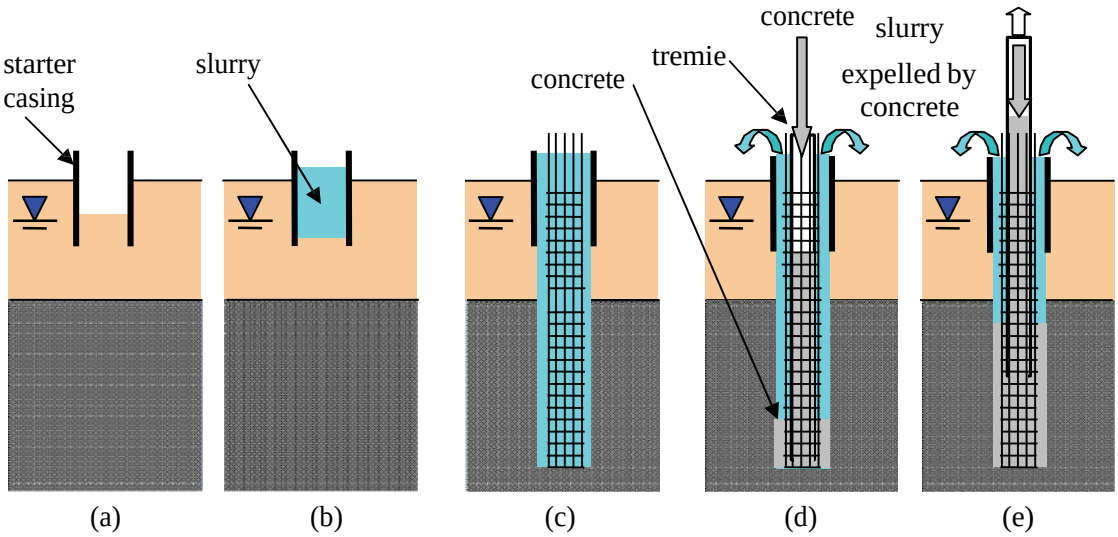

Figure 2.2. Diagram of the slurry method of stabilization.

Although both mineral and polymer slurry have been shown to be effective in stabilizing an excavation (and now both permitted in most cases), the mechanisms by which they provide this stability are quite different. Mineral slurries depend on minimum clay mineral concentration (0.3-1.0lb/gal) to quickly seal the excavation walls. The layer of clay minerals that form on the walls is called a filter cake (where the clay particles are filtered out of the slurry by the surrounding permeable soils). When mineral slurry is mixed correctly, very little flow into the surrounding soil occurs and the excess head differential between the slurry elevation and the ground water table is directly converted to a lateral force.

Polymer slurry is more viscous than water which allows it to bind sandy soil in a quasi-cohesive manner making it less susceptible to low pressure sloughing behind the auger. The concentration of polymer products in the slurry are approximately $1/100^{th}$ that of mineral slurry and no filter cake forms. While polymer slurry will continue to flow, the flow rate will slow but will not completely seal off the excavation walls (Mullins and Winters 2014). Nonetheless, similar to mineral slurry, this outward flow also causes radially outward pressure on the walls, but to a lesser level. As the density and lateral flow / pressure are lower for a given head differential, polymer slurry levels must be maintained at higher levels than mineral slurry.

Depending on the soil type and slurry level maintenance, the excavation process may also be accompanied by stress relaxation in the surrounding soil (Clayton and Milititsky 1983; O'Neill 2001). Filling the borehole with fluid concrete can partially or completely restore the in situ lateral soil stresses (Bernal and Reese 1983; Chang and Zhu 2004). The available side shear resistance depends on how much effective stress in the soil near the borehole is lost before the borehole is concreted, how effective the concreting process is at restoring lateral stress in the soil, the degree

of roughness in the borehole, and the pore pressure response of the resulting modified soil (O'Neill 2001).

Bentonite is the common name for a type of mineral slurry, which is a processed powdered clay consisting predominately of the mineral sodium montmorillonite. Other processed, powdered clay minerals, such as attapulgite (calcium montmorillonite) and sepiolite, may also be used, typically in saline groundwater conditions (Brown et al. 2010).

When introduced into a drilled shaft excavation, the mineral slurry contributes to borehole stability through two mechanisms: formation of a filter cake, which effectively acts as a membrane on the sidewalls of the borehole, and a positive fluid pressure acting against the filter cake membrane and borehole sidewalls from increased density (Figure 2.3, Brown et al. 2010).

The filter cake is formed due to the hydration of the clay minerals (attapulgite, montmorillonite and other expansive minerals), which creates the double layer, generating plate-like particles that accumulate on the pores of permeable materials. The infiltration of this material exhibits an aptness to form larger and larger nets that builds a seal in the geomaterial voids, significantly decreasing the permeability. This phenomenon was observed by Terzaghi (1925), Macey (1942) and Grace (1953), as summarized in Mesri and Olson (1971). The filter cake may affect the effective shaft dimensions, especially in small diameter shafts, as observed by Majano (1992).

The bentonite slurry will have a density a little greater than water alone from the suspended slurry products; mineral slurry also develops gel strength which aids in the transport of cuttings during excavation and concrete placement. During recirculation, the solids that are suspended on the slurry increase the slurry density and can make it thicker (more viscous). If the slurry becomes

too heavy or viscous the integrity of the shaft can be at risk as it becomes more difficult to be displaced by the fluid concrete.

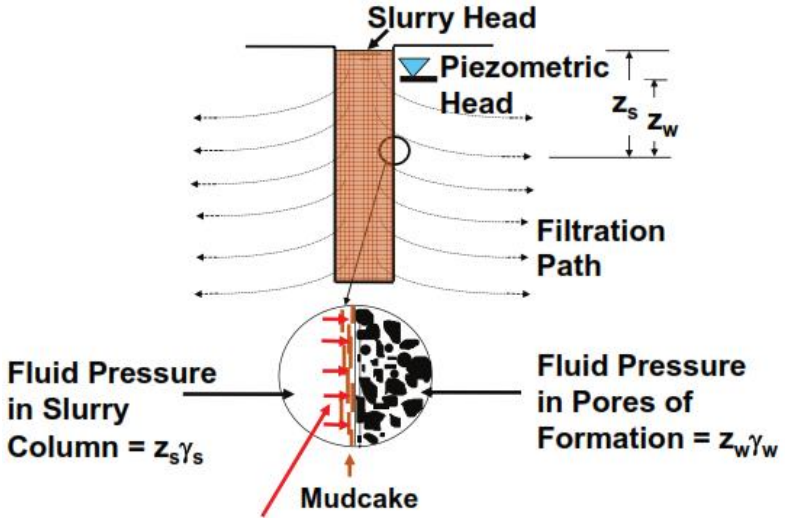

Figure 2.3. Formation of filter cake and positive net pressure in granular soils.

The term polymer refers to any natural and synthetic compounds, usually of high molecular weight, consisting of individual units (monomers) linked in a long, chain-like hydrocarbon molecules. Synthetic polymer slurries made from acrylamide and acrylic acid, specifically termed anionic polyacrylamide or PAM, entered the drilled shaft market in the 1980s. More recently, advanced polymers made by combining polyacrylamides with other chemicals have been introduced in an effort to improve performance while minimizing the need for additives. Commercial polymer products vary in physical form (dry powder, granules, or liquids) and in the details of the chemistry of the hydrocarbon molecules (molecular weight, molecule length, surface charge density, etc., Brown et al. 2010).

Synthetic polymers can be made by modifying natural polymers. For example, carboxy-methylcellulose (CMC) is made by reacting cellulose with chloracetic acid and NaOH, substituting $CH_2COO^-Na^+$ for H. In the cellulose unit, there are three OH groups, and each one is capable of substitution. In general, the average number of carboxy groups (OH-C-H) on the chain per unit

cell is known as the “degree of substitution”. The carboxy group has the function of imparting water solubility (or dispersability) to the polymer. It is also responsible for stretching linearly the chains of polymer by creating negative charges that repel every unit from each other, therefore increasing the viscosity of the polymer-based slurry.

Another common type of water soluble polymer is made of a polyacrylamide base. This type of polymer is also an anionic polyelectrolyte which is made by converting some amides on a polyacrylamide chain to carboxylates through hydrolysis (Majano 1992).

When polymer slurry is introduced, there is an initial fluid loss into the formation. This penetration of polymer slurry into a porous formation allows the polymer to interact with the soil particles by chemical adhesion, creating a bonding effect and improving stability. The strength of adhesion varies significantly between polymer types and can be affected by various additives (Brown et al. 2010).

Polymer slurries are designed to perform through continuous infiltration through permeable formations (sand, silt, and permeable rock). The fluid loss is dependent on the viscosity, time of excavation and slurry type. Care must be taken on rising the tool because it generates zones of lower pressure behind the extracting tool, which can pull the soil walls in. There must be excess pressure head to prevent this, even if the head is kept above the water table. The borehole stability is produced by a combination of hydrostatic pressure and continuous percolation of the slurry through the zone containing the polymer strands, in addition to the adhesion and three-dimensional lattice or web-like structure that forms gradually over time, as illustrated in Figure 2.4 (Brown et al. 2010).

Commercial polymer products vary in physical form (dry powder, granules, or liquids) and in the details of the chemistry of the hydrocarbon molecules (molecular weight, molecule length, surface charge density, etc.).

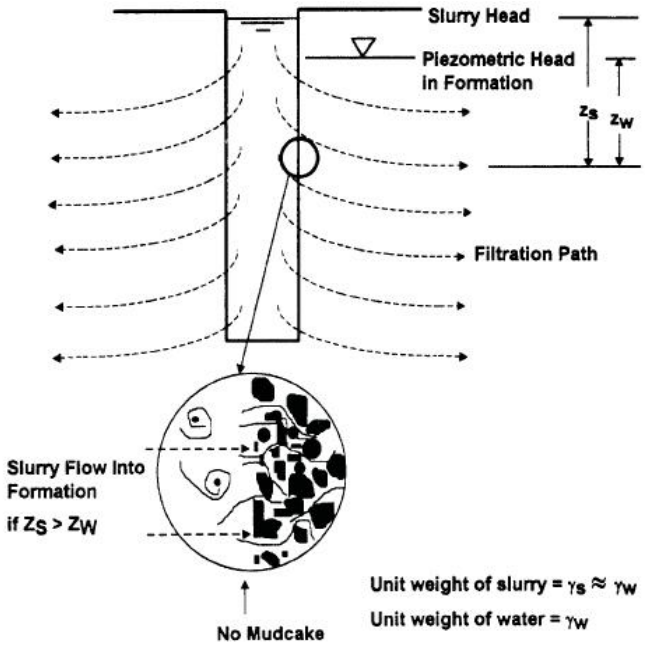

Figure 2.4. Borehole stabilization through polymer slurries.

The simpler PAM slurries may be sensitive to the presence of chloride (salt), free calcium, magnesium and chlorine in the mixing water or groundwater (low pH). Unless the polymer has been developed to remain stable in hard waters, typical upper limits for the concentration of chloride, calcium and magnesium, and chlorine are 1500ppm, 100ppm and 50ppm, respectively (Matrix 2016).

Usually, the quantification of the hardness of the water is done indirectly taking pH measurements. If the pH is low, it has to be corrected to a range between 8 and 11, according to design manuals. A commonly used product in the field is the soda ash. Some manufacturers have developed its own products to correct the pH (Matrix 2016).

As mineral and polymer slurries are so different, different values for density, viscosity and sand content (due to contamination during drilling) are imposed by state and federal specifications.

Tables 2.1 and 2.2 summarize slurry properties recommended for mineral and polymer slurries, respectively. Often, only synthetic slurry systems which have been approved by the Owner may be used. The anticipated subsurface conditions and construction methods should also be considered in slurry selection (AASHTO 2016).

The State of Florida allows the use of polymer slurries only in the construction of drilled shafts for miscellaneous structures (e.g. high mast lighting, signal poles, and signs). The slurry properties required by FDOT (2017b) are also included in Tables 2.1 and 2.2. It is interesting to note that the maximum allowed sand content on polymer slurries in the State of Florida is more restrictive than the national standards (after Deese 2004). The presence of sand on the drilling slurry is due to the excavation activity. It increases the density of the slurry and could form a layer of loose sediment that could drastically reduce the end bearing of the shafts.

Table 2.1. Specified property ranges for mineral slurry.

Property	**Required range of values**	
	AASHTO (2016); FHWA (2010)	FDOT (2017b)
Density (lb/ft^3)	64.3 to 72	64 to 73 (fresh water) 66 to 75 (salt water)
Viscosity (s/qt)	28 to 50	28 to 40
pH	8 to 11	8 to 11
Sand Content (%)	≤ 4.0	≤ 4.0

Table 2.2. Specified property ranges for polymer slurry.

Property	**Required range of values**	
	AASHTO (2016); FHWA (2010)	FDOT (2017b)
Density (lb/ft^3)	≤ 64	62 to 64 (fresh water) 64 to 66 (salt water)
Viscosity (s/qt)	32 to 135	Manufacturer range
pH	8 to 11.5	Manufacturer range
Sand Content (%)	≤ 1.0	≤ 0.5

2.2.2 Cased Stabilization of Drilled Shafts

There are different methods for installing and extracting temporary casings during the construction of drilled shafts, each one may have a different effect on the side shear. Temporary casing can be placed through a pre-drilled hole to seat the casing into an underlying formation of more stable material (Figure 2.5), or advanced ahead of the excavation in cases where the hole will not stand open for short periods or where slurry drilling techniques are considered less attractive from a cost or performance standpoint (Figure 2.6).

When the casing is installed after excavation (Figure 2.5), a surface (starting) casing is often used, similarly to slurry excavations (a). The casing is then placed into the excavation (b), the reinforcement cage is installed (c) and concrete is placed (d). The casing is then extracted and the concrete must be fluid enough to flow through the cage, expel the slurry (if any) and create a bond with the soil I. A minimum head of concrete inside the casing has to be maintained. The use of slurry is necessary to stabilize the excavation prior to temporary casing installation.

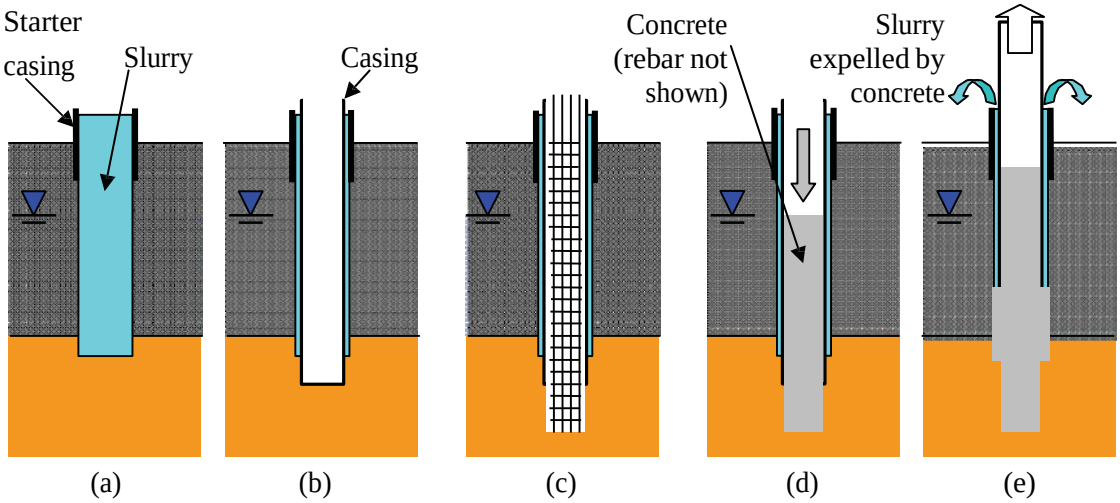

Figure 2.5. Construction using casing through slurry-filled starter hole.

More commonly, the casing is advanced ahead of excavation (Figure 2.6). The casing is either driven, rotated or oscillated into a formation that can provide a good seal (a). The soil or soft rock inside the casing is then excavated (b). Steps (c), (d) and I are the same as those described and shown of Figure 2.5. This method can be used in dry or saturated conditions. When in saturated high water table conditions, fluid levels inside the casing should be maintained at or above the ground water elevation to prevent ground water (from soil or pervious rock below the casing) from flowing into the excavation.

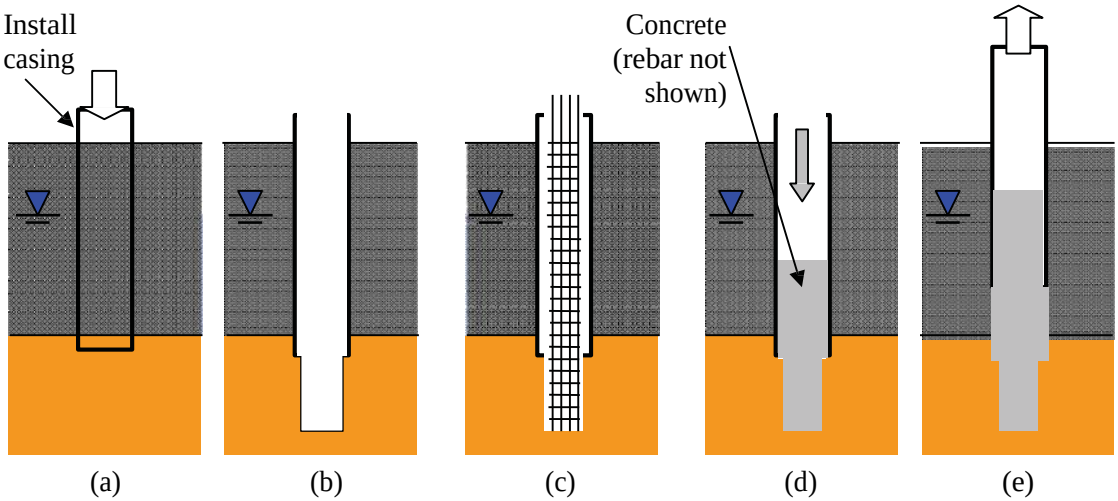

Figure 2.6. Construction using casing advanced ahead of excavation.

Oscillators are hydraulic-powered tools attached to a crane to advance and extract casing. The casing often is a segmental pipe with bolted joints. The oscillator grips the casing with hydraulic-actuated jaws and twists the casing back and forth through a small angle (less than 90 deg) while other hydraulic cylinders apply downward or upward force.

While an oscillator twists back and forth, a twisted casing system can rotate the casing through a full 360° when advancing it. This system couples to the drill rig by attaching a twister bar so that the rig can apply torque and crowd onto the casing. Sometimes the casing is equipped with cutting teeth or carbide bits at the bottom to penetrate hard layers (Brown et al. 2010).

Vibratory hammers are also hydraulically activated with two functions: (1) the gripping jaws which grabs either side of the casing and can be adjusted to fit a wide range of casing diameters, and (2) horizontally oriented hydraulic motors with an eccentric weight; the up and down cyclic motion of the eccentric weight produces large axial forces that advance the casing with the addition of the self weight of the hammer and casing. During casing extraction the hammer is lifted via crane to offset self weight and help overcome side shear (Brown et al. 2010).

If the concrete slump becomes low, it will not easily flow through the cage to fill the space between reinforcing and the sides of the hole, which can result in near zero side shear (Mullins and Winters 2014). Arching of the concrete can also occur, and the concrete will move up with the casing, creating a gap into which slurry, groundwater, or soil can enter. Finally, the casing should be pulled slowly in order to keep the forces from the downward-moving concrete to prevent moving the rebar cage (Brown et al. 2010).

Casing sometimes needs to be used to stabilize deeper shafts and/or into stronger soils or soft rocks, in which casing removal may be difficult. In such instances, contractors may choose to “telescope” the casing. With this approach, the upper portion of the shaft is excavated and a large-

diameter casing sealed into a suitable stratum. A smaller-diameter shaft will then be excavated below the bottom of the upper casing and a second casing, of smaller diameter, will be sealed into another suitable stratum at the bottom of the second-stage of excavation. The process can be repeated several times to greater and greater depths until the plan tip elevation is reached. With each step, the borehole diameter is reduced, usually by about 6 inches. The casings should be extracted starting with the innermost (Brown et al. 2010). The importance of casing extraction order is discussed later.

A flight auger specially designed for rock can be used to drill relatively soft rock (hard shale, sandstone, soft limestone, decomposed rock). Hard-surfaced, conical teeth, usually made of tungsten carbide, are used on rock augers. The geometry, pitch and orientation of the teeth are usually designed to promote chipping of rock fragments. Core barrels can also be employed if the augers are ineffective (Brown et al. 2010).

The simplest form of core barrel is a single, cylindrical steel tube with hard metal teeth at the bottom edge to cut into the rock. The chisel teeth would be used in soft rock, while the conical points would be suitable in somewhat harder material. The oscillated/rotated casing is a type of core barrel which commonly employs the button teeth. If the rock is hard and a significant penetration is required, a double walled core barrel may be more effective (Brown et al. 2010).

All procedures used to install and extract temporary casings change soil properties; in some cases these changes are for the better making loose or medium dense sand denser. When loose deposits underlie rock layers or clays, vibration from casing installation densifies the soil resulting in a void in the upper portion of the layer over the now higher relative density sand; if below the water table, this void is the result of an exchange of loose soil volume with ground water. When a temporary casing is extracted up and through this voided region, the cover concrete will flow out

first to fill the void and some exchange of water and concrete occurs. This was described by Sliwinski et al. (1984) and illustrated in Figure 2.7, where a water-filled void around the casing (1) is filled by denser, higher pressure fluid concrete (2) resulting in trapped water inside casing or shaft volume (3).

In a local case in south Florida (Mullins 2014a), the scenario described by Sliwinski was observed where a significant drop in concrete level inside the temporary casing occurred during casing extraction. Figure 2.8 shows the predicted shaft radius from thermal profiling which indicated concrete within the permanent casing region (above 30ft depth) was less than that of the casing. Below the cap rock, the shaft was oversized (design radius was 30in). This problem can be a by-product of temporary casing (Mullins 2014a).

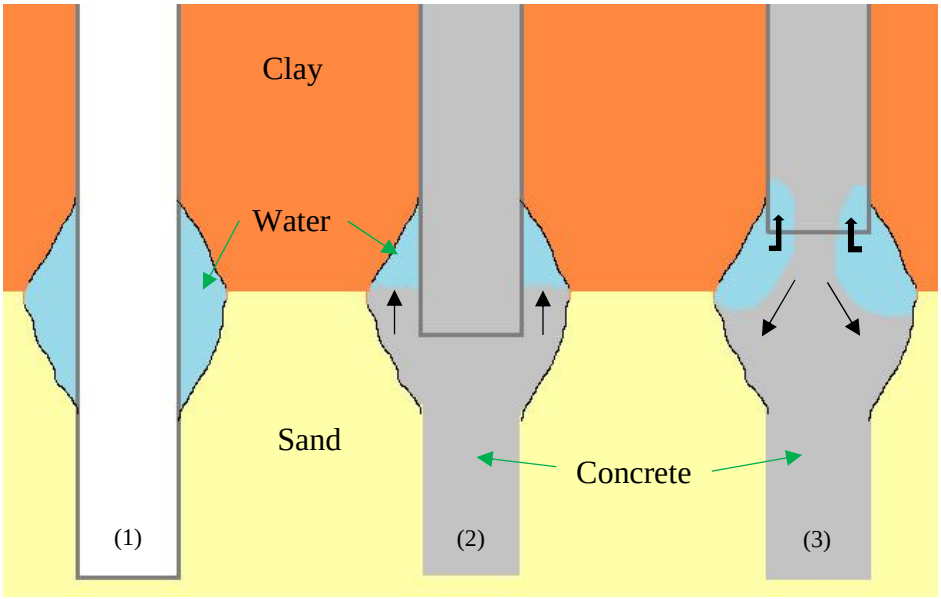

Figure 2.7. Conceptual process during casing extraction.

In the case shown by Figure 2.8 the concrete was sufficiently fluid to flow into the surrounding void, and where no alternate exit for the incompressible water in the void was available. It should also be noted that the core concrete level falls much slower due to the cage obstruction making the cover region more prone to water intrusion/fluid exchange. Unfortunately,

the concrete level measurement was performed inside the cage and not outside the cage, making the true severity of the drop appear less drastic than actual (Mullins 2014a).

The FHWA (2010) Drilled Shaft Manual (Brown et al. 2010) cites providing an exit and use of telescoping casings with a progressive casing extraction technique. Unfortunately, most of these conditions go undetected during construction and the designer could not have predicted the effects of the contractor's approach on the final soil conditions or shaft integrity. In essence, the as-built soil strata may not even come close to reflecting the boring log conditions used for design.

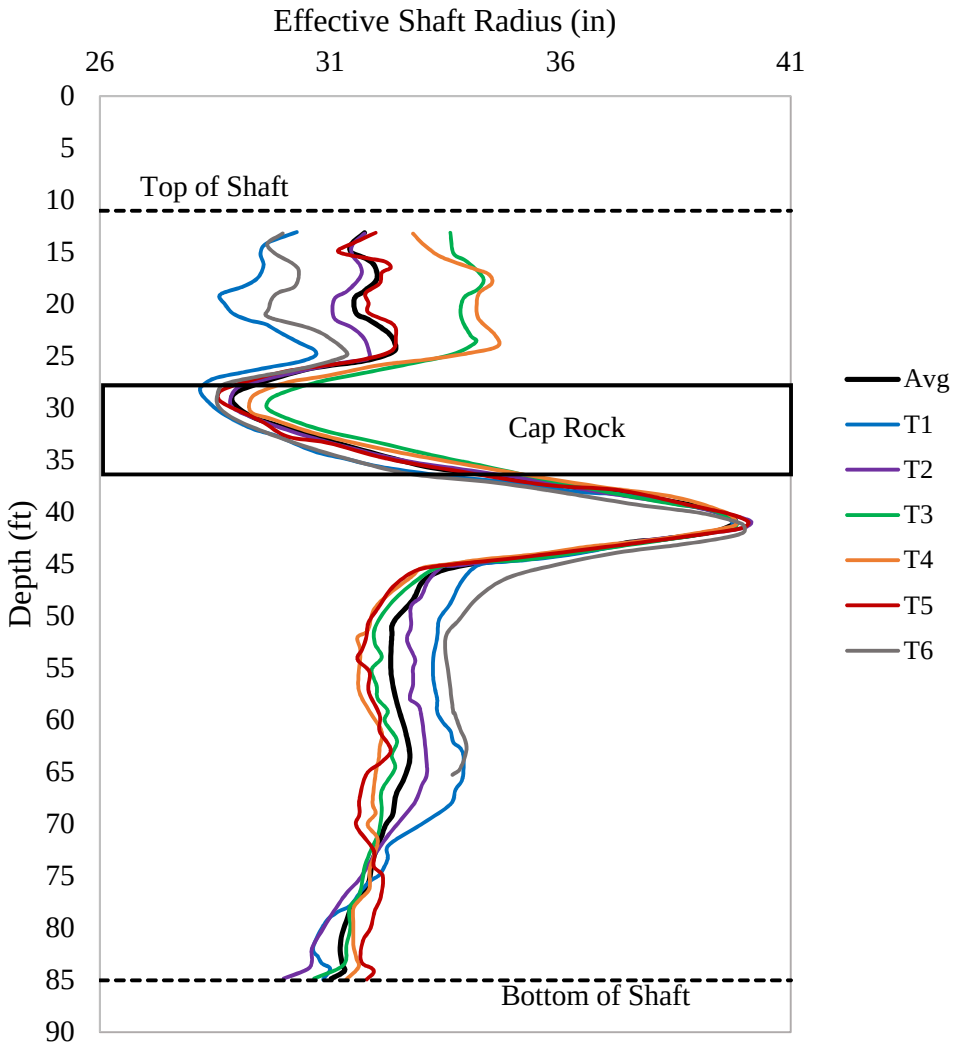

Figure 2.8. Example case where concrete / water exchange was detected by field integrity test.

Concrete properties have been shown to affect side shear capacity and flow-ability through the cage. Some state and federal specifications recommend minimum clear cage spacing or spacing to max aggregate diameter ratio (CSD) to ensure concrete presses unrestricted against the side wall of the excavation. Figure 2.9 shows the results of concrete flow tests performed on a wide range of CSD ratios (Mullins and Ashmawy 2005). The study findings showed that tighter cage spacing (small CSD) caused the concrete level inside the cage to rise before squeezing out into the annular concrete cover region. Higher concrete placement / flow rates had a similar effect. Such effects were not addressed in this study as the discussions and results presented herein were limited to small scale sockets with high slump, no coarse aggregate and no reinforcement cage.

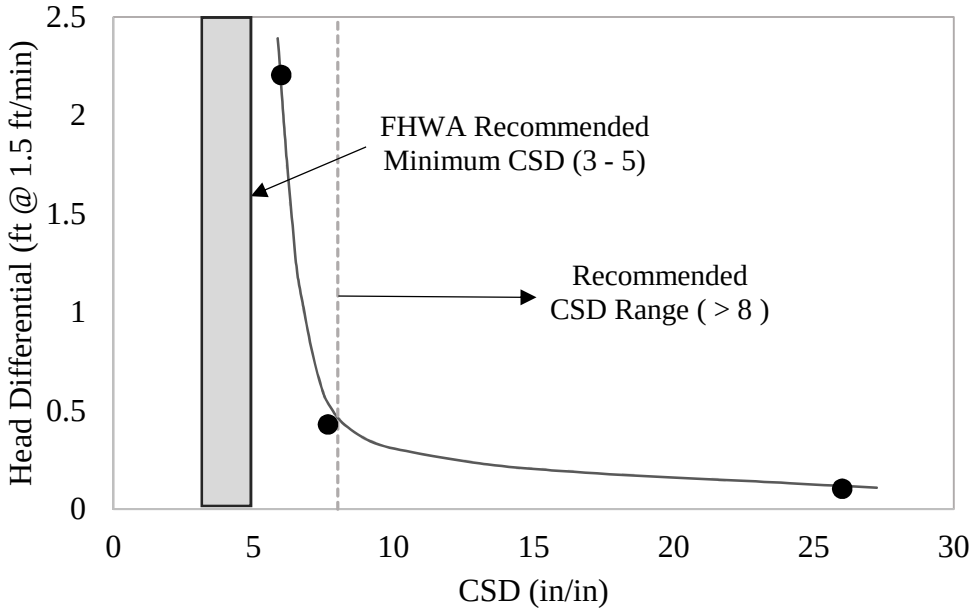

Figure 2.9. Concrete level differential (inside vs outside cage) with respect to cage tightness.

2.3 Design Methods for Side Resistance of Drilled Shafts

Side shear resistance develops in sands, clays and rock by different mechanisms. The design methods attempt to reflect this based on the unique mechanical behavior of each different geomaterial (e.g. internal friction angle, cohesion, and unconfined compression, respectively). A brief discussion of each design method is provided.

2.3.1 Design Methods for Sandy Soils

Side shear resistance is the dominant load carrying component in shafts; end bearing can be considered, but only to a far lesser degree. This study again focuses on side shear and how it is affected by construction methods.

Several methods to estimate the ultimate side shear resistance for shafts in sand have been developed. Two of them are discussed in this dissertation: (1) Reese and Oneill (1988a) and O'Neill and Hassan (1994), which were last updated in the 1999 version of the FHWA Drilled Shafts Manual (O'Neil and Reese 1999), and (2) Brown et al. (2010), based on the work of Chen and Kulhawy (2002), which was recommended by the 2010 version of the FHWA Drilled Shafts Manual and by AASHTO after 2014.

Essentially, in sandy soils cohesion I is zero and the side shear resistance (f_{smax}) becomes a function of the effective internal friction angle (ϕ') and the effective vertical overburden stress (σ'_v). Based on this, Touma (1972), and Touma and Reese (1972) presented analyses of side shear behavior of drilled shafts in sandy soils using the following equation, in which alpha (α) does not relate to the alpha method; instead, it was the beginning of the beta methods:

$$f_S = \alpha * \sigma'_V * \tan(\phi') \qquad \text{eqn. 2.1}$$

O'Neill and Reese (1978) suggested that the side shear resistance of drilled shafts in sands would be proportional to a parameter then called β, and it would be a function of the ratio between the final (after construction) lateral earth pressure coefficient and the corresponding at rest value, and the ratio between the shaft to concrete and soil to soil friction angle. The parameter β was suggested as a representation of how construction would change these ratios. The side shear resistance of drilled shafts was further defined as a relationship between β and the effective vertical overburden stress, σ'_v (O'Neill and Reese 1978):

$$f_{smax} = \beta * \sigma'_v \qquad \text{eqn. 2.2}$$

The two methods discussed herein derive from this same approach, though one of them recommended equations for β based on analysis of case studies, and the other suggested that a more theoretical approach would be more suitable.

The original beta method was last updated by O'Neill and Reese (1999) in the 1999 FHWA Drilled Shaft Manual, which was also adopted by AASHTO until 2014. The resulting equations for calculating beta were based on the work of Reese and O'Neill (1988a), with contributions of O'Neill and Hassan (1994). The equations recommended for the β coefficient were based on the following equation:

$$\beta = \frac{K}{Ko} * Ko * \tan \phi' \frac{\delta}{\phi'} \qquad \text{eqn. 2.3}$$

In equation 2.3, K_0 is the at rest lateral earth pressure, K is the resulting lateral earth pressure after construction, ϕ' is the soil friction angle and δ is the friction angle between soil and shaft concrete. Note that equation 2.3 can be simplified, but it highlights the ratios (K/K_0) and (δ/ϕ'), which have been investigated by several authors.

Both (K/K_0) and (δ/ϕ') are very difficult to evaluate for any particular drilled shaft because they are highly dependent on the construction procedures. Whether the contractor is using a drilling tool that is appropriate to the soil encountered or is excessively rotating the tool in the hole; the length of time the borehole remains open; whether drilling slurry is used and when during the drilling process the slurry is introduced into the borehole; the length of time drilling slurry (especially mineral slurry) remains unagitated in the borehole; the diameter of the borehole; the grain-size distribution of the soil (as it relates to arching of stresses in the soil), and many similar factors which had not been individually quantified (O'Neill and Reese 1999).

O'Neill and Reese (1999) recommended that full-scale loading tests should be considered in granular soils at the construction site, using the equipment and techniques that the contractor expects to use in constructing the production shafts. The β coefficient could then be empirically calculated as:

$$\beta = \frac{f_{max}\,\text{measured}}{\sigma'_v} \qquad \text{eqn. 2.4}$$

When β is obtained from a load test using equation 2.4, it becomes a "local" factor, applied to one particular depth, and not an average value for the entire drilled shaft (O'Neill and Reese 1999); f_{max} is the maximum side shear resistance.

Alternatively, if definitive information on K and δ is not available to the designer, O'Neill and Reese (1999) recommended the use of a function for β that is near the lower bound of the values obtained from a data base of compression loading tests (Reese and O'Neill 1988a; b).

For granular soils with uncorrected SPT N-values < 15 blows/ft, the beta parameter is calculated using equation 2.5. If the SPT N-values are larger than 15 blows/ft (max SPT N = 50), equation 2.6 should be used. For very gravelly sands or gravels, with uncorrected SPT N ≥ 15 blows/ft, equation 2.7 should be used, but based on limited data (O'Neill and Reese 1999).

$$\beta = \frac{N}{15}\ \{1.5 - 0.135[Z(\text{ft})]^{0.5}\} \qquad 0.25 \le \beta \le 1.20 \qquad \text{eqn. 2.5}$$

$$\beta = 1.5 - 0.135[Z(\text{ft})]^{0.5} \qquad 0.25 \le \beta \le 1.20 \qquad \text{eqn. 2.6}$$

$$\beta = 2.0 - 0.15[z(\text{m})]^{0.75} \qquad 0.25 \le \beta \le 1.80 \qquad \text{eqn. 2.7}$$

Equation 2.6 is the same as the recommended by O'Neill and Reese (1978) and Reese and O'Neill (1988a). Equation 2.5 had applied the recommendation from O'Neill and Hassan (1994) for SPT-N values lower than 15, and equation 2.7 is the same as proposed by O'Neill and Hassan (1994). The unit side resistance should be limited to 4,200 psf when using equations 2.4, 2.5 and 2.6, unless a higher value can be confirmed by load testing (O'Neill and Reese 1999).

The beta method proposed by Reese and O'Neill (1988a) was based on 41 case studies (Table 2.3). The numbers in the cells represent the number of case studies that were analyzed for each type of stabilization method and soil type.

Only 1 case study pertained to an entirely sandy soil profile (but with temporary casing), and other 20 (about half of the case studies) consisted of interbedded layers of sandy and clayey soils. Among the 20 cases on interbedded layers, 6 were excavated using slurry (which refers to mineral slurry only, no polymer included at this point).

O'Neill and Hassan (1994) incorporated 45 more load test results on the original database (Reese and O'Neill 1988b) and proposed equations for beta method that were included on O'Neill and Reese (1999). The number of slurry excavated shafts is unclear. O'Neill and Reese (1999) also incorporated the work of Majano (1992), which analyzed differences in behavior due to the use of mineral or polymer slurry and its effects over exposure time. However, the tests performed by Majano (1992) were conducted on very small model drilled shafts (about 1in diameter).

Table 2.3. Classification of the 41 case studies presented in Reese and O'Neill (1988b).

Construction Procedure	Soil Type			
	Clay	Sand	Interbedded	Total
Dry	18	0	11	29
Slurry	0	0	6	6
Casing	2	1	3	6
Total	20	1	20	41

The 2010 Drilled Shafts Manual (Brown et al. 2010) proposed a different approach for calculating β, based on the work reported by Chen and Kulhawy (2002). In this approach, it was assumed that the unit side resistance is directly proportional to the normal stress acting on the

interface, regardless of the construction procedure and its possible effects on the maximum mobilized side shear. Figure 2.10 (adapted from Brown et al. 2010) illustrates the variables involved, and the maximum (ultimate) side shear resistance, $fs_{,max}$, is defined in equation 2.8, from O'Neill and Reese (1978):

$$f_{max} = \sigma'_v * K * \tan\delta \qquad \text{eqn. 2.8}$$

where σ'_v is the vertical effective stress at the middle depth of the analyzed layer, K is the coefficient of horizontal soil stress, and δ is the effective friction angle between the shaft and the soil.

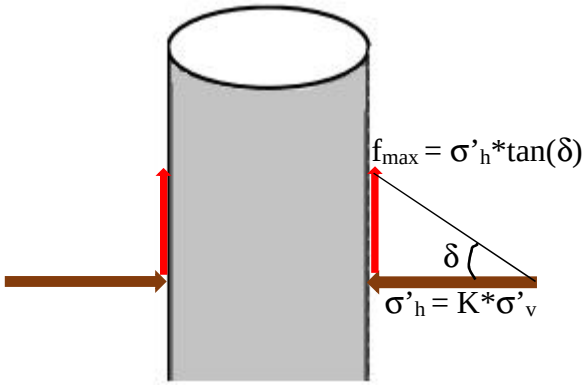

Figure 2.10. Representation of the friction model for side shear in granular soils.

Brown et al. (2010) proposed the following equation for calculating β:

$$\beta \approx (1 - \sin\emptyset') \left(\frac{\sigma'_p}{\sigma'_v}\right)^{\sin\emptyset'} \tan\emptyset' \qquad \leq K_p * \tan\emptyset' \qquad \text{eqn. 2.9}$$

where ϕ' is the effective friction angle of the granular material, σ'_v is the vertical effective stress at the middle depth of the analyzed layer, K_p is the coefficient of passive earth pressure, and σ'_p is the effective vertical preconsolidation stress. For clean quartzitic sands and sandy silts, the effective vertical preconsolidation stress can be approximately obtained using equation 10, and for gravelly soils, through equation 2.11.

$$\frac{\sigma'_p}{p_a} \approx 0.47(N_{60})^m \qquad \text{eqn. 2.10}$$

$$\frac{\sigma'_p}{p_a} = 0.15N_{60} \qquad \text{eqn. 2.11}$$

where p_a is the atmospheric pressure, and N_{60} is the corrected SPT N-value, corresponding to an efficiency of 60%.

In the approach described above, it is assumed that no change in horizontal stress, and therefore no change in K, should occur because of construction (Brown et al. 2010).

The beta method proposed by Kulhawy and Chen (2002) was based on 58 field load test results (27 in uplift and 31 in compression). Among the 27 shafts tested in uplift, 5 were constructed using slurry and 22, dry. Slurry was used on 7 of the compression shafts, 3 used casing and 21 were constructed dry (Kulhawy and Chen 2002). It is unclear if polymer was used as a type of drilling slurry.

The methods for design side shear of drilled shafts in sands (β methods) were, again, developed considering all used construction procedures and did not account for particular effects on the actual side shear, although differences were observed by O'Neill and Reese (1999) and Kulhawy and Chen (2002). The shafts constructed using slurry were minority; most of the shafts on the methods database were excavated dry.

2.3.2 Design Methods for Rock Socketed Shafts

The side shear strength of rock-socketed drilled shafts is similar to that of clayey soils in that it is dependent on the in situ shear strength of the bearing strata. In this case, rock cores are taken from the field and tested using various methods. Specifically, mean failure stresses from two tests are commonly used: the unconfined compression test, q_u, and the splitting tensile test, q_t. Local experience and results from load tests can provide the best insight into the most appropriate approach (Mullins 2014b).

Side resistance in rock depends upon factors other than solely the strength of the geomaterial. These include the roughness of the socket, the presence of soft seams within the geomaterial, and the angle of friction between the concrete and geomaterial. The first recommendation that O'Neill and Reese (1999) provided was to decide whether the socket will be smooth or rough, since roughness of the borehole wall has a large effect on side resistance.

It was recommended that, unless the sides of the borehole are artificially roughened during construction, the socket is considered smooth; however, procedures must guarantee that no smeared material remains on the sides of the borehole. For design purposes, a smooth socket contains a roughness naturally created with the drilling tool, but without leaving smeared material on the sides of the borehole wall (Hassan and O'Neill 1997).

For smooth rock socket in a rock layer, the maximum side shear (f_{max}) should be calculated using a method based on the work of Horvath and Kenney (1979) (O'Neill and Reese 1999):

$$f_{max} = 0.65 p_a \sqrt{\frac{q_u}{p_a}} \leq 0.65 p_a \sqrt{\frac{f'_c}{p_a}} \qquad \text{eqn. 2.12}$$

where f'c is the 28 day compressive cylinder strength of the drilled shaft concrete.

There is a slight difference between the methods proposed by Horvath and Kenney (1979) and Brown et al. (2010). The last authors suggest the use of a very similar equation as the one recommended by AASHTO until 2014, but based on the work of Kulhawy et al. (2005). In this approach, the "C" coefficient was introduced and ranges from 0.63 to 1.00.

The C value of 1.00 represents the mean of "normal sockets", constructed with conventional equipment and result in clean sidewalls, without use of artificial roughening. Sockets constructed into rock formations that are prone to smearing and/or rapid deterioration, which may the case of limestone, are not included within the "normal sockets" definition. In such

circumstances, Brown et al. (2010) not explicitly suggests using a lower bound value for "C" of 0.63, which encompasses 90% of the load test results analyzed by Kulhawy et al. (2005).

$$F_{max} = C * p_a \frac{\overline{q_u}}{p_a} \qquad \text{eqn. 2.13}$$

In this research program, the design side shear of the sockets was calculated using both C equal to 0.63 and 1.0 (called the lower and upper design side shear, respectively).

The FDOT (2017a) methodology was based on the work of McVay et al. (1992), applicable to rock socketed drilled shafts in Florida limestone formations. McVay et al. (1992) performed a parametric finite element study for the purpose of examining the maximum skin friction at the shaft-rock interface. They considered that, since the shaft typically has the greatest stiffness, followed by the rock and then soil, failure typically initiates from the juncture of the shaft and top of rock and then migrates downward along the shaft-rock interface.

Failure of the rock was described through a Mohr-Coulomb strength envelope, established in stress space by its cohesion and friction angle. The authors concluded that the Mohr circles grow toward a common failure state, and that the failure state propagates from one element to the adjacent, and as the rock elements adjacent to the shaft fail in shear, the load is transferred further down the rock-shaft interface.

Multiple triaxial compression tests at different confining pressures could be performed to determine the cohesion more precisely. Alternatively, q_u (unconfined compression strength) could be obtained from unconfined compression tests, and, q_t (indirect split tensile strength) could be obtained from split tensile tests, which are simpler and cheaper to be executed. Making use of trigonometric relationships and using the results provided by the numerical analysis, McVay at al. (1992) proposed that the maximum side shear resistance would be a function of q_u and q_t.

$$f_s = \frac{1}{2} \overline{q_u} \ \overline{q_t} \qquad \text{eqn. 2.14}$$

Hudyma and Hiltunen (2014) argued that the large variability of the Florida limestone properties should be incorporated into the design in order to obtain the design side shear (ultimate/nominal) by applying the average recovery from the coring. FDOT (2017a) recommends that the design side shear should be calculated as:

$$f_s = REC * \frac{1}{2} \quad \overline{q_u} \quad \overline{q_t} \qquad \text{eqn. 2.15}$$

where REC is the recovery expressed in decimals.

The method proposed by McVay et al. (1992) for rock sockets into Florida limestone and adopted by FDOT (2017a) was supported by 14 case studies and over a thousand unconfined and split tensile tests performed on recovered rock cores. The unconfined compressive strength (UCS) from McVay at al. (1992) database ranged from 160psi to 1,400psi on the limestone samples tested, and the split tensile strength, from 47psi to 166psi. The particular effects of using casings (permanent or temporary) were not considered in the basis of this design method.

2.4 Case Studies

2.4.1 Case Studies with Slurry Stabilized Excavations

Numerous studies about the effects of slurry type on drilled shaft capacity have been published, and yet there is no consensus agreement about the differences in side shear due to use of bentonite or synthetic polymer slurry. Depending on the soil type, bentonite may leave no filter cake (i.e. clayey soils) (Clayton and Mililitsky 1983) due to little radial permeation into those soils. Furthermore, the availability of publications that discuss the effects of longer exposure times to bentonite and polymer slurry are scarce and, in general, limited to 36h.

Research by Reese et al. (1973) and Fleming and Sliwinski (1977) has showed that proper use of slurry does not reduce the side resistance of drilled shafts, provided that the slurry and fluid concrete are handled so that the slurry is displaced during concrete placement and concrete is

placed as soon as possible after the excavation is complete (Turner 1992). This could be virtually true if actual 0h exposure times could occur either in practice or research. For longer exposure times, soil relaxation may introduce changes on the K/K_0 ratio.

In reality, most variations between test shafts are due to soil strength, concrete or inadvertent construction variations. Studies reported by Mullins (2012) and Mullins and Winters (2014) showed that using of polymer slurry did not adversely affect side shear capacity but rather a modest improvement was noted. This finding was also reported by Majano (1992). Intuitively many feel that the slick / slippery texture of polymer slurry materials may lubricate the soil particle interfaces, but the high pH of the concrete is hypothesized to break down the polymer and eliminate this effect. However, the concrete does not penetrate the soil as deeply as the slurry and would not prevent "lubrication" of the more peripheral soils.

Chang and Zhu (2004) monitored the changes in horizontal stress in the ground during the construction of a 2.6ft diameter and 98ft long drilled shaft, adjacent to the excavation, at a piling site at Singapore. The upper part of the ground consisted of over 26ft of compacted residual soil fill, classified as predominantly sandy silt, containing a fraction of clay. The ground water table was encountered at 62ft depth.

One flat dilatometer was installed and left in place 1.6ft away from the borehole wall, at the depth of 14.7ft (within the compacted fill) 5 days prior to pile construction. The initial membrane lift off pressure (p_{0i}) was measured before the excavation, and subsequent membrane lift off pressure (p_0) measurements were performed to monitor the changes in horizontal stress throughout the construction (Figure 2.11). After some localized collapses (indicating loss of stability), the piling contractor decided to fill up the excavation with water. Casting of concrete

(w/c = 0.55) was subsequently conducted by the tremie method 4hrs after excavation. Dilatometer p_0 pressures were taken at regular time intervals during shaft construction.

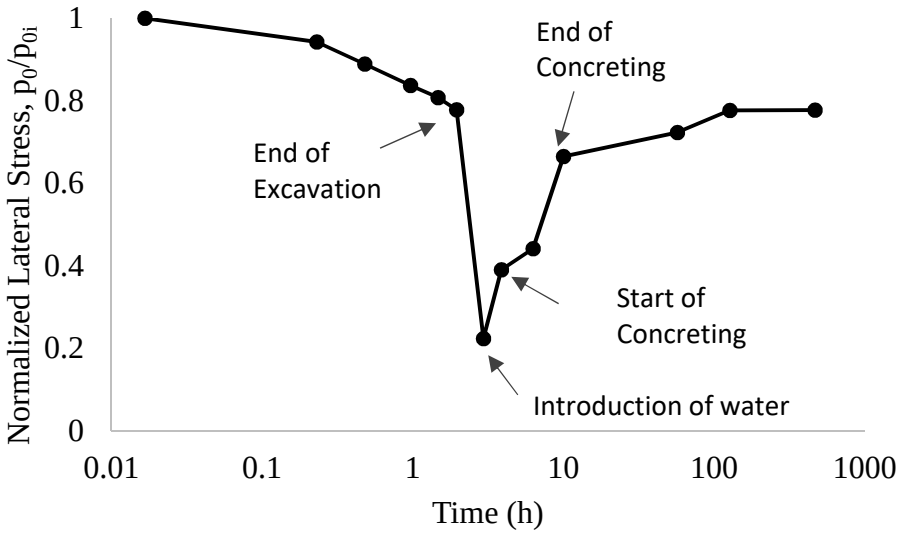

Figure 2.11. Measured normalized lateral stress changes during shaft construction.

The change in p_0 clearly showed that borehole excavation led to a significant reduction in horizontal stress in the surrounding soil. The normalized membrane lift off pressure was about 0.77 after completion of excavation, and reached about 0.22 after the borehole was left open for 1h after excavation was complete, prior to pouring of water. After the borehole was filled with water, the normalized p_0 raised to 0.40. At the completion of concrete casting, the normalized lift off pressure was of about 0.67, and stabilized at 0.78 after 4 days.

The University of South Florida recently performed a research study to investigate the influence of the drilling slurry viscosity on the side resistance of drilled shafts. Both bentonite and polymer slurries were investigated at various concentrations (viscosities). The full scale drilled shafts were between 14.2ft and 17.4ft long and about 2ft nominal diameter. The concrete slump ranged from 8in to 9.5in. The polymer product type used in the construction of these shafts was the solid vinyl. The construction site was located in Clearwater, FL, and was comprised by a 15ft thick silty sand, followed by clay to silty clay. The results of viscosity and slurry types versus

ultimate side resistance are shown in Figure 2.12, but no appreciable effects from either slurry type or viscosity were apparent (Mullins and Winters 2014).

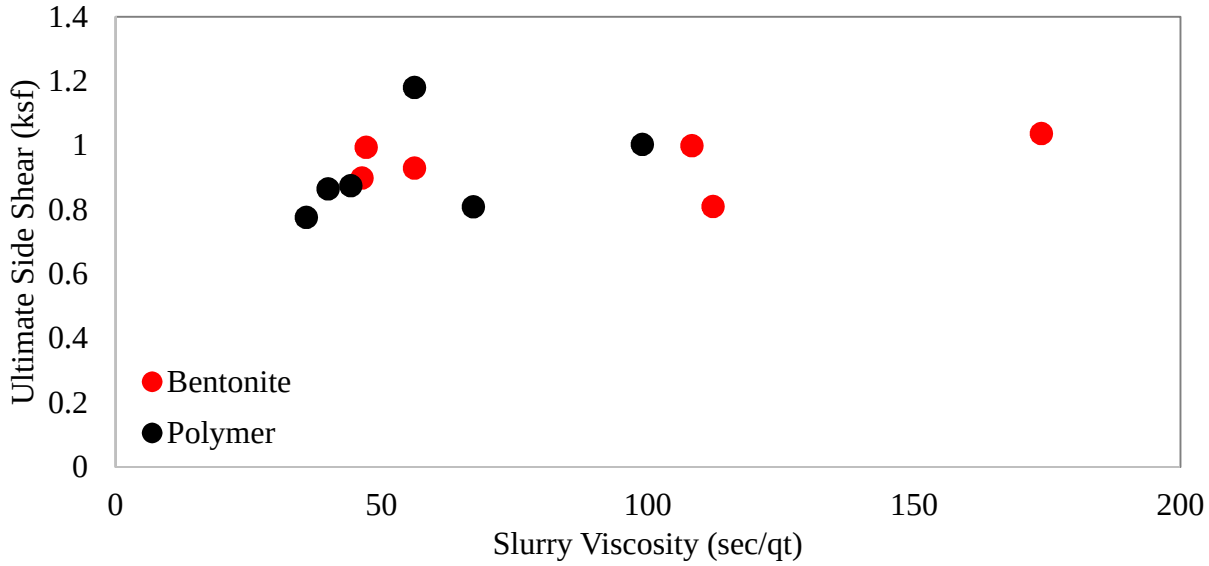

Figure 2.12. Ultimate side resistance vs viscosity and slurry type.

Investigating the effects of contact time with the drilling slurries was not part of the cited project scope, but the exposure times of six shafts, three bentonite and three polymer, were recovered from field records. Figure 2.13 shows the ultimate side shear as a function of exposure times for the six shafts that pertained to phase two of the cited research program.

In Figure 2.13, B and P are the bentonite and polymer shafts, respectively, and the numbers are the slurry viscosity, in seconds per quart. Since effects of exposure time were not the focus of this research, conclusions based solely on the presented results may not be readily evident. Further, due to construction sequencing, all bentonite shafts were constructed first followed by polymer shafts. As a result, a somewhat longer open excavation time was experienced by the bentonite shafts (5 to 7hrs) when compared to the polymer shafts (1 to 4hrs). One of the conclusions was that more research is required to properly quantify such effects.

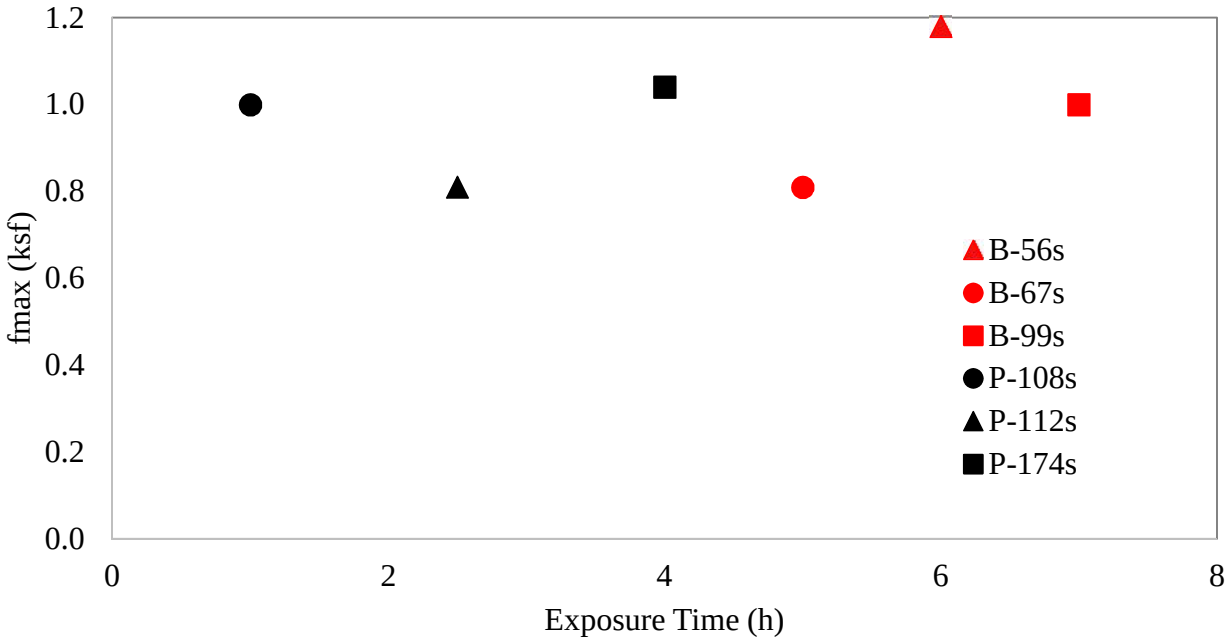

Figure 2.13. Variation of unit side shear with exposure time.

Auburn University in 2002 showed some effect of exposure time from polymer and bentonite slurry types. In that study, dry polymer pellets (DP) were used as well as liquid polymer (LP) (Brown and Vinson 1998; Brown and Drew 2000; Camp et al. 2002; Brown 2002). In total, 10 drilled shafts were constructed with 3ft nominal diameter and 36ft long. In two shafts, excavation was stabilized with bentonite slurry, four with polymer slurry, and four using temporary casing. The four polymer shafts were constructed using PHPA type, two in the dry form (solid), and the other two contained an emulsifying agent (liquid). The exposure time to the drilling fluids was either 1h or 24h. Some reduction was noted as a result of exposure which may have been due to soil relaxation and not exposure.

The construction site was located at the Auburn University National Geotechnical Experimentation Site, at Spring Villa, Alabama. The subgrade materials were comprised of Piedmont residual soils, which may have a significant spatial variability due to the remaining parent rock characteristics (such as foliation and structural arrangements). This case study was developed within the top 49ft, where the soils were classified as micaceous sandy to clayey silt.

On the construction site, the grain size distribution showed about 47% sand, 33% silt and 10% clay. In this zone, the SPT-N values ranged between 8 and 14.

All shafts were tested via static axial compression load tests. The load was applied with the use of a hydraulic jack acting against a reaction frame, in increments of 45kips to 67kips held for 5min. Each test was about 1 hour long.

The solid PHPA hydration process is not clear, and comparisons between solid and emulsified polymers may lead to imprecise conclusions. Brown (2002) attributed the reduced performance of the bentonite shafts, in comparison to the other methods, to the filter cake formation, even in short exposure times (e.g., 1h). As an example, the peak shaft resistance on the 1h bentonite was about half of the 1h emulsified polymer. The shafts constructed with polymer slurry showed, overall, an improved side resistance in comparison to the bentonite. Some strain softening can be observed, that was associated to the possible dilatant behavior of the local Piedmont soils. It is unclear, however, the degree of disturbance that might have occurred due to the specific construction methods.

One observation not included in the study findings is that about the same absolute resistance reduction was seen between the 1h and 24h shafts, regardless of the slurry type. Figure 2.14 quantifies this effect. The dashed lines were used because it is not possible to determine how the resistance changed between the 1h and 24h times. The 1h performance of the bentonite shafts was notably lower by a factor of two relative to standard liquid polymer.

The differences between bentonite and polymer slurries with 1h exposure might be attributed to the slurry types and the presence or absence of trapped bentonite presented as filter cake. However, it may be inferred that the differences between 1h and 24h exposure was due to the soil relaxation, not effects of any particular product (in this particular case study).

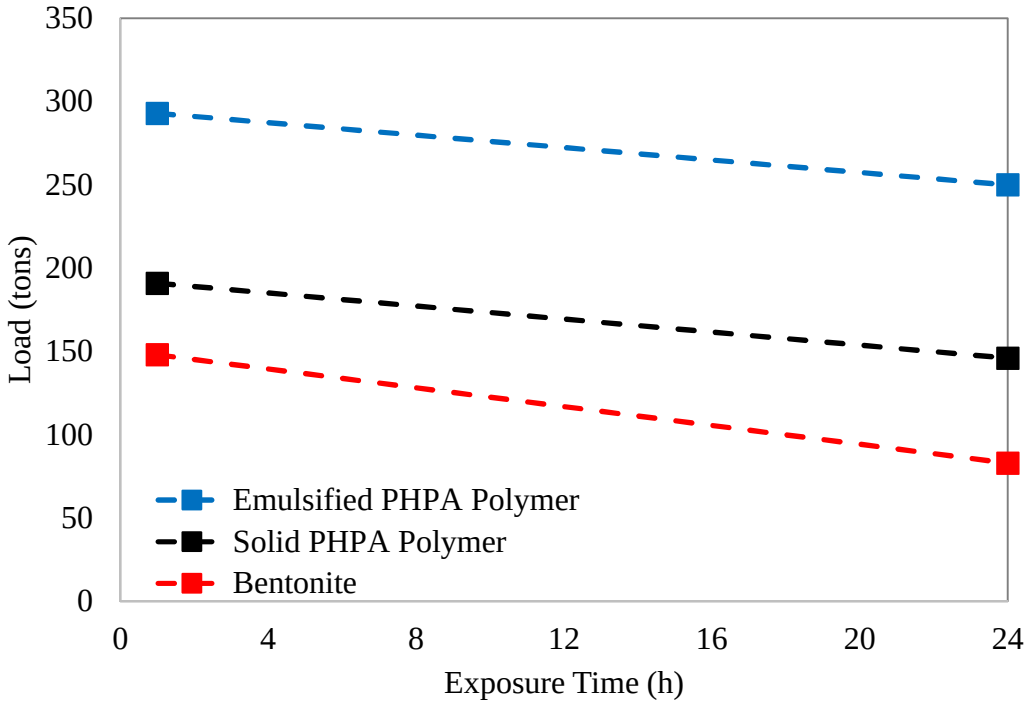

Figure 2.14. Time effect on side shear from Opelika test shafts.

Lam and Jefferis (2015) analyzed two case studies addressing exposure time effects of bentonite and polymer slurry on the side shear of drilled shafts. The first was originally presented by Wheeler (2003).

The construction site was located in Canary Wharf, east London. The subground materials consisted predominantly of sands, with two interbedded relatively thin clay layers, one in the top 9ft, and the other between 27ft and 39ft. The other layers consisted of sands to very dense sands, proportionally to the depth. The ground water table was not provided. Four test shafts were constructed to investigate if any observable difference in side shear over time could be attributed to the use of different slurry types (bentonite and solid PHPA polymer). In other words, the core question was if the recommendations derived for bentonite slurry would also be applicable / adaptable to polymer slurries.

The test shafts were 2.5ft diameter and 85ft long. Three of them were constructed with solid PHPA polymer slurry, and one of them with bentonite. No information about the viscosity or the mixing process was provided. The bentonite shaft and two of the polymer excavations remained open and in contact to the drilling fluid for 12h, and one of the polymer shafts was exposed for 37h. Further details about the construction procedure, such as cage layout, concreting procedure and concrete properties, were not presented. Details regarding the load test procedure were also not available.

The authors concluded that no significant difference could be observed between the polymer and bentonite shafts. Since all shafts achieved the working load with no clear signs of failure (estimated at about 800 tons), it was proposed that all polymer shafts (including the one left exposed for 37h) behaved satisfactorily and could be adopted as the production shafts. Based on the estimated working load, a displacement of about 0.3in (1% of shaft diameter) was used to obtain the mobilized shaft resistance and these values were plotted against the exposure times to the bentonite and polymer slurries, as shown in Figure 2.15. It is not clear what led the bentonite shaft to behave similarly to the polymer shafts at the same exposure time.

Care must be taken when interpreting these results and the conclusions proposed by Lam and Jefferis (2015). One may consider that soil relaxation may, once again, be included as one of the variables influencing the side shear of drilled shafts. The effects of time on the side shear cannot be determined from this study.

Lam and Jefferis (2015) reported another case study in east London, but at a construction site located at Stratford. The subground materials consisted of clays, ranging from stiff to very stiff, proportionally to a depth of 55ft, followed by a very dense sand layer, where the shaft tips were positioned (about 83ft below ground surface).

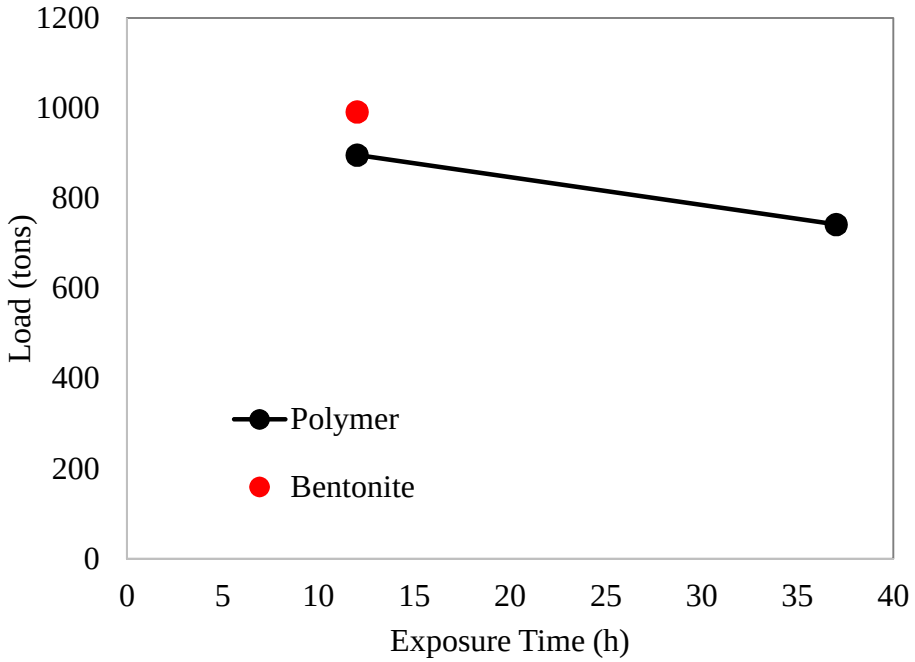

Figure 2.15. Effects of exposure time, Canary Wharf site.

Three 4ft diameter and 89ft long shafts were constructed, similarly to the Canary Wharf case study, to investigate the influence of different drilling fluids and exposure times on the side shear of drilled shafts. Two shafts were constructed with the aid of solid PHPA polymer slurry, and one with bentonite slurry (same products as the Canary Wharf case study). The load vs displacement curves are presented on Figure 2.16.

In this case, the polymer shafts outperformed bentonite. No appreciable difference could be observed between the 7.5h and 26h exposure times to polymer slurry. Soil spatial variation could be one of the variables, but no further information was provided that could explain these results. Once again, the tests did not reach clear failure, and no means for computing the changes in side shear were provided.

Lam and Jefferis (2015) concluded that, even under the working load, estimated to be about 1000 tons, no significant difference existed between the three shafts. No further discussions can be properly proposed herein since the amount of available data is limited.

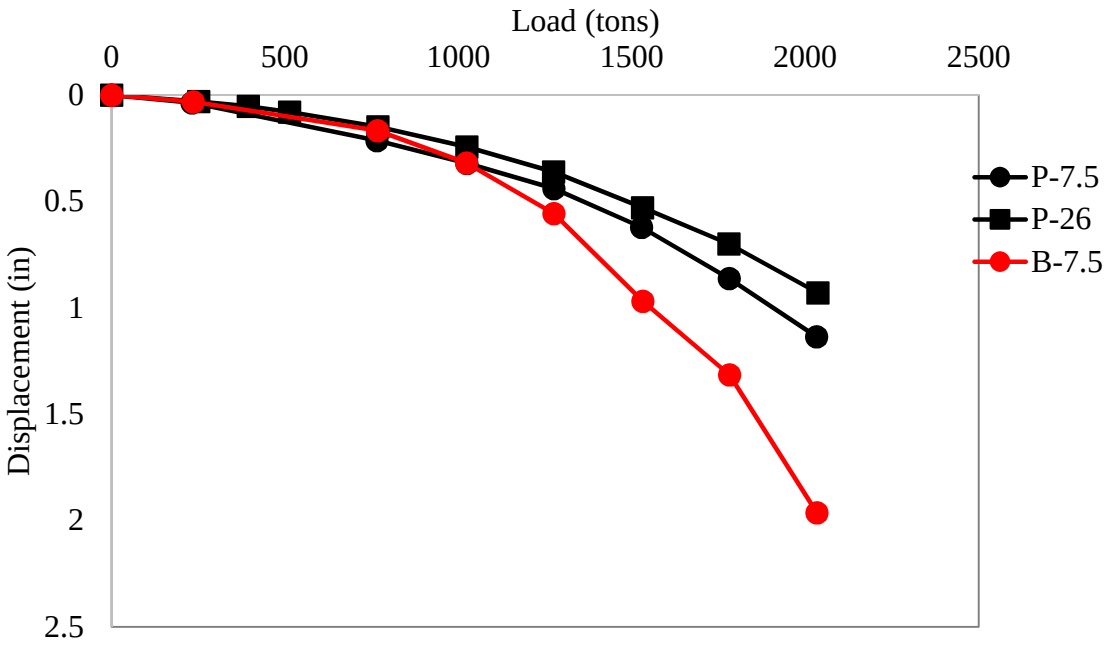

Figure 2.16. Load vs displacement curves, Stratford site.

Frizzi et al. (2004) reported the results of a load test program in three 6ft diameter, 120ft long test drilled shafts, in downtown Miami, FL. The objective was to evaluate the effects of using bentonite and polymer slurry on full-scale drilled shaft load carrying capacity.

The subgrade was comprised of interbedded layers of limestone, sandstone and sand. Frizzi et al. (2004) had the objective of investigating the effects of three different construction methods on the overall performance of drilled shafts recommend an appropriate construction method for the production shafts. Three test shafts were constructed with different stabilization methods: one with bentonite slurry, one with polymer and temporary casing, and the other with polymer slurry. All shafts were 6ft diameter and 120ft long (nominal dimensions) with a 6.6ft diameter, 15ft long surface casing.

No specific details regarding the construction sequence were provided. It is not clear if the temporary casing on one of the polymer shafts was installed prior to or after excavation below the surface casing had begun, but the authors cited some possible effects on the sand layers due to the casing vibration during installation and extraction.

All shafts were load tested by the use of O-cells. The results were presented in terms of mobilized end bearing versus displacement and equivalent load on top versus displacement, making possible to estimate the mobilized side resistance versus displacement for the three shafts described by Frizzi et al. (2004). These inferred results are presented on Figure 2.17.

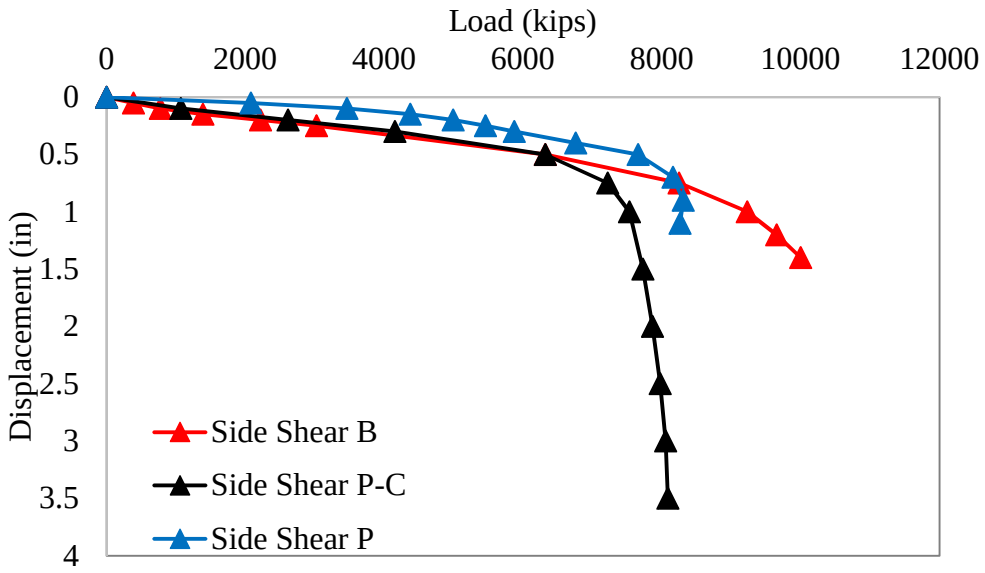

Figure 2.17. Estimated side shear resistance.

From Figure 2.17, the polymer shaft showed the best response in terms of side shear versus displacement at side resistances below 6,000 kips, where the polymer-cased and the bentonite shaft exhibited very similar results. At higher side resistance levels (beyond 8000 kips), the bentonite shaft showed a better response. Based on the available information, explanations for these differences and results do not seem appropriate.

Majano (1992) presented a series of small scale laboratory pull-out tests carried out on model shafts constructed in sand, under different slurry types, concentrations and times of contact with the soil. The lab model shafts were constructed in compacted sand, collected from the San Jacinto River, which contained about 2% silt and clay. Five slurry product types were used in various concentrations (viscosities) and different exposure times. The extraction cell reported by Majano (1992) and Majano and O'Neill (1993) was designed to accommodate 3in diameter by

6.5in long sand soil samples. The pull-out tests and extractions were performed using a triaxial-like cell.

After the extraction, the model shaft “as built” dimensions were measured so the unit perimeter load transfer could be computed and presented. The filter cake thickness (if any) was also measured (Majano 1992; Majano and O’Neill 1993). Figure 2.18 shows the maximum side shear observed on the pull-out tests on the specimens that were exposed up to 24h. The bentonite results presented on Figure 2.18 refer to the nominal shaft dimensions, because of the large filter cake that formed. In Figure 2.18, S represents the solid polymer shafts, B, the bentonite shafts, and the numbers followed by “s” are the viscosity, in sec/qt, of each slurry analyzed by Majano (1992).

According to Majano (1992), the effects of contact time in laboratory does not necessarily correspond to those occurring in the field. Majano (1992) stated that the side shear observed on bentonite shafts with longer exposure times are misleading, since visual inspections indicated severe geometrical deteriorations on the shafts. In the field, such effects could mean integrity problems in the foundation elements.

Majano (1992) and Majano and O’Neill (1993) suggested that longer exposure times adversely influenced the behavior of mineral supported drilled shafts in comparison to the polymer supported ones, which presented a tendency of increasing the side shear with time.

From the series of performed tests, presented in Majano (1992) and Majano and O’Neill (1993), the importance of better understanding the effects of exposure times to polymer slurries on the side shear of drilled shafts has become even more evident. Limitations, such as the very small scale tests, sand specimen preparations and constant confining pressures throughout the tests, impose restriction in extrapolating these results to the side resistance behavior of full scale drilled shafts.

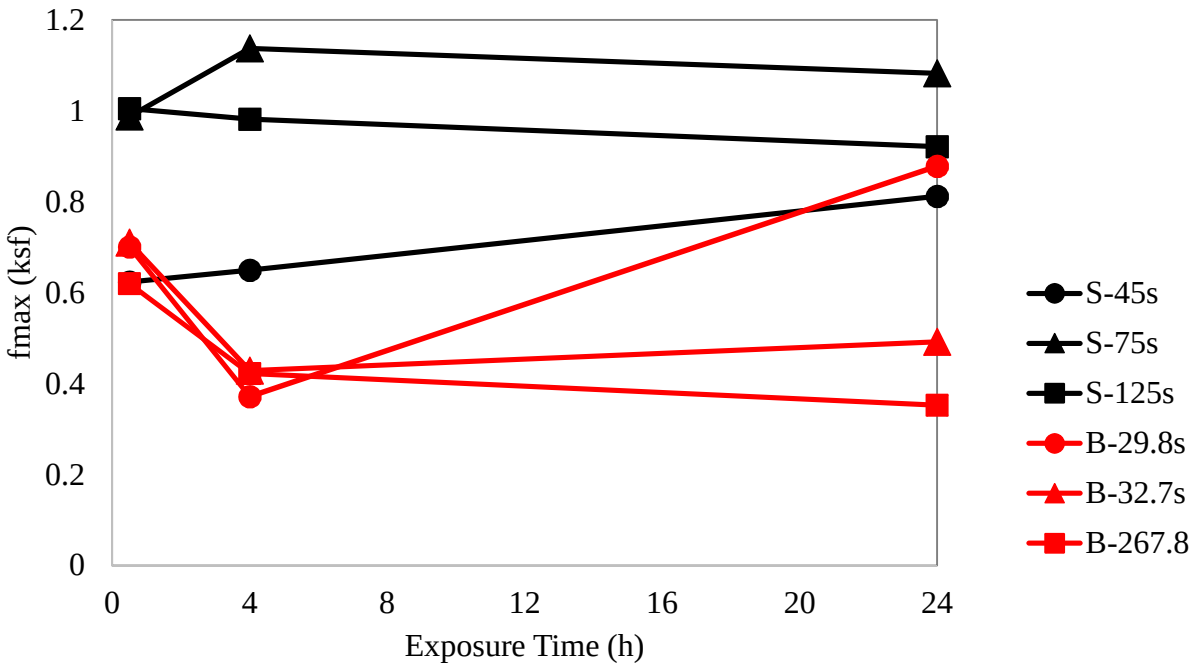

Figure 2.18. Side shear vs exposure time.

2.4.2 Case Studies with Temporary Casing Supported Excavations

Three selected case studies are presented herein showing effects of temporary casing supported excavations on the side shear of drilled shafts; two in rocks (limestone) and one in sandy soils.

Law (2002) reported two test piles built and load tested in downtown Jacksonville, Florida, during the construction of an office building. The objective was investigating the changes in side resistance due to different construction procedures.

The two test shafts were very similar in terms of design side shear and depths, but completely different in construction procedures. A 13ft thickness overburden layer overlaying a 16ft thickness variably cemented limestone layer, followed by a marl layer, comprised the site. The ground water table was near the surface. The drilled shaft tip was at a depth of 43ft. For design purposes, the overburden material resistance was disregarded, as well as the tip resistance in the marl. An Osterberg cell was installed at a depth of 36ft in both shafts (Law 2002).

In the first test shaft, an outer surface temporary casing, with outer diameter of 42.5in, was installed with a vibratory hammer to the top of rock elevation, and an earth auger removed the spoil from inside this casing. Next, a 15ft long, 36.75in outside diameter core barrel cored the entire limestone layer at once. Then, a telescopic casing, with outer diameter of 36in, was placed in the annular space excavated by the core barrel, and rotated into the marl formation. The rock plug and the marl were drilled with a rock auger, the borehole was cleaned and the concrete was poured by free fall (dry excavation). The temporary casings were extracted from outside-in (Law 2002).

In the second test shaft, the limestone was penetrated using a rock auger, which removed the inner rock from the borehole during the excavation. The major difference was that the temporary casings were extracted from the inside out.

The results of the load tests performed on the two test shafts were completely different. For the first test shaft, the upper portion of the shaft failed in side shear when the applied O-cell load reached around 205kips. For the second test shaft, no signs of failure were identified in the upper portion up to the maximum applied O-cell load of around 1,220kips. Figure 2.19 shows the load vs displacement curve for the two test shafts.

Law (2002) suggested that firstly extracting the outer casing could have caused degraded materials to infuse into the annular space generated between the outer and inner casings, so concrete could not establish bond with the excavated walls.

After the failure of the upper portion of test shaft in which the outer casing was extracted first, no significant residual side shear could be observed. The displacement went back to zero by the action of the upper shaft portion self-weight, estimated to be about 40kips. No information about fluid concrete, cage or construction time was provided. Nonetheless, this extreme

discrepancy unquestionably emphasizes the importance of construction procedures on the side shear of drilled shafts and its overall performance.

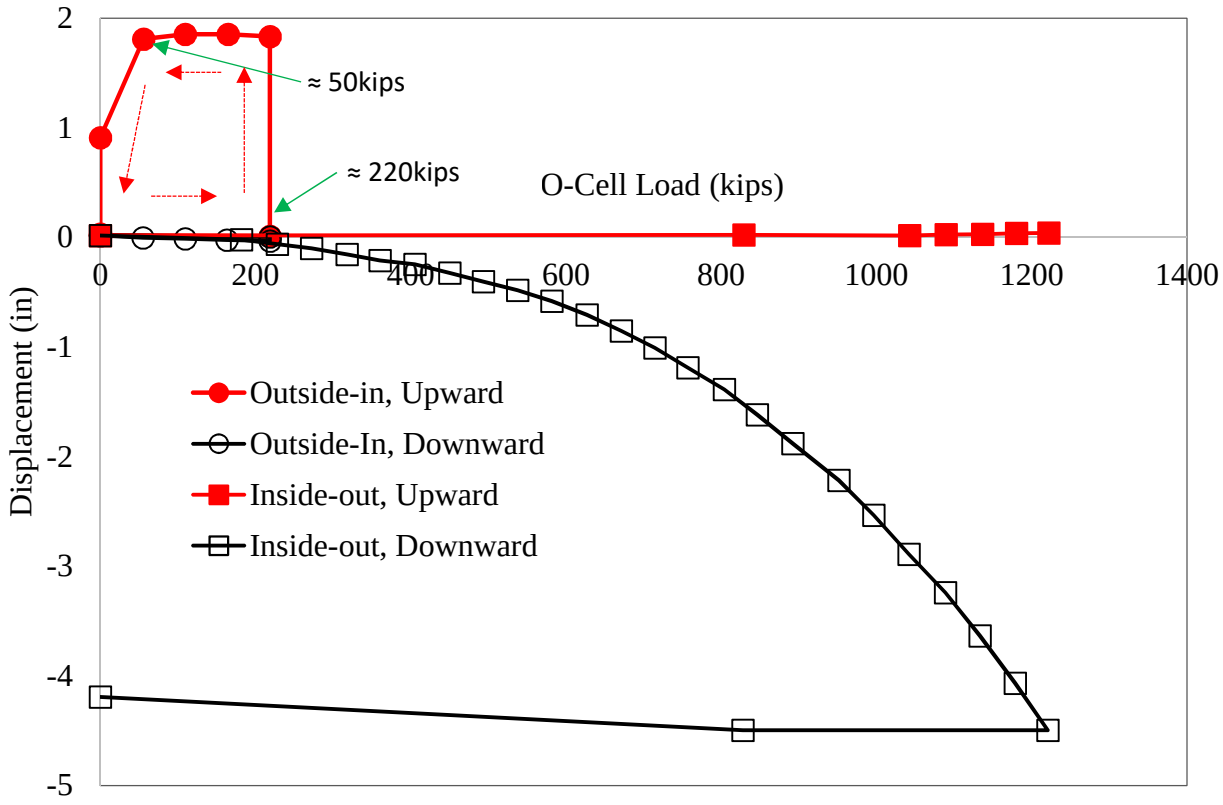

Figure 2.19. Load-displacement at top for test shafts in Jacksonville.

Castelli and Fan (2002) presented the results of load tests conducted in two drilled shafts constructed with temporary casings into the limestone, during the replacement of the existing I-95 Fuller Warren Bridge over the St. Johns River in Jacksonville, Florida.

The bridge alignment was underlain by three formations, including overburden soils, limestone, and marl. The limestone was found to be porous, weakly-cemented to well-cemented (SPT N-values from less than 10 blows per foot to over 50/2 inches), having a thickness up to 20ft. The top of the limestone stratum was typically encountered at elevations -15 to -35ft, and contained interbedded seams of calcareous sand, silt, and clay, and was underlain by marl (Hawthorne

formation). Both test shafts were constructed by driving a temporary casing into the limestone. Table 2.4 summarizes the results. The load tests were performed using O-cells.

The mobilized side shear of the bottom segment of socket 1 and throughout socket 2 did not reach failure, and according to Castelli and Fan (2002), a higher ultimate side shear would be expected. It seems not possible to determine whether the temporary casing caused any notable reduction on the side shear.

Table 2.4. Maximum side shear.

Test Shaft ID	Shaft Diameter (in)	Elevation (ft)	Limestone Description and SPT N-Value	Maximum Side Shear (tsf)	Upward Disp. (in)
1	36	-18 to -21	Decomposed Limestone, N ≈ 7	0.5	0.94
		-21 to -25	Cemented Limestone, N ≈ 50/1in to 50/5in	8.2	
		-25 to -28		19.0	
		-29 to -34.3		5.6*	
2	48	-17.7 to -21.7	Decomposed Limestone, N ≈ 16	2.1*	0.50
		-21.7 to -25.6	Cemented Limestone, N ≈ 50/3in	6.2*	
		-25.6 to -29.5	Cemented Limestone, N ≈ 50/3in	14.1*	
		-29.5 to -32.3	Weakly Cemented Limestone, N ≈ 20 to 50/4in	4.1*	

* Failure was not observed on these segments.

Seavey and Ashford (2004) presented a final report to the California Department of Transportation with the objective of identifying some issues that would require further research regarding how construction methods affect the axial capacity of drilled shaft, and one of the topics was construction with temporary casing. The authors cite a study presented by Reese et al. (1985), consisting of three test shafts constructed with temporary and/or permanent casing.

The subgrade consisted of a loose to firm sand/soft clay mixture for the top 20ft, soft to medium clay to 30ft, a very dense sand layer for the next 10ft, with SPT N-values around 175 (it

is not clear why refusal was not noted). This dense sand layer was classified as an IGM and was underlain by a soft to medium silty clay, with an undrained cohesive strength, s_u = 0.4tsf.

The first shaft was 60ft long and 48 inches diameter, constructed with temporary casing to the depth of 52ft, and augering the soil from inside. The remaining length was excavated with slurry, but the type of slurry was not provided. As the concrete was poured, the casing was removed. This pile was chosen to be the control shaft. The second shaft was constructed with a temporary 48 inch diameter casing that was driven to 50ft. The inner 36 inches were excavated with slurry, and a permanent 36 inch diameter casing was placed inside the first casing and the concrete poured. The third shaft used surface casing for the upper 10ft, and was excavated with the slurry method for the remaining depth with a permanent 36 inch casing placed down to 40ft (Reese et al. 1985), from Seavey and Ashford (2004).

Test shaft 1 showed the highest measured side shear among these three piles (Table 2.5). The side resistance dropped significantly when permanent casing was installed, especially on test shaft 2, where a combination of temporary and permanent casing was used in construction. In test shaft 2, upon removal of the outer temporary casing, the soil experienced a significant relaxation and possibly moved inward, indicating a void space between the pile and soil; thus, side resistance was expected to be low. The ultimate side shear was estimated between 2.1 and 2.8tsf for the IGM layer (Reese et al. 1985; Seavey and Ashford 2004). From these results, it is possible to infer that constructing with temporary casing, and then extracting it, did not affect the side shear in comparison with the designed / calculated values. No information regarding how the casings were installed and extracted was presented.

Table 2.5. Calculated versus measured side shear (Reese et al. 1985).

	Test Shaft 1	Test Shaft 2	Test Shaft 3
Nominal Diameter (in)	48	36	36
Casing method	Temporary	Temporary + Permanent	Permanent (installed after excavation with slurry)
Calculated ultimate side shear (tsf)	2.1 to 2.8	2.1 to 2.8	2.1 to 2.8
Measured Side Shear (tsf)	2.3	0.5	1.5

2.5 Need for Further Study

Design methods for side shear of drilled shafts, either in soils or rocks, are based on soil and rock mechanics theory and calibrated, sometimes, by analyses of load test results. Even those that were calibrated using load test results do not account for differences in side shear behavior due to any specific construction method (e.g. bentonite or polymer slurry, time that the open excavation was exposed to each type of slurry, or casing types and installation/extraction methods)

While the effects of exposure time for mineral slurry have been partially quantified in literature, the time-dependent effects of polymer slurry exposure have not, especially for periods over 36h (Mullins 2014a).

A small number of publications can be found that provide a better understanding about the differences in side shear behavior between the different types of temporary casing and its installation/extraction methods. Drastic differences could occur depending, among other variables, on the construction procedure (recall the case study reported by Law 2002).

Furthermore, the resistance factors that are proposed in design manuals also incorporate all types of construction method, with no attempt to quantify possible variations due to the procedure used during construction. The resistance factors were calibrated also without differentiate particular construction procedures. Further discussions regarding resistance factors are presented on Chapter 5.

This research program provides evidence that the side shear behavior of drilled shafts in sands and rock socketed shafts in limestone is influenced not only by the geotechnical properties of the foundation geomaterial, but also by the construction procedures.

CHAPTER 3: CONSTRUCTION PROCEDURE AND TESTING RESULTS: SLURRY SHAFTS

3.1 Research Program Overview

As part of this research program, thirty-two, $1/10^{th}$ scale (4in diameter; 84 – 96in long) drilled shafts were cast and tested for pull out resistance where open excavation exposure times were 0h, 1h, 2h, 4h, 8h, 24h, 48h and 96h, for each slurry type. In practice, 0h exposure is an unachievable number, since the procedure for concrete pouring takes a finite amount of time to be completed. However, in this work, the denomination of "0h shafts" will be used as a reference. Among these 32 shafts, the fluid level was continuously monitored and maintained for 8 of the shafts up to 96h (phase 2 shafts).

Additionally, 4 small-scale excavations (phase 3) were also monitored to acquire complementary data to study flow rate. Such excavations were left opened for up to 16h, and as pull-out tests were not performed, no concrete placement was required.

Three commonly used polymer products were selected: (1) Cetco ShorePac, with no additives; (2) KB International Enhanced SlurryPro CDP, with the EnhancIT 100, EnhancIT 200 and SlurryPro MPA additives, and (3) Matrix Big-Foot, with the Fortify additive. The bentonite product was PureGold Gel from Cetco which is an API 13A, Section 10 pure bentonite product, with no polymer additives.

Figure 3.1 shows the plan view layout of the 36 shafts at the Geo-Park. All shafts pertaining to the same test series (same product) in the first phase of this study were constructed with a distance of 6ft, center-to-center. Each series (rows using different products) was staggered with spacing 3ft on center, but constructed at different times. The space between the 96h exposure series and the Cetco series was also 3ft, whereas between the 96h and 48h series (phase 2) and phase 3 shafts, this spacing was 6ft from center as shown.

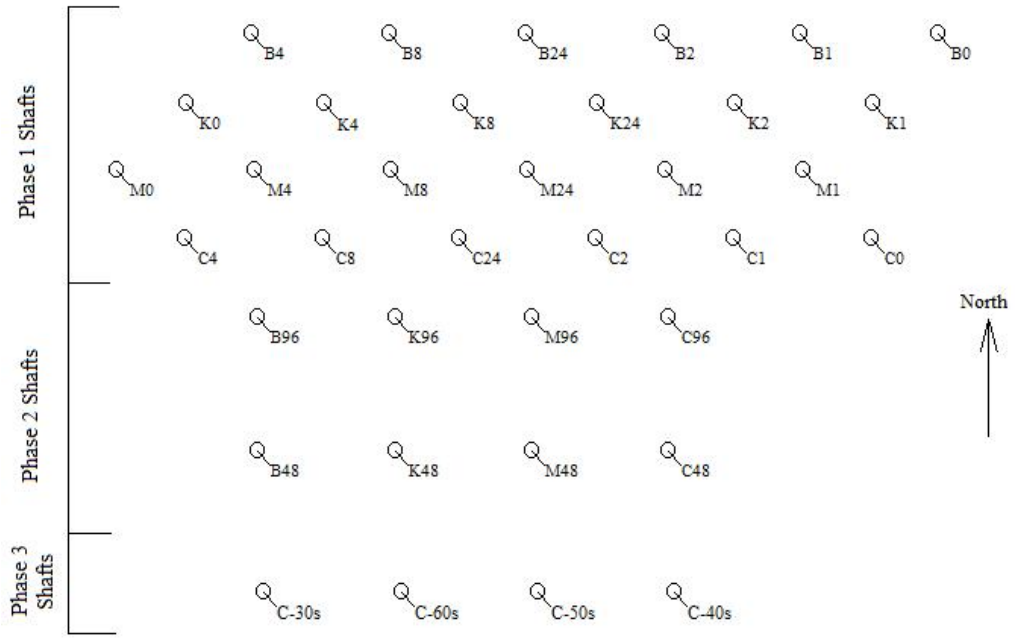

Figure 3.1. Plan view layout of all 36 test shafts.

The testing program was conducted in the Geo-Park, a geologic research site on the University of South Florida's Tampa Campus (Figure 3.2). The geotechnical characteristics of the underlying soils were obtained by performing 32 CPT tests, one for each shaft, using a truck-mounted miniature CPT rig at each shaft location. The depths of each CPT varied from 14ft to 25ft. The test site was mostly comprised of silty sands from 0-8ft over sandy clay / clayey sand interbedded layers from 8-25ft, followed by limestone. The length of the shafts were limited to 8ft to stay out of clay and promote slurry infiltration for both bentonite and polymer slurries.

The equivalent SPT-N, calculated based on correlations with the CPT test results (Robertson 1990), ranged from about 4 to 20, typically. The CPT test results of the 0h through 24h shafts are presented in Allen (2016). The CPT results of the 48h and 96h shafts are presented herein in Appendix 1. Figure 3.3 illustrates the geotechnical profile including the ranges of SPT-N values that were typical for each layer.

Figure 3.2. Overview of the testing site.

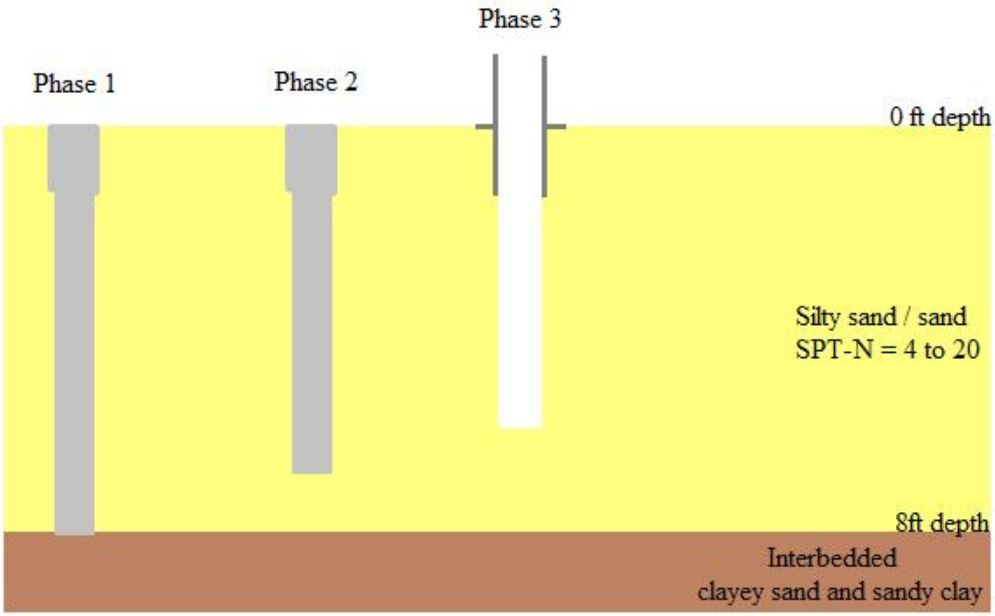

Figure 3.3. Simplified geotechnical profile and illustration of the shafts positioning.

3.2 Shafts Construction

All 32 shafts pertaining to phases 1 and 2 were of similar construction. The slurry mixing and excavation procedures for the phase 3 shafts were the same, but no concrete was placed. The slurry used during shaft construction was prepared prior to construction. Shaft excavation was performed using a hand auger, and the concrete was placed by tremie. More details about phase 1 shafts can be found elsewhere (Allen 2016).

3.2.1 Slurry Mixing

Prior to mixing the slurry, soda ash was added to the mixing tank in order to elevate the pH from 6.5 to a range of 8 – 10. This was accomplished using a Hootonanny dry powder mixing educator attached to the side of the mixing tank. After all soda ash was added, the tank was recirculated for 20 minutes.

The overall setup used for slurry mixing for phase 2 shafts is shown in Figure 3.4. Figures 3.5 through 3.8 show the mixing of each of the 4 products used. Centrifugal pumps were used to do prepare and recirculate the mineral slurry. Preliminary mixing of the polymer slurry was performed via centrifugal pump, but subsequent recirculation implemented diaphragm pumps and air bubbling system to prevent cleaving the polymer chains. This helped the polymer to maintain viscosity during the pumping and recirculation processes.

Figure 3.5 illustrates the bentonite mixing. After all bentonite was introduced via the Hootonanny, the tank was recirculated for 20min, resulting on a viscosity of 39.2s. This value is comparable to the value obtained on the first 24 shafts and also within the recommended ranges of FDOT (2017b), FHWA (2010) and AASHTO (2016). During the testing, viscosity measurements were taken at least once a day, and the slurry was also recirculated at least once a day to maintain a constant viscosity.

Figure 3.4. Phase 2 mixing and testing setup.

Figure 3.5. Bentonite slurry mixing.

The Hootonanny was attached to the top edge of the tank while the water was pumped in, pulling in the Cetco ShorePac polymer (Figure 3.6). Two 300gal tanks were used to achieve the

desired 450gal. The slurry was mixed between tanks to ensure consistency. The viscosity was 65s/qt.

Figure 3.6. Cetco polymer mixing.

The mixing of the KB polymer slurry first introduced the Enhanced SlurryPro CDP (main product), and the additives the EnhancIT 100 and EnhancIT 200 through the Hootonanny. The SlurryPro MPA was sprayed on the tank afterwards, but while the mix was being recirculated. The slurry viscosity was 71.0s by the end of mixing process.

Figure 3.8 illustrates the mixing of Matrix polymer, which resulted in a viscosity of 69s. The Big Foot and the Fortify were also first introduced using the Hootonanny as the clean pH treated water was pumped in with a centrifugal pump.

Phase 3 shafts used only Cetco polymer slurry to investigate the influence of viscosity variations on the fluid loss. The target viscosity values were 30s, 40s, 50s and 60s. The mixing setup was similar to that used in phases 1 and 2 (Figure 3.9). Once the desired viscosities were achieved, the experiment was setup at the Geo-Park for the complementary fluid loss study (Figure 3.10).

Figure 3.7. KBI polymer mixing.

Figure 3.8. Matrix polymer mixing.

All the slurry used to refill the holes and the samples used for viscosity tests were collected from the same valves, at the bottom of the tanks. Figure 3.11 shows the viscosity test being performed.

Figure 3.9. Phase 3 shafts slurry mixing.

Figure 3.10. Setup for the viscosity vs fluid loss study.

Table 3.1 shows the main product concentration, pH and viscosity for all shafts. It should be noted that the KBI system did not call for pre-treatment of the mixing water (KBI 2015). However, for the 48h and 96h KBI polymer shafts, the pH of the mixing water was treated with soda ash, as part of a trial to obtain higher viscosity than those in Phase 1 (which fell below the manufacturer's recommended range).

Figure 3.11. Viscosity measurement during the construction of phase 2 shafts.

Both AASHTO (2016) and FHWA (2010) recommend the same ranges for pH and viscosity. For mineral slurry, the pH should range between 8 and 11, and the viscosity between 28sec/qt and 50sec/qt. For polymer slurry, the recommended pH ranges between 8 and 11.5, and the viscosity between 32 and 135sec/qt. FDOT (2017b) recommends limiting the mineral slurry viscosity to 40sec/qt.

All viscosity and pH values shown in Table 3.1 were within state and federal recommendations with the exception of the bentonite slurry for the 48h and 96h shafts, in which the viscosity was slightly above the FDOT (2017b) upper limit, but still very close to that of the 0h – 24h shafts. In Table 3.2, B = bentonite, C = Cetco polymer, K = KBI polymer. In phases 1 and 2 shafts, the numbers on the "Shaft ID" column represent the exposure time, in hours. In phase 3 shafts, the numbers are the viscosity, in seconds.

The KBI polymer slurry viscosity observed in the 0h to 24h shafts was lower than the manufacturer recommended range of 65-100sec/qt. For the 48h and 96h shafts, the viscosity was within the manufacturer suggested range (65 – 100 sec/qt) and comparable to the other polymer

slurries. Both Cetco and Matrix polymer viscosities were above the manufacturer's recommended range of 45 – 55 sec/qt for Cetco and 50 – 55 sec/qt for Matrix (CETCO 2017; KBI 1991; Matrix 2016).

Table 3.1. Summary of slurry data for all shafts.

Slurry Product	Shaft ID	Main Product Concentration (lb/gal)*10^{-3}	pH	Viscosity (sec/qt)
Pure Bentonite	B0 to B24	667	10.0	39
	B48	616	10.5	41 – 43
	B96	616	10.5	41 – 43
Cetco Polymer	C0 to C24	5.67	10.0	74
	C48	11.45	10.5	70 – 76
	C96	5.57 – 11.45	10.5	58 – 77
	C-30s	0.84	10.0	29 – 30
	C-40s	4.19	10.0	40 – 42
	C-50s	14.67	10.0	47 – 51
	C-60s	12.51	10.0	59 – 63
Matrix Polymer	K0 to K24	8.82	7.0	47 – 54
	K48	6.19	11.5	68 – 80
	K96	6.19	11.5	68 – 93
KBI Polymer	M0 to M24	5.70	10.0	73
	M48	4.44	10.5	72 – 75
	M96	4.44	10.5	72 – 78

3.2.2 Excavation

For all 36 shafts, the excavations were performed using a hand auger with 3.8in outer diameter and 8in long collection bucket with two cutting teeth on the bottom. When the excavation reached 1ft depth, a 4in inner diameter steel surface casing (0.25in thick and 2ft long) was installed 1ft into the ground. Its purpose was to prevent surface collapse, serve as a guide for the remaining excavation and allow slurry to be filled above the ground surface up to 1ft. As soon as the surface casing was in place, it was filled with slurry so that excavation could proceed. After one or two passes with the hand auger, the slurry level within the hole dropped and was replenished. Figure 3.12 illustrates the excavation of phase 2 shafts and the silty-sand characteristic of the top 8ft.

Figure 3.12. Phase 2 shafts excavation (left) and predominant silty-sand soil (right).

3.2.3 Concrete Placement

All concrete (mortar) was tremie-placed where the upper hopper/funnel was removable and could serve as the transport vessel between the concrete mixer and the excavation (Figure 3.13).

The tremie was first sealed with a plug and a 12ft long anchor rod assembly was placed into the tremie before attaching the hopper. Each anchor assembly consisted of ¾in diameter all-thread steel rods attached to a 2.75in diameter, 1/2in bearing plate nutted on both sides of the plate; the all-thread portions were sleeved with 1in diameter SCH40 PVC pipes to prevent bonding between concrete and steel. This ensured a direct load path to the bottom of the shafts, where the upward tensile force from the rod could transfer compression to the shaft bottom upward. Since the shaft was placed in direct compression (from the bottom up), no reinforcement steel cage was necessary.

For phase 2 shafts, the concrete was mixed using a 1 cubic yard capacity mixer and all shafts were constructed for the same batch (Figure 3.14). In phase 1, a $1ft^3$ concrete mixer was used (Allen 2016). The concrete was mixed immediately before pouring and had the same material ratios (w/c, cement content per cubic yard and cement to sand ratio). The concrete mortar had slumps ranging from 9.5in to 10.5in, with a minimum compressive strength of 3ksi.

Figure 3.13. Illustration of concrete placement.

Figure 3.14. Concrete mixing for phase 2 shafts.

3.3 Pull-Out Load Tests

Investigating the effects of exposure times to different commercially available slurry products on the side shear of drilled shafts was one of the major objectives of this study. In this section, the testing procedures and the pull-out test results are presented.

3.3.1 Testing Procedures

The pullout testing setup and procedure was the same for all 32 shafts, as described by Allen (2016) and Caliari de Lima et al. (2016). First, a load frame was threaded over the rod cast in the shaft. Next, a 10MT capacity hollow-core jack and load cell were positioned on the top of the assembly and restrained by a steel plate and nut. An 8ft reference frame was positioned orthogonal to the reaction beam to avoid undesired effects of displacements caused by the load frame (Allen 2016). Figure 3.15 illustrates the small-scale pull-out tests setup during phase 2 shafts testing.

The data was recorded using an Omega Model USB OMB-55 data acquisition device and a field computer enclosure was not crucial to the data collection, merely a convenience (Allen

2016). A manual-activated hydraulic pump was used to slowly apply and control jack pressure. The loads were applied in increments of 0.5kips, and each step was held for 2min. After observing failure, the test was continued until the displacement gage stroke was fully used (4in). All pull-out tests were performed between 7 and 9 days after concreting. Phase 1 shafts were extracted for as built dimension measurements and computation of cake thickness; phase 2 shafts were not. Figure 3.16 shows an overall view of the testing area.

Figure 3.15. Small-scale pull-out load tests setup.

Figure 3.16. Overview of the phase 2 testing area.

3.3.2 Results

Figure 3.17 shows the field load vs displacement results for all 32 tested shafts, organized by each set of products. In the legends, B denotes bentonite, C the Cetco polymer, K the KBI polymer and M the Matrix polymer. Again, the numbers after the letters represent the exposure time in hours.

When looking strictly at the pull-out load, the bentonite shafts were somewhat comparable to polymer shafts for exposure times up to 4h. After longer exposure times, the polymer shafts outperformed bentonite.

The maximum load achieved by the 96h bentonite shaft was about half of the 0h bentonite shaft. This significant reduction on the maximum load can be associated with the filter cake buildup over time (Allen 2016). Reductions due to longer exposure times were not observed in the polymer shaft results. Majano (1992), Majano and O'Neill (1993) and Majano et al. (1994) also reported similar observations.

Figures 3.18 and 3.19 show the variation of the maximum pull-out load and the side shear resistance variations over time, respectively. The letter P on the legend represents the averaged values for all three polymer products used. Again, little changes in the polymer performance were noted; bentonite shafts showed almost a linear capacity loss with time after 4h.

Variations in both local soil strength and shaft dimensions can have an effect on the side shear when comparing side-by-side load test results. Some variations are real, like shaft length, and some are artificial, such as filter cake build up. Phase 1 shafts were exhumed and measured, and smaller diameters caused by filter cake buildup after washing are not truly the correct dimensions when computing side shear and, therefore, the actual failure surface was used which included the filter cake thickness or the true sheared surface diameters (Allen 2016).

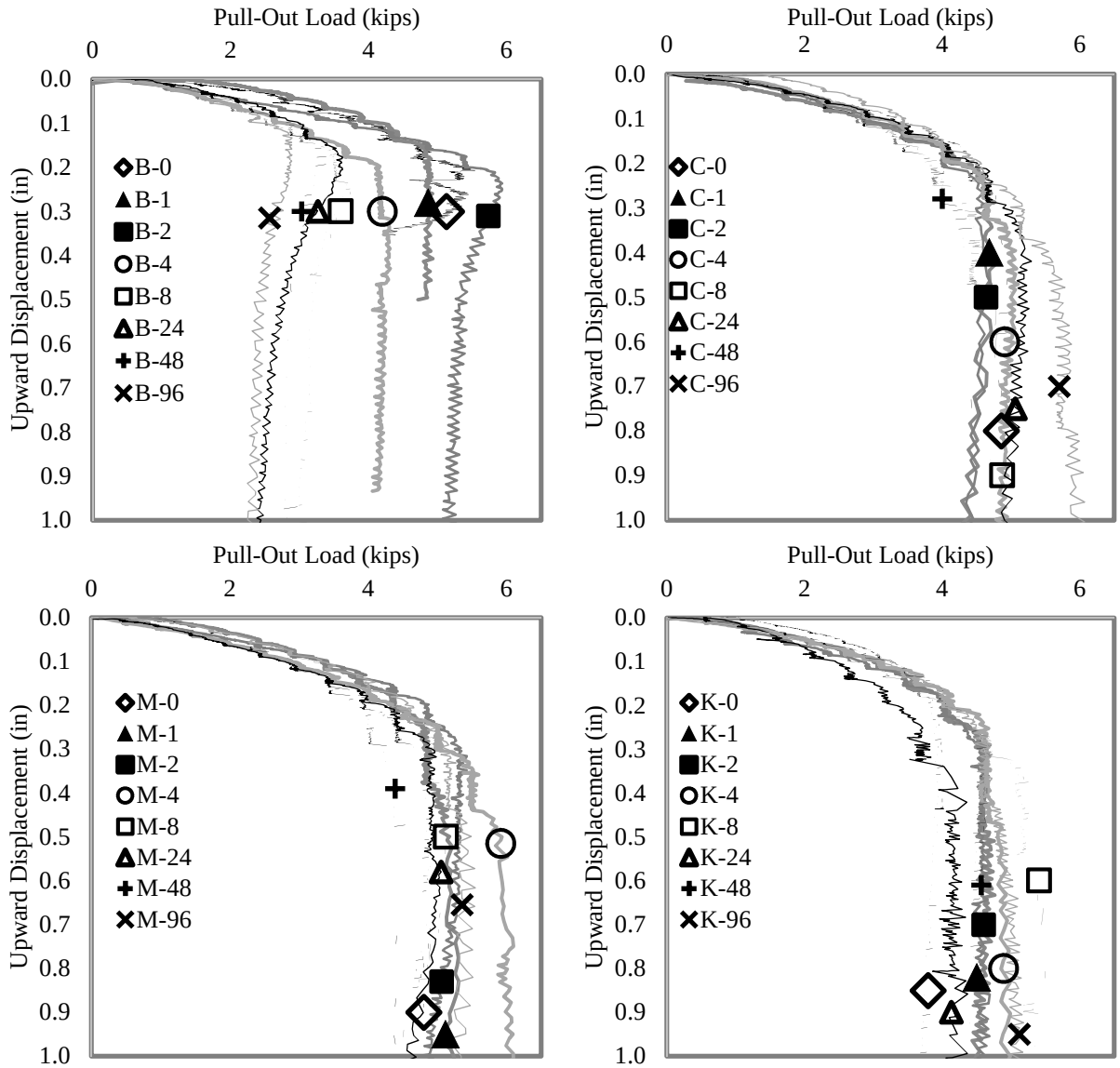

Figure 3.17. Field pull-out load vs displacement for the 32 small-scale shafts.

The results shown for side shear in phase 2 shafts apply a somewhat smaller shaft diameter for bentonite shafts which modestly increases the resulting side shear resistance. This should not be taken as real; the true shaft dimension including the filter cake should be used, which takes into account the actual failure surface. This means that the computed side shear on the 48h and 96h bentonite shafts should have been slightly smaller. Majano (1992) noted the same effect and warned that load is sometimes a better indicator of side-by-side performance. Measurements of

the filter cake and the polymer soil cake were taken on phase 1 shafts, and presented in Allen (2016) and Caliari de Lima et al. (2016).

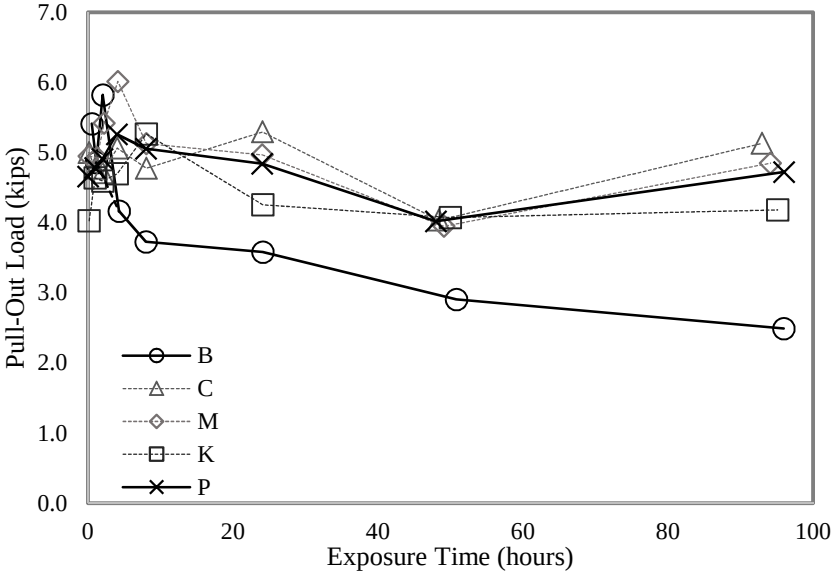

Figure 3.18. Maximum pull-out load vs exposure time.

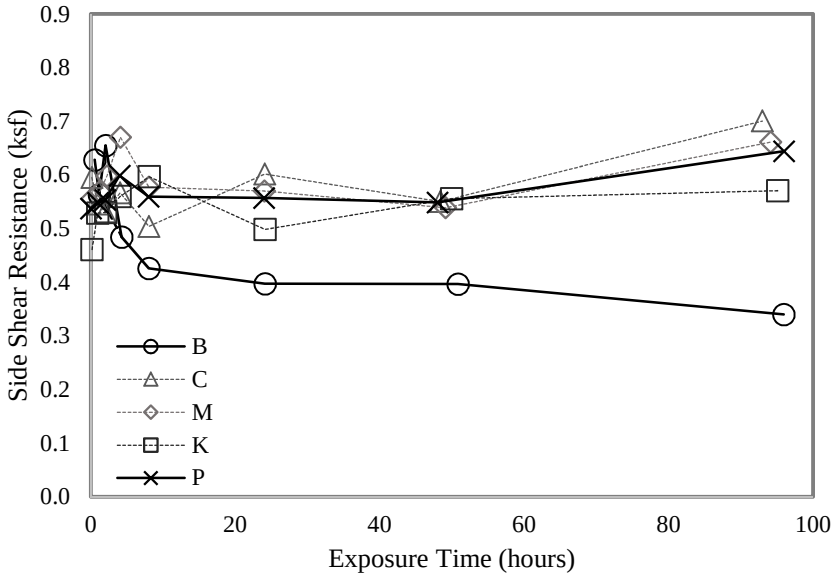

Figure 3.19. Side shear resistance vs exposure time.

Different types of drilling slurry (bentonite and polymer), as well as the time of exposure, seemed to also affect the stiffness of the shafts. Figure 3.20 shows the variation of stiffness vs exposure times, and Figure 3.21 shows the normalized stiffness variation in relation to shaft B24. The stiffness values shown in Figures 3.20 and 3.21 relate to changes in load corresponding to

upward displacements from 0.04in to 0.1in (1% and 2.5% of the shaft diameter, respectively). The stiffness observed on the polymer shafts was relatively constant with time, whereas in the bentonite shafts, a continuous decreasing trend was noted.

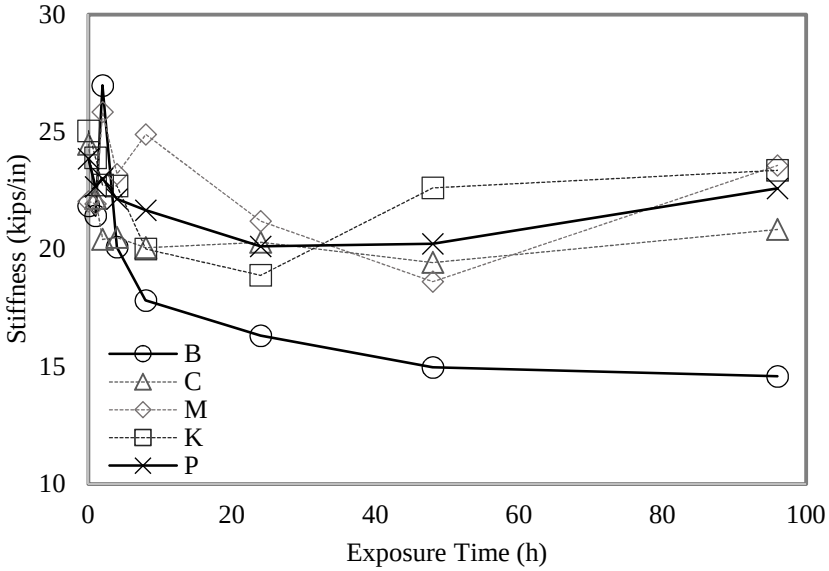

Figure 3.20. Variation of shafts stiffness over time.

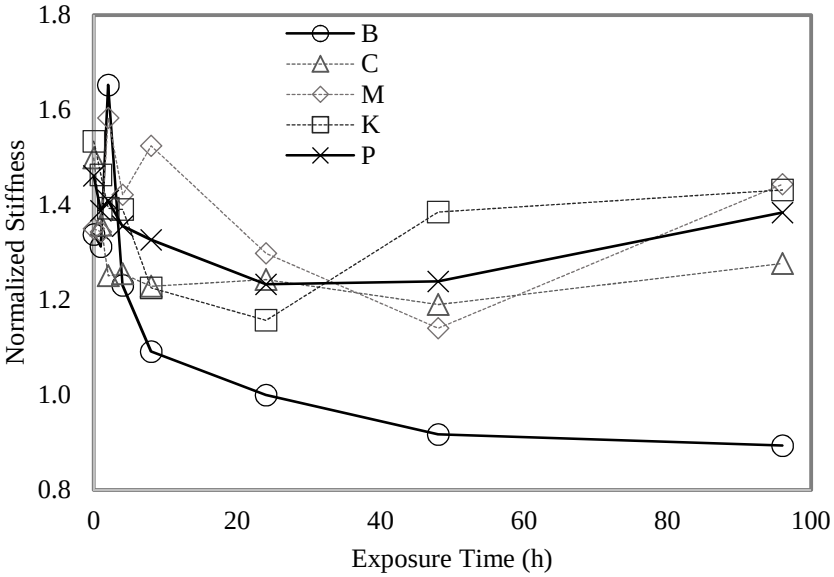

Figure 3.21. Variation of normalized stiffness over time.

In practice, exposure times often exceed 8h, reaching 24h or days; FDOT currently allows 36h exposures for a majority of the shaft length. Figure 3.22 shows the variation of the normalized unit side shear using the data shown in Figure 3.19, admitting shaft B24 as reference for the

computations. Note that, from Figure 3.19, after 4h of exposure (including 4h) independently of the bentonite shaft selected as reference, all polymer shafts have a normalized side shear higher than 1.0. After 2h of exposure, the polymer shafts displayed at least 35% larger side shear than the 24h bentonite shaft. After 96h, this difference increased to 76%.

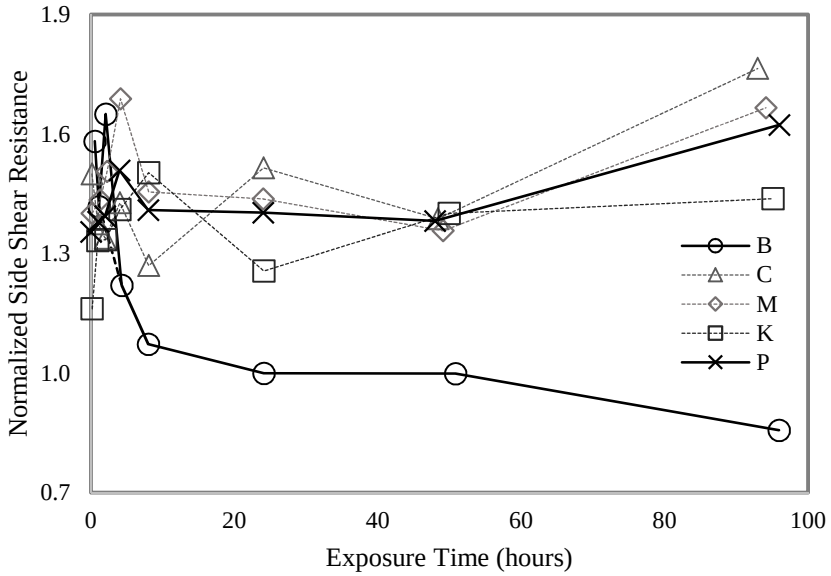

Figure 3.22. Normalized side shear over time.

3.4 Flow Rate Study

The flow rate study was executed in phases 2 and 3 small-scale shafts. During phase 2 tests, which had significantly higher exposure times than phases 1 and 3, larger amounts of polymer slurry were prepared several days before the beginning of excavation.

3.4.1 Testing Procedures

In the phases 1 and 2, as soon as the excavation reached 1ft depth, the surface casing was installed (recall). Immediately after the casing installation, the slurry was introduced. After every 1 or 2 passes with the hand auger, the hole was filled up to the ground surface. Whenever the excavation reached the desired depth, the hole was topped-off with slurry up to the ground surface again and this was considered the start time for the fluid loss study.

During the tests, the slurry level inside the excavations was allowed to oscillate between the ground surface to 3.0ft below the ground level (2.0ft below the bottom of the surface casing) (Figure 3.23).

Figure 3.23. Monitoring of fluid level on phase 2 shafts.

Whenever the slurry level reached the triggering depth, 5gal buckets were used to refill the holes. A 400mm ruler was inserted into the buckets containing the slurry before and after each refill to quantify the volume that was being introduced into the holes every time it needed to be refilled (Figure 3.24). Measurements of the buckets volume were taken to calibrate the ruler. When full with 5gal, the height of slurry inside the buckets marked 340mm, and every millimeter corresponded to 0.00147gal (1gal = 68mm). Different buckets were used for each slurry type.

Figure 3.24. Volumetric measurement of the slurry being introduced in the shafts (phase 2).

The fluid loss tests in the 8 shafts pertaining for phase 2 were 96h long total. The holes were continuously monitored and refilled, day and night (Figure 3.25), which required the cooperation of the entire team taking turns on the readings and keeping track of the data.

To prevent many of the logistical problems in phase 2, the 5gal buckets containing the slurry for refills were replaced in phase 3 by 1.25gal buckets with opaque sides that allowed seeing through it. Furthermore, the fluid level was allowed to oscillate only between the ground surface and the bottom of the casing. Since every refill should have a volume of 0.65gal, all used buckets were labeled with this volumetric mark (Figure 3.26), calibrated individually using a graded container with known volume.

Since the purpose of these last 4 shafts was not to be cast and pullout load tested, it was not necessary to continue the fluid loss tests once the flow rate had reached approximately a constant value (in less than 24h).

Figure 3.25. Illustration of the testing being performed overnight.

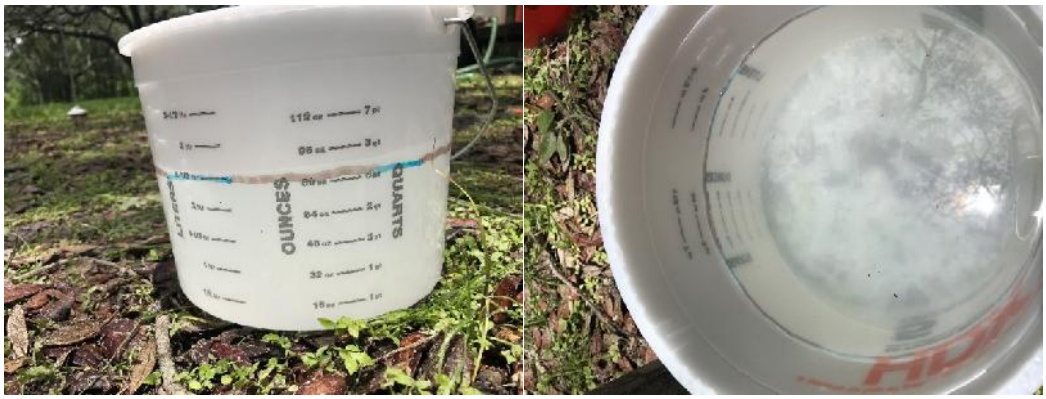

Figure 3.26. Labeled buckets used on phase 3 shafts.

3.4.2 Results

Figure 3.27 summarizes the viscosity of the four products used to stabilize the 8 first shafts over time. Note that the excavation of the 48h exposure shafts began 48h after the 96h shafts were excavated.

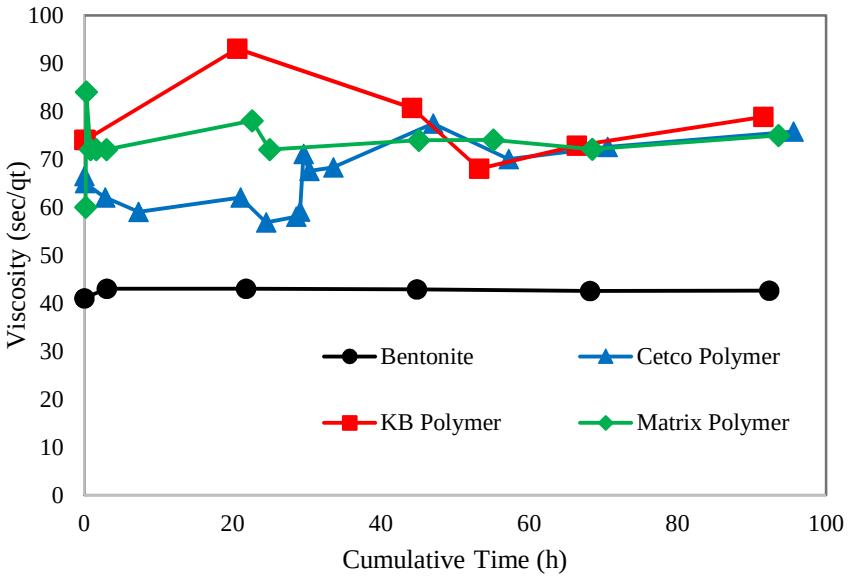

Figure 3.27. Viscosity variation over time.

In the first 48h, the KBI polymer viscosity was about 85sec/qt, while Matrix and Cetco polymer displayed about 75 and 62sec/qt, respectively. This may have influenced the flow rate in a way that Cetco was the one that showed the highest flow rate in the beginning of the 96h shafts construction. After 48h of exposure (which includes all the 48h exposure shafts), all polymer slurry viscosities were somewhat similar (about 74sec/qt average), yet small differences may be noted. All slurry tanks that were used during this study were recirculated throughout the test at least once a day, including the bentonite slurry, which had a near constant viscosity of about 43s.

Figure 3.28 shows the cumulative added slurry volume over time, for the 48h and 96h exposure shafts. The 96h exposure shaft to the Cetco polymer had a clearly larger volume of slurry added, and the 48h exposure shafts to Cetco and Matrix polymers had comparable added volumes over time. The 96h exposure shafts to Matrix polymer had smaller added volumes than all Cetco and Matrix shafts. This can be attributed to the differences in viscosity in the beginning of each shaft construction, which seems to infer that the flow rate depends on the slurry viscosity on the polyacrylamide-based polymers.

In general, a clear inverse relationship between viscosity and flow rate was noted. For example, the first 24 hours of the Cetco 96h shaft exhibited high flow rates that were drastically slowed by increasing viscosity to a value closer to the other products. Initially the viscosity was 58s, and more ShorePac was added to the mix. The resulting viscosity increased to 71s, and the flow rate reduced from 0.44ft3/h to 0.12ft3/h after 1.3h (72.7% reduction).The KBI slurry shafts had the highest viscosities and the slowest flow rates. Bentonite slurry showed virtually no flow with time as expected.

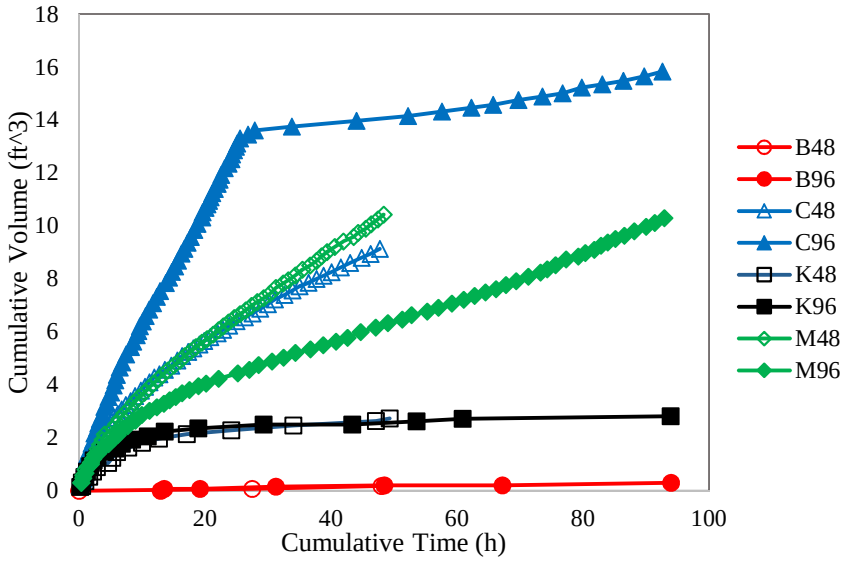

Figure 3.28. Cumulative volume of slurry introduced on the shafts over time.

Figure 3.29 shows the flow rate versus time for the 48h and 96h of exposure shafts. Overall, the Cetco and Matrix polymer exhibited higher flow rate values again related to the viscosity achieved at the time of mixing. Depending on the viscosity, a larger plume of slurry around the shaft was required to begin the slow of slurry inflow. The KBI polymer at 85s showed a strong reduction in flow rate after 2cuft of slurry had migrated into the surrounding soil. Shaft M96 with a 75s viscosity required 50% more volume (3cuft) before starting to slow. C48 and M48 with viscosities near 62s took an additional 1cuft (4cuft) before slowing could be seen. The lower viscosity C96 shaft (57s initial value) showed almost no change in flow rate up to 14cuft of slurry

and which only reduced by increasing the viscosity. Regardless, all products showed a tendency of reduction in flow rate after prolonged exposure and where viscosity (not polymer brand) was the key contributor to decreasing flow rate.

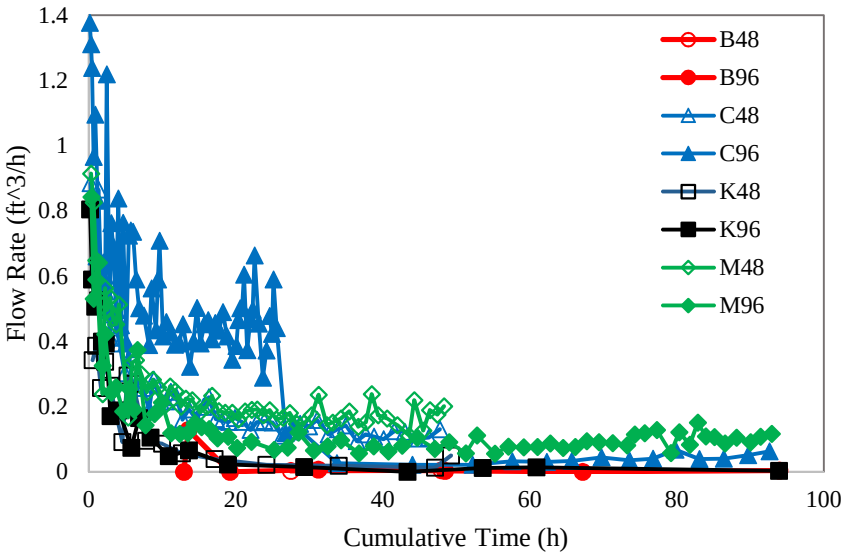

Figure 3.29. Flow rate vs exposure time, phase 2 shafts.

Figure 3.30 shows the cumulative volume that was added over time for phase 3 shafts (viscosities of 30s, 40s, 50s and 60s). After 1h of testing, the 30s shaft showed a strong discontinuity in the flow rate. In the field, it meant that one member of the team had to be exclusively dedicated to refill this shaft. Overall, this shaft required between 0.65gal/min and 1.95gal/min. Nonetheless, it is clear that the polymer slurry viscosity plays an important role on the fluid loss. It also seems evident that polymer slurry with lower viscosity values should be avoided due to limitations in the construction practice, meaning that very large volumes would be required, including enormous mixing and storage tanks.

Figure 3.31 shows the flow rate variation over time due to different viscosity values. Again, it is clear that the viscosity influenced the fluid loss. It is recommended that such low polymer slurry viscosity values, such as 30s, should be avoided in practice. The flow rate of the 40s Cetco

polymer slurry was 2.3 times larger the value observed on the 50s slurry after 4h of exposure, and 4.4 times larger than the 60s slurry after 4h of exposure.

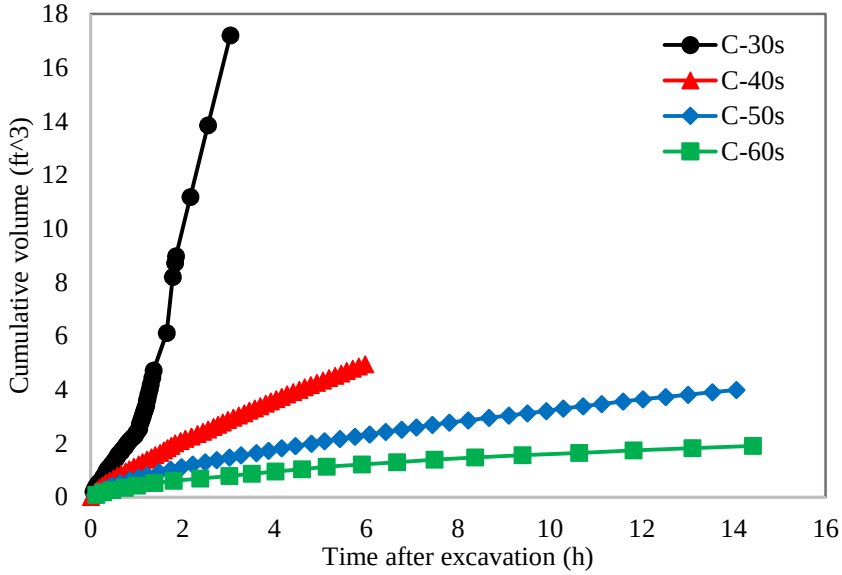

Figure 3.30. Cumulative slurry volume over time for different viscosities.

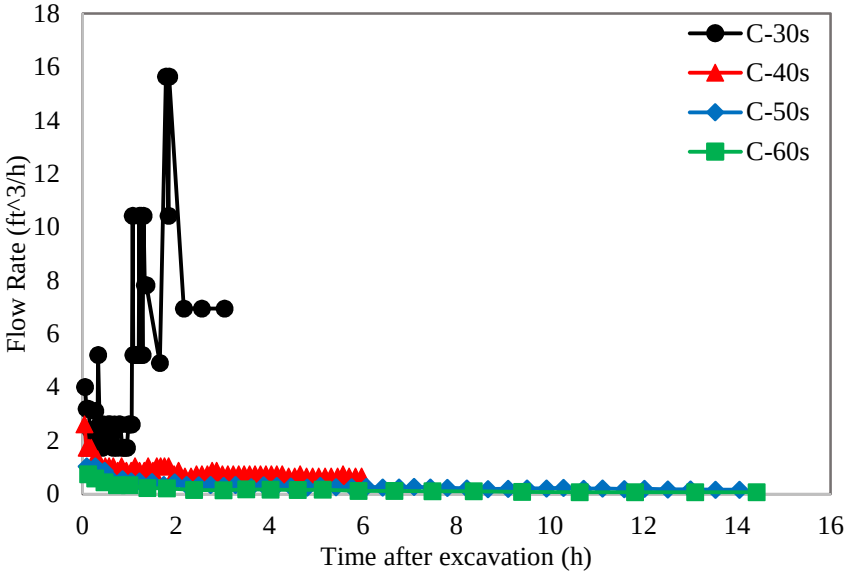

Figure 3.31. Flow rate over time for different viscosities.

CHAPTER 4: CONSTRUCTION PROCEDURE AND TESTING RESULTS: ROCK SOCKETED SHAFTS

4.1 Research Program Overview

A total of 29 small scale rock sockets (nominally 4.6in to 4.8in diameter and 18in long) were constructed. The sockets were excavated into different simulated limestone materials, using different casing installation and extraction procedures. Among these sockets, 11 were selected to be inspection holes (control specimens), in which the casings were extracted before concrete placement and the open excavation was cleaned out with water and then inspected prior to concreting. The intent of the control specimens was to set a baseline for comparisons between temporarily cased and uncased construction conditions.

All sockets were pull-out tested with tension loads applied on sleeved anchor bars, which extended to a bearing plate on the bottom of the excavation, subjecting the socket concrete to compression (similar to what was performed with the small-scale slurry shafts). After extraction, the dimensions of the sockets were determined on the observable failure surface.

4.2 Simulated Limestone Material

The search for representative simulated limestone materials was a challenge itself involving over 200 unconfined compression test specimens prepared from 29 different mixes. All mixes were cast using varying ratios of sand, coquina shells, calcium hydroxide, cement and water. The simulated limestone mixes targeted strengths between 100psi and 600psi. Similarly, texture and porosity needed to replicate the porous structure typical of natural Florida limestone.

Figure 4.1 shows side-by-side images of field (left) and the simulated limestone samples (right). Details addressing the simulated limestone development and the unconfined compressive strength test results are presented in Hagerman (2017).

Figure 4.1. Field retrieved limestone cores (left); core from simulated limestone bed and simulated limestone cylinder specimen (right).

Upon identifying a suitable simulated limestone, larger scale samples were prepared in large diameter beds. The simulated limestone beds were 42in in diameter and 23in tall, cast inside circular steel formworks, which remained in place until the subsequent pullout tests and extractions were completed. A steel reinforcing cage consisting of 6 vertical #3 bars, 23in long and 4 - #3 stirrups 38in in diameter was installed to provide confinement during load testing and to prevent bed cracking from an adjacent test.

A 1 cubic yard mobile mixer was used for mixing the materials and dispensing into the steel formworks (Figure 4.2). When the fresh limestone reached a height of 6in inside the formwork, 6in diameter plastic disks were placed at the corresponding plan view socket positions to debond the bottom of the cored rock socket excavations without causing needless damage to the parent limestone beds (Figure 4.3). After the bed casting was completed centering rods were installed in the fresh limestone at the same position as the plastic disks to serve as drilling guides and to prevent the core barrel from walking across the surface of the simulated limestone.

Cylinders of the limestone bed material were also prepared at the time of casting for unconfined compression tests and visual inspection (Figure 4.4).

Figure 4.2. Casting of simulated limestone bed.

Figure 4.3. Debonding plastic disks (left) and centering rods (right).

Figure 4.4. Preparation of cylinders from limestone bed material.

4.3 Sockets Construction

Each bed provided adequate room to cast five rock socket specimens without interfering with the adjacent specimen. Figure 4.5 illustrates the sockets layout used on the 6 simulated limestone beds. One of the beds (B3) had 4 rock sockets instead of the desired 5 because one of the holes was lost during the bed preparation. For all casing installation / construction methods, an aluminum tripod with an overhead hoist was used to support the casing installation equipment. Table 4.1 lists the different construction procedures used on the 29 rock sockets. The bed ID numbers refer to the chronological order of construction which did not correspond to any trend in UCS values.

Three different procedures for casing installation and extraction were used: driven (DR), rotated with fine cutting teeth (FT), and rotated with coarse cutting teeth (CT). Figure 4.6 shows the casing components including extensions, coring bits, coring head, and pipe wrenches used for assembling and disassembling the casings. The control casing types for each bed were varied to provide different comparison combinations (DR-C, FT-C and CT-C, Table 4.1). Figure 4.7 shows details of the coring bits used on this research program.

A driven control was constructed on all beds along with a rotated option (except bed 3). The control specimens provided baseline capacity measurements for comparison with the temporary casing methods commonly used and similar to field practice. The construction methods are further described in this Chapter.

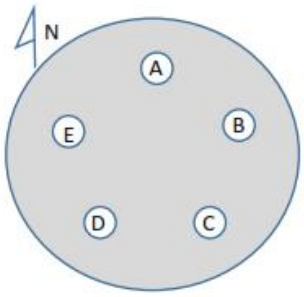

Figure 4.5. Rock socket construction layout on each simulated limestone bed.

Table 4.1. Types of construction used on the rock socket specimens.

Bed UCS (psi)	Bed ID Number	Construction Method				
		A	B	C	D	E
64.8	4	CT	FT	FT-C	DR	DR-C
163.4	5	CT	FT	DR	DR-C	CT-C
487.4	3	CT	FT	DR-C	DR	None
502.8	1	CT	FT	FT-C	DR	DR-C
685.6	6	CT	FT	FT-C	DR	DR-C
885.0	2	CT	FT	DR	DR-C	CT-C

Figure 4.6. Casing cutting tips, drive shoe, casing extensions and drill rod couplers.

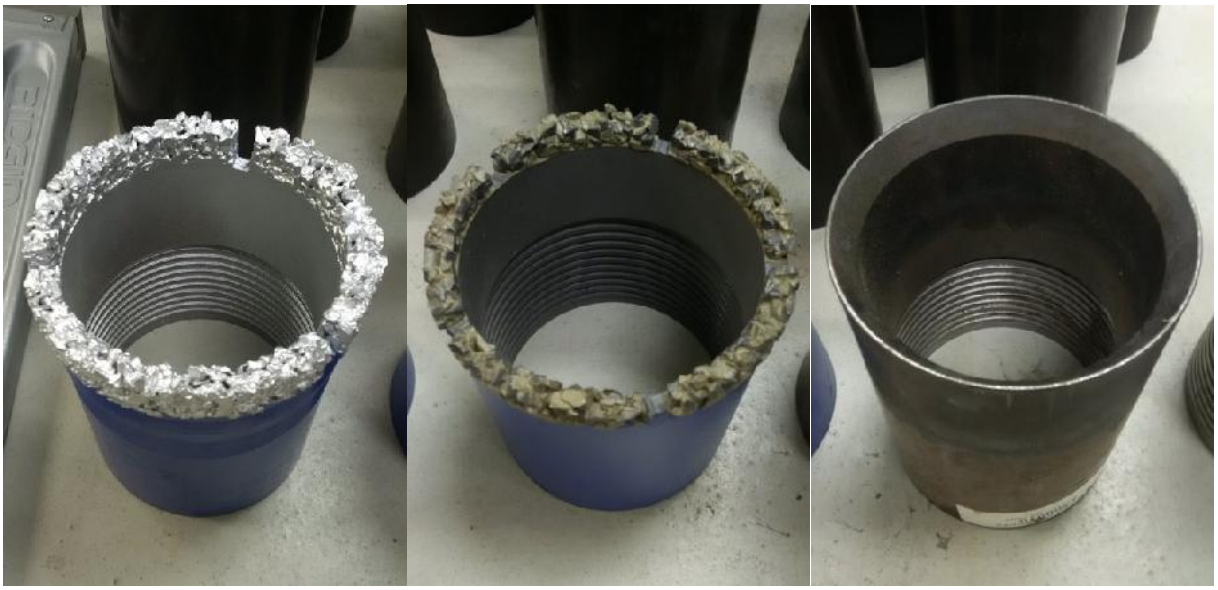

Figure 4.7. Fine-tooth (left), coarse-tooth (center) and driving shoe (right).

4.3.1 Rock Socket Excavation

The rock socket specimens were constructed between 7 and 21 days after the beds were cast. Before starting the excavation, the gap between the top of the simulated limestone and the formwork edges (1in to 2in) was flooded with water (Figure 4.8). All excavation and concreting was performed via the wet method, simulating common field conditions. All inspected, control excavations were flooded again before concrete casting.

Figure 4.8. Top of simulated limestone beds flooded with water and being pre-cored.

The driven casing specimens (both temporary casing and control) were cast and removed first. The purpose was preventing disturbances caused by vibration and consequent consolidation of other sockets on the same bed. Rotated temporary specimens were cast next, and finally, the control sockets with no casing were cast.

4.3.1.1 Driven Casing Sockets

A pilot hole was cored prior to driven casing installation to prevent excessive stress development and cracking of the beds. A coring machine was positioned on the corresponding socket positions and a 16in long, 4in diameter, coring bit was attached (Figure 4.9). The resulting pilot holes were smaller than the driving shoe outer diameter (4.6in) thereby producing the desired crumbled / pulverized material outside the driven casing.

A standard SPT safety hammer, attached to a rope, overhead pulley system and cathead motor was used to drive and extract the casing. The fragments that remained inside the installed casings were flushed out with the use of an air vacuum (Figure 4.10) before concrete placement or casing extraction (temporary driven casing or driven control specimens, respectively).

A cathead motor was used to lift the hammer and provide just enough drop energy to advance the casing. Increasing drop heights were required as the embedment depth increased (Figure 4.9). For extraction, the same setup was used, but the blows were applied upward with smaller strokes to avoid damaging the just-cast specimen and the bed.

Figure 4.9. Pre-drilling (left) and driving the casing (right).

Figure 4.10. Airlift vacuum used to clean up fragments from inside the installed casings.

4.3.1.2 Coarse-Tooth and Fine-Tooth Rotated Casing Sockets

The construction procedure for the rotated fine and coarse-tooth casings was the same. The assembled coring bit with the 2ft extension attached to the coring head were lifted and positioned with support of the overhead hoist. The coring assembly was attached to a gas-powered rotary reduction gear box and continuously flushed with water to prevent the cutting from binding the casing. After the casing reached the desired depth, an internal drill bit was used to break up material that could not be extracted as a core (Figure 4.11). This procedure was eventually necessary on the driven casing specimens as well, whenever the pre-coring procedure was not able to reach the full desired depth inside the beds.

The vertical alignment was checked before and during coring. After concrete placement, the casings were extracted by slowly rotating it with 2 pipe wrenches while applying upward force small enough to keep the casings coming up without causing damages to the beds and the shafts.

Figure 4.11. Rotatory casing installation (left) and drill bit (right).

During the installation of the rotated casings, part of the crumbled material that would normally form outside the casing was flushed out from the annulus space between the outside of the casings and the intact bed material. This normally would not occur in field applications where circulation is not used during casing installation. The material flushed out of the annulus was reintroduced before concreting and subsequent casing extraction to more closely simulate field conditions (Figure 4.12).

4.3.1.3 Control Specimens

Two rock sockets on each bed were selected to be control specimens (except on bed 3, which had only 1 control). These holes were flushed out before and after casing extraction, removing all remaining smeared and crushed rock fragments, and drained for inspection. On the majority of these inspection holes, high-resolution pictures (borescope) were taken and the excavated diameter was measured (Figure 4.13). The obtained high-resolution pictures are presented on Hagerman (2017).

Figure 4.12. Cuttings replacement on the outer perimeter of the casings.

Figure 4.13. Example of high-resolution pictures taken on the control holes.

The rotated casings were extracted the same way as the temporary rotated specimens, but before concreting. The driven control casing also was extracted using the same method as on the driven temporary sockets, also before concreting.

4.3.2 Concrete Placement

The shaft concrete was actually mortar mixed in a 1 ft^3 mixer and designed to have a compressive strength of 10ksi. In order to achieve this strength and keep the fresh concrete with slump near 10in, a superplasticizer additive was introduced after mixing the cement with sand and water (w/c ratio = 0.34). Details about mix design and compressive strength are presented in Hagerman (2017).

A 3in diameter tremie pipe with a hopper attached at the top, capped at the tip, was pushed to the bottom of the sockets. The hopper was large enough such that it could hold all shaft mix volume necessary to cast the entire shaft. The fresh concrete (mortar) was poured from the mixer into 5 gallon buckets and poured in the hopper (Figure 4.14). Next, the tremie/hopper assembly was slowly raised to expel/displace water in the excavation leaving the fresh concrete in the holes. No drilling slurry was used.

Immediately after pouring the concrete and extracting the tremie, a 1in diameter (120ksi yield stress) steel all-thread rod was pushed into the fresh concrete. Each rod was sleeved with a thin-walled, 1.25in inner diameter PVC tube (Figure 4.15). The rod was attached at the bottom to a 0.5in thick, 4in diameter steel plate to ensure that the pullout load, applied to the rod, would cause only compression stress on the concrete during the pullout (actually push up) tests.

A debonding plastic sleeve, 8in long and adjustable to the socket diameter, was inserted at the top of the fresh concrete to prevent undesired side shear to develop too close to the surface, that could damage other sockets nearby (Figure 4.16). Figure 4.17 shows several beds cast and ready for load testing.

Figure 4.14. Concrete casting on the rock sockets.

Figure 4.15. PVC tube containing the all-thread rod being pushed into the fresh concrete.

Figure 4.16. Debonding plastic sleeves on top 8in of the sockets.

Figure 4.17. Sockets immediately after concreting (left), ready for load testing (center and right).

4.4 Pull-Out Load Tests

The pullout tests were performed 7 days after concreting of the shafts, on all beds. Cylinders made from the corresponding simulated limestone materials during casting of the beds were broken the same day of the pullout tests to provide the shaft and bed UCS strength. The reaction system was setup directly on the surface of the simulated limestone beds using steel blocks with dimensions of 6in x 3in x 3in, preventing stress concentration and its undesired affects. These blocks were placed just outside of the concreted shaft area to prevent unquantifiable influences on the results.

A 1in steel plate with a 1.25in diameter hole on the center was carefully placed on the steel blocks. The all thread steel bars passed through the hole and extended to a height tall enough to permit installing the load cell and the hydraulic jack. Pieces of lead shims were placed as necessary to keep the steel blocks leveled on the bed surface, preventing misalignment during the pullout tests. Figure 4.18 shows a load testing in progress.

Figure 4.18. Pull-out load test in progress.

Depending on the expected load carrying capacity of the sockets, the pullout load was applied by either a 30ton or a 60ton capacity jack. A manually operated pump provided the hydraulic pressure, and the load readings were acquired by load cells with capacities of 15ton or

50ton, installed just above the jack. A 1.5in stroke LVDT was used to track displacement and all data was recorded by a MEGADAC data acquisition system.

After all specimens in a given bed were pulled upward 1.5 in, each specimen was fully extracted and its bonded zone was measured to compute shear stress that developed on the observable failure surface. Figure 4.19 shows examples of the fully removed rock socket samples. Table 4.2 shows the shaft bonded dimensions considered in the side shear calculations, which effectively contributed to the load-carrying capacity. Complete details about the testing procedures, equipment and extracted shafts can be found at Hagerman (2017) and Caliari de Lima et al. (2017).

Figure 4.19. Extracted sockets from bed 5 (left), bed 1 (center) and bed 4 (right).

4.5 Test Results

The load versus displacement data from each pull out test was plotted by bed ID denoted by the UCS strength of the bed (Figure 4.20). The graphs are arranged by increasing UCS strength (top left to bottom right). Tables 4.3 and 4.4 list the maximum load and corresponding displacement, respectively, for each pullout test.

Table 4.2. Measured dimensions of the extracted sockets.

Bed UCS (psi) and ID Number	Socket Construction Method	Socket ID	Bonded Diameter (in)	Bonded Length (in)	Bonded Surface Area (ft^2)
64.8 (B4)	DR	D	5.06	14.06	1.55
	CT	A	6.11	16.00	2.13
	FT	B	6.31	14.88	2.05
	DR-C	E	5.85	16.00	2.04
	FT-C	C	5.92	15.63	2.02
163.4 (B5)	DR	C	4.83	9.62	1.01
	CT	A	5.19	16.34	1.85
	FT	B	5.16	8.46	0.95
	DR-C	D	5.14	9.17	1.03
	CT-C	E	5.75	9.14	1.15
487.4 (B3)	DR	D	4.73	11.70	1.21
	CT	A	4.89	12.80	1.37
	FT	B	4.93	11.00	1.18
	DR-C	C	4.81	13.75	1.44
502.8 (B1)	DR	D	4.68	14.07	1.44
	CT	A	4.92	8.02	0.86
	FT	B	4.81	8.61	0.90
	DR-C	E	4.81	9.48	1.00
	FT-C	C	5.09	7.53	0.84
685.6 (B6)	DR	D	4.70	8.13	0.83
	CT	A	5.04	9.54	1.05
	FT	B	4.86	9.26	0.98
	DR-C	E	4.61	9.14	0.92
	FT-C	C	4.89	9.18	0.98
885.0 (B2)	DR	C	4.64	9.56	0.97
	CT	A	4.93	8.25	0.89
	FT	B	4.80	8.69	0.91
	DR-C	D	4.73	9.13	0.94
	CT-C	E	4.93	8.03	0.86

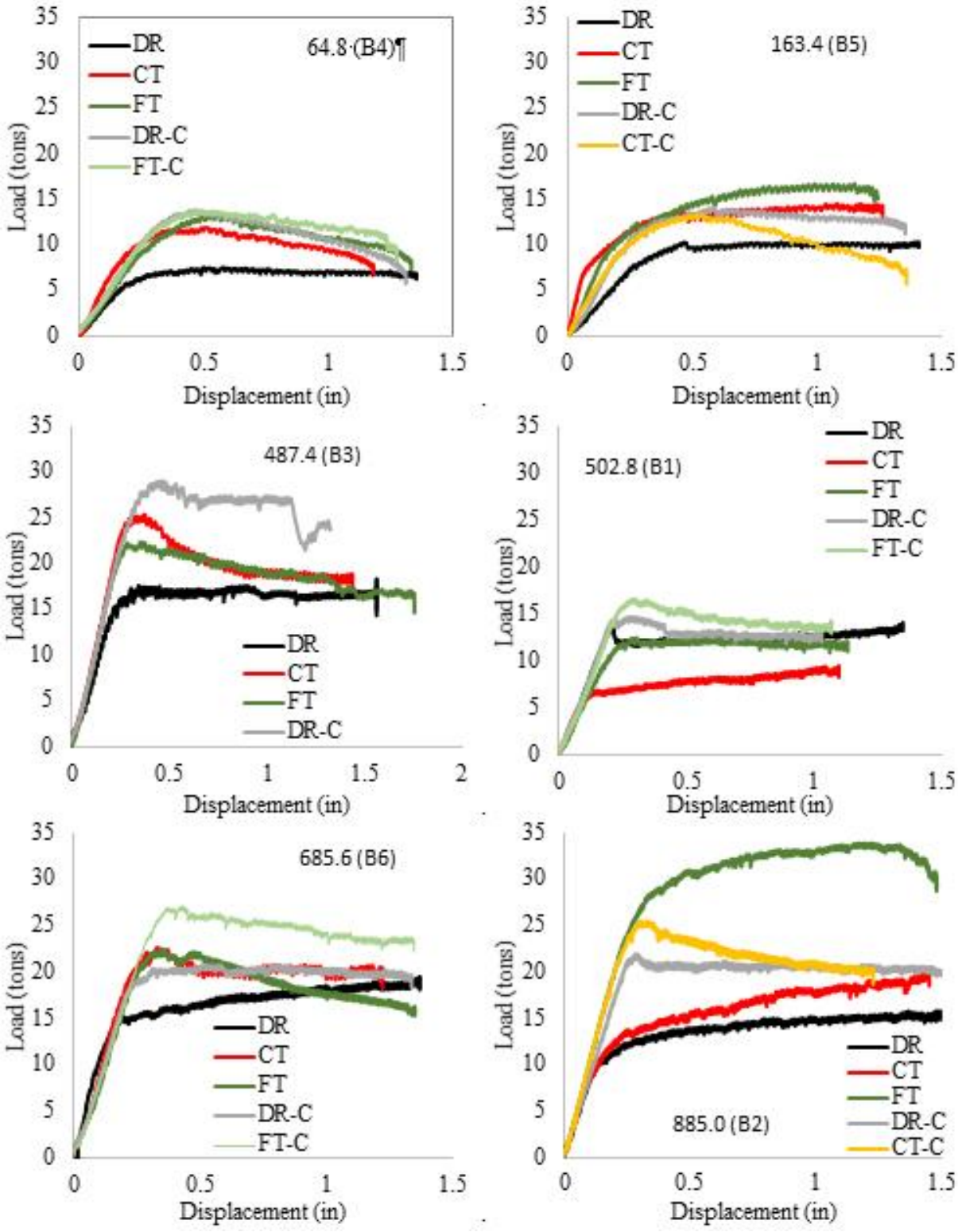

Figure 4.20. Load vs displacement for all sockets.

Table 4.3. Maximum load for all sockets.

Bed UCS (psi)	Bed ID	Peak Load (tons)					
		DR	CT	FT	DR-C	CT-C	FT-C
64.8	B4	7.49	11.70	13.15	13.62	-	13.79
163.4	B5	10.30	13.74	15.23	14.00	13.28	-
487.4	B3	16.16	25.40	21.91	28.57	-	-
502.8	B1	13.53	6.94	12.43	14.55	-	16.51
685.6	B6	15.11	22.38	22.47	20.34	-	26.81
885.0	B2	10.72	13.70	28.13	21.88	25.23	-

Table 4.4. Displacement at peak load for all sockets.

Bed UCS (psi)	Bed ID	Upward Displacement at Maximum Load (in)					
		DR	CT	FT	DR-C	CT-C	FT-C
64.8	B4	0.52	0.39	0.61	0.48	-	0.49
163.4	B5	0.48	0.47	0.58	0.59	0.54	-
487.4	B3	0.34	0.37	0.31	0.44	-	-
502.8	B1	0.21	0.15	0.31	0.30	-	0.29
685.6	B6	0.21	0.34	0.35	0.32	-	0.39
885.0	B2	0.16	0.25	0.33	0.28	0.31	-

In general, a trend of increasing pullout load was noted proportional to the bed UCS. However, given the variations in socket dimensions (Table 4.5) this can be misleading. Figure 4.21 presents the same results in terms of side shear stress and displacement determined by dividing the

pullout load by the surface area of the sockets. Table 4.5 presents the maximum side shear resistance for all sockets, computed at the displacements shown on Table 4.4.

Table 4.5. Maximum side shear strength for all sockets.

Bed UCS (psi)	Bed ID	Maximum Side Shear (tsf)					
		DR	CT	FT	DR-C	CT-C	FT-C
64.8	B4	4.82	5.49	6.43	6.67	-	6.84
163.4	B5	10.16	7.44	15.99	13.60	11.59	-
487.4	B3	13.40	18.59	18.51	19.81	-	-
502.8	B1	9.42	8.05	13.76	14.62	-	19.74
685.6	B6	18.11	21.34	22.89	22.12	-	27.40
885.0	B2	11.08	15.43	30.89	23.21	29.20	-

From Figure 4.21 and Table 4.5, it becomes clear that the side shear is proportional to the geomaterial strength, as considered in design methods. Figure 4.22 shows the same results in terms of normalized side shear (relative to the bed UCS) versus displacement.

Further observations may also be made after analyzing Figures 4.21 and 4.22. In all beds, the driven temporary sockets (DR) exhibited lower strength than the corresponding control sockets (DR-C). The DR and CT sockets showed the lowest side shear resistance among the construction methods investigated, whereas the fine-tooth rotated sockets (FT) exhibited the highest side shear values when considering the temporary casing sockets only. The control sockets consistently showed higher side shear resistance as well, comparable to the temporary casing specimens. Table 4.6 shows the summary of maximum normalized side shear. These ratios were obtaining by dividing the maximum side shear by the bed unconfined compressive strength, both in tons per square foot (tsf).

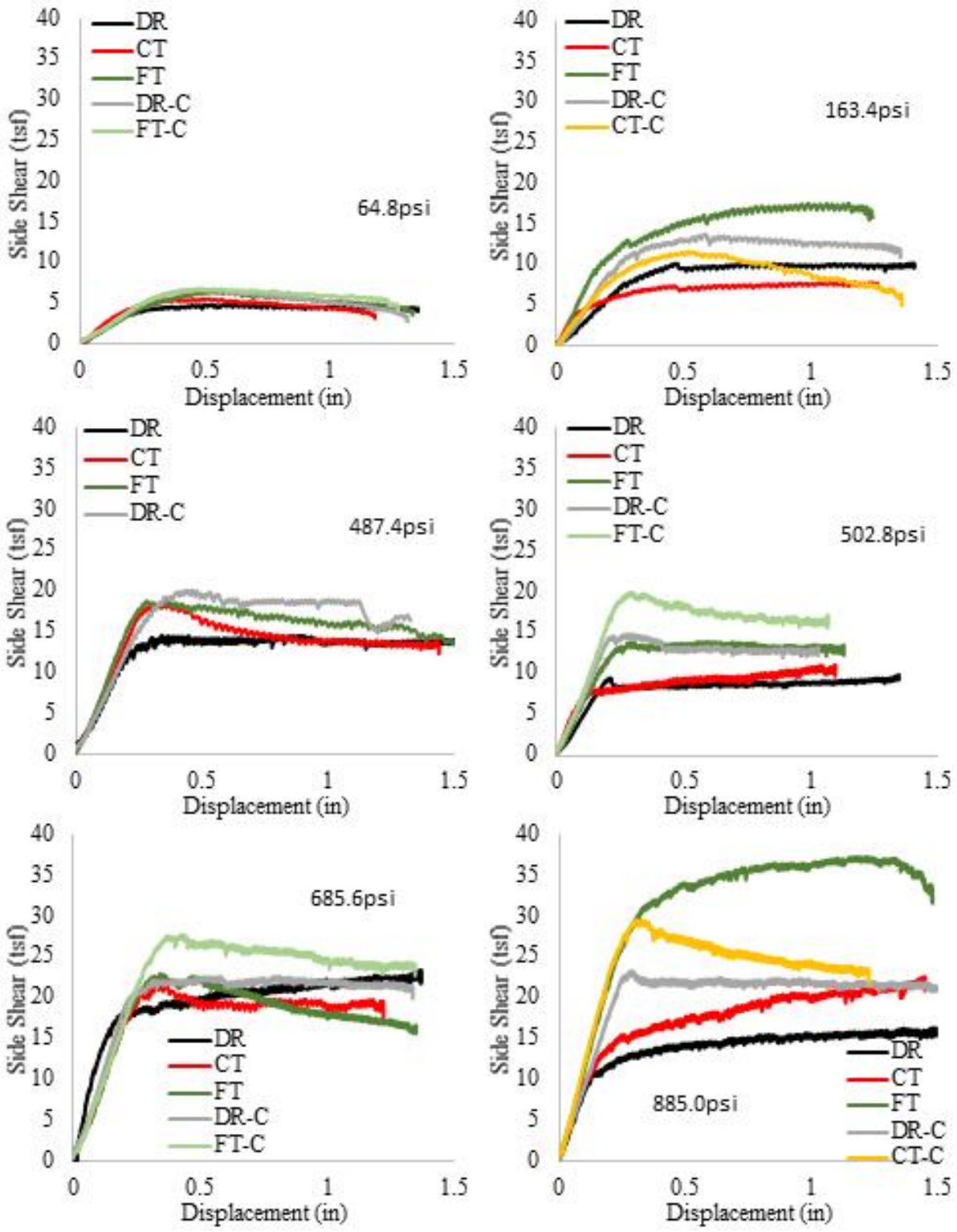

Figure 4.21. Side shear resistance vs displacement for all sockets.

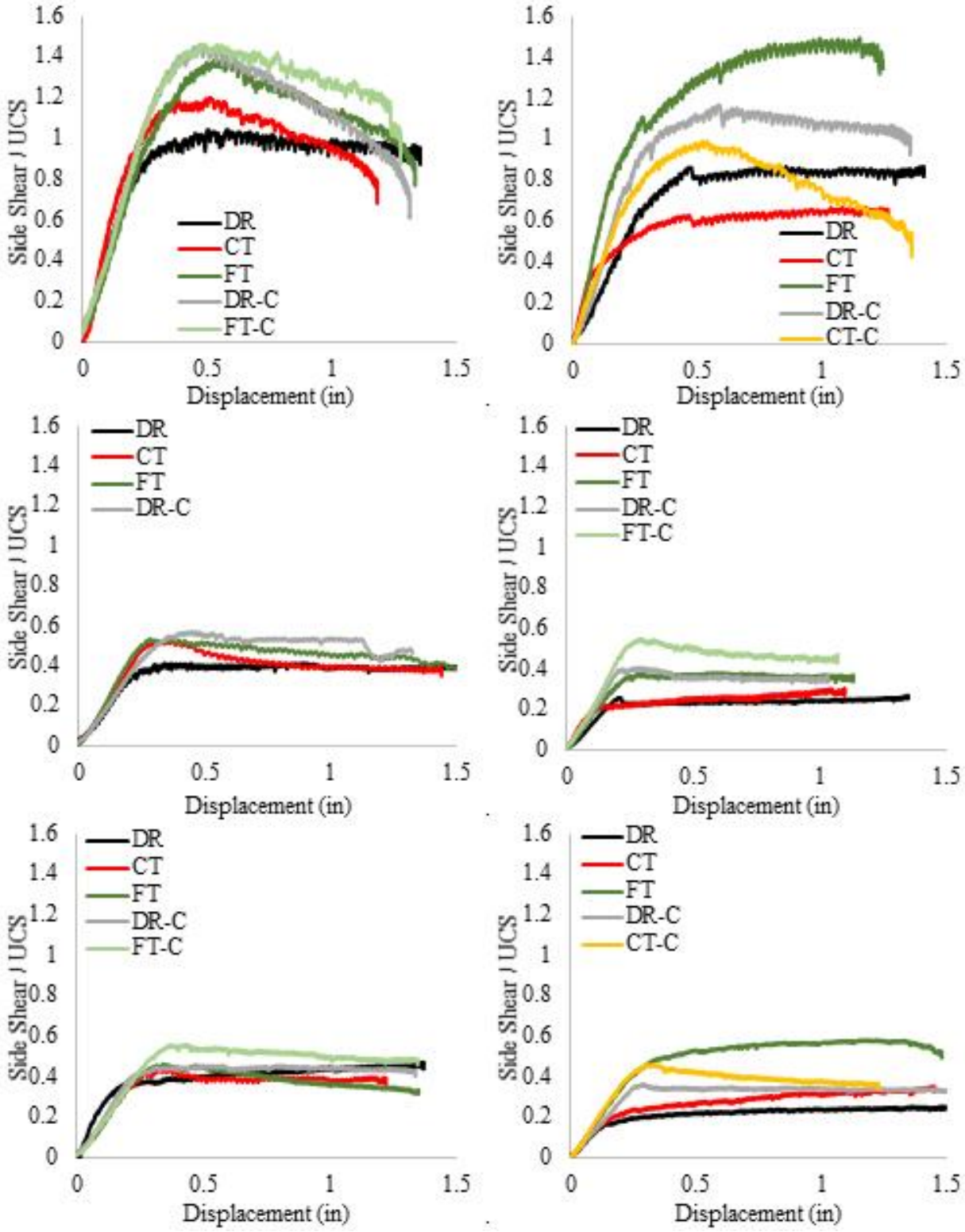

Figure 4.22. Normalized side shear resistance (by bed UCS) vs displacement.

Table 4.6. Maximum normalized side shear.

Bed UCS (psi)	Bed ID	Maximum Normalized Side Shear (Side Shear / UCS Ratio)					
		DR	CT	FT	DR-C	CT-C	FT-C
64.8	B4	1.03	1.18	1.38	1.43	-	1.47
163.4	B5	0.86	0.63	1.36	1.16	0.99	-
487.4	B3	0.38	0.53	0.53	0.56	-	-
502.8	B1	0.26	0.22	0.38	0.40	-	0.55
685.6	B6	0.37	0.43	0.46	0.45	-	0.56
885.0	B2	0.17	0.24	0.48	0.36	0.46	-

Table 4.7 shows the ultimate side shear ratios between the temporary casing and the control sockets, using the values shown on Table 4.4. Figure 4.23 shows the side shear ratios versus displacement.

Table 4.7. Side shear ratios between temporary and respective control casings.

Casing Type	Bed UCS (psi) and ID	Peak Displacement (in)	Ultimate Stress Ratio	Average Peak Stress Ratio
Driven (DR)	64.8 (B4)	0.52	0.72	0.68
	163.4 (B5)	0.48	0.75	
	487.4 (B3)	0.34	0.68	
	502.8 (B1)	0.21	0.64	
	685.6 (B6)	0.21	0.82	
	885.0 (B2)	0.16	0.48	
Coarse-Tooth Rotated (CT)	163.4 (B5)	0.47	0.64	0.59
	885.0 (B2)	0.25	0.53	
Fine-Tooth Rotated (FT)	64.8 (B4)	0.61	0.94	0.82
	502.8 (B1)	0.31	0.70	
	685.6 (B6)	0.35	0.84	

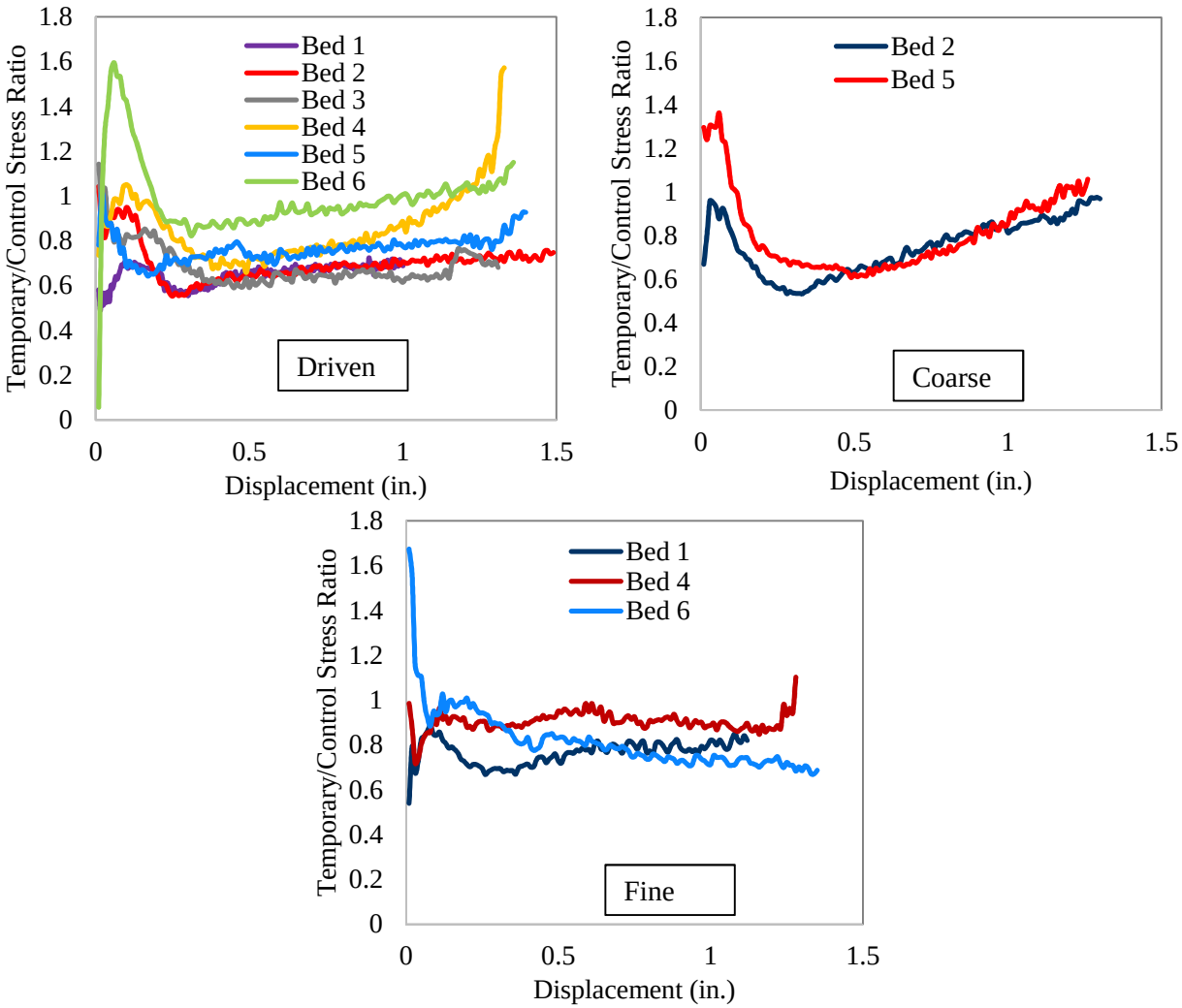

Figure 4.23. Temporary / control side shear ratio vs displacement.

CHAPTER 5: DISCUSSIONS AND CONCLUSION

5.1 Overview

Present design methods for side shear resistance of drilled shafts in soils and rock were derived and/or verified from full scale case studies, but do not make any distinctions for a wide range of construction techniques. Instead, the design parameters encompass all excavation procedures, and therefore the resulting calculated side shear is solely dependent on the soil type regardless of whether slurry, temporary casing or dry construction is used.

This research program separately investigated the effects of slurry and casing stabilization of drilled shaft excavations. For slurry excavations, the type of slurry (e.g. mineral or polymer) and open excavation / slurry exposure time was altered to identify how sandy soils might be affected (Chapter 3). Clayey soils were not addressed as very little slurry inflow occurs into clay and slurry stabilization is often not needed. Similarly, the effects of different procedures to install and extract temporary casings in simulated limestone were examined (Chapter 4).

This Chapter presents further discussions regarding the results, which evidence even more that there are significant differences in side shear due to the different excavation stabilization methods.

5.2 Slurry Constructed Shafts

Thirty two small scale drilled shafts were constructed and pull-out tested for quantifying the effects of 4 different commercial drilling slurry products used in the field (one bentonite and three polymers). The shafts were, nominally, 4in diameter and 7ft to 8ft long.

The test site was located at the Geopark, in the University of South Florida (Figure 5.1). The exposure time for each product ranged from 0h to 96h. For each tested shaft, the resistance bias factor (λ_R), defined as the ratio between measured and predicted pullout capacity (using the methods presented in Chapter 2), was determined. This factor is a fundamental part of the Load and Resistance Factor Design, LRFD, calibration (TRB 2005). The National Research Council (NRC 1995) highlights that the measured quantities used to determine these factors may refer to full-size foundation systems in the field, scaled down elements and laboratory tests.

Figure 5.1. Partial view of freshly concreted test shafts.

The resistance bias was calculated as the ratio between measured ($f_{max\ field}$) and predicted ($f_{max\ design}$) side shear:

$$\lambda_R = \frac{f_{max\ field}}{f_{max\ design}} \qquad \text{eqn. 5.1}$$

Figure 5.2 shows a comparison between measured and design side shear resistance using the method developed by O'Neill and Reese (1999), which was a combination of Reese and O'Neill (1988a) and contributions from O'Neill and Hassan (1994) (Chapter 2). Figure 5.3 shows

the bias obtained from the slurry shafts. However, as the bias is sensitive to the prediction method, the same computations were performed using the newer prediction method for shaft side shear in sand Brown et al. (2010). Figures 5.4 and 5.5 show a slight reduction in the bias as the prediction method produces slightly higher predicted strengths. In these figures (Figures 5.2 – 5.5), B denotes bentonite shafts, C = Cetco Polymer, K = KBI Polymer , M = Matrix Polymer, D = design capacities, and P = all polymer shafts. In Figures 5.2 and 5.4, the solid lines are the field measured side shear, and the dotted lines are the design side shear values. The side shear observed on all shafts exceeded its corresponding expected design capacity.

For each shaft a unique predicted capacity was determined based on the local soil strength (32 different CPT soundings) and the selected design/prediction method.

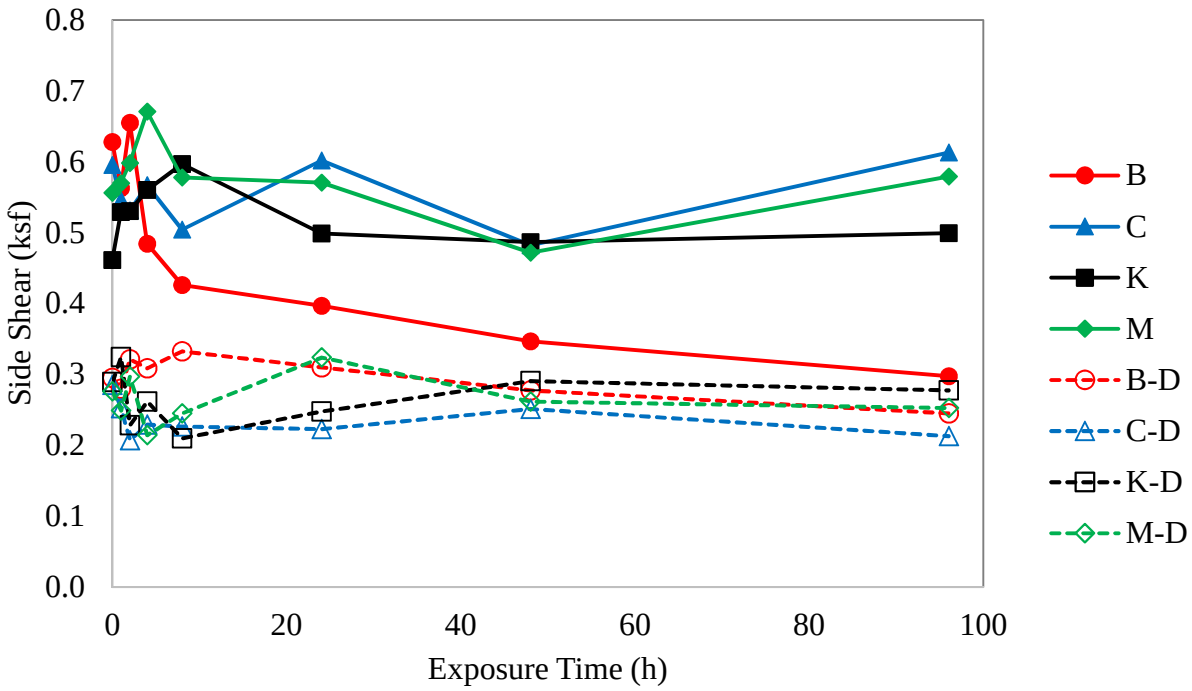

Figure 5.2. Measured vs design side shear (O'Neill and Reese 1999).

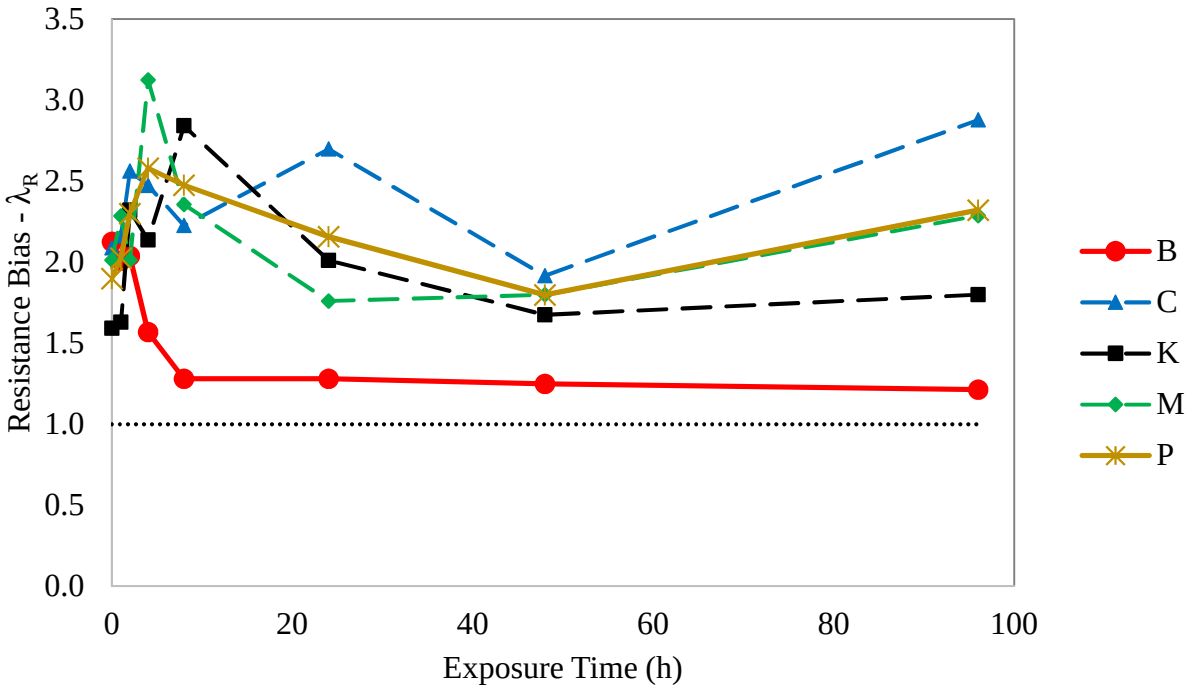

Figure 5.3. Resistance bias factor based on O'Neill and Reese (1999).

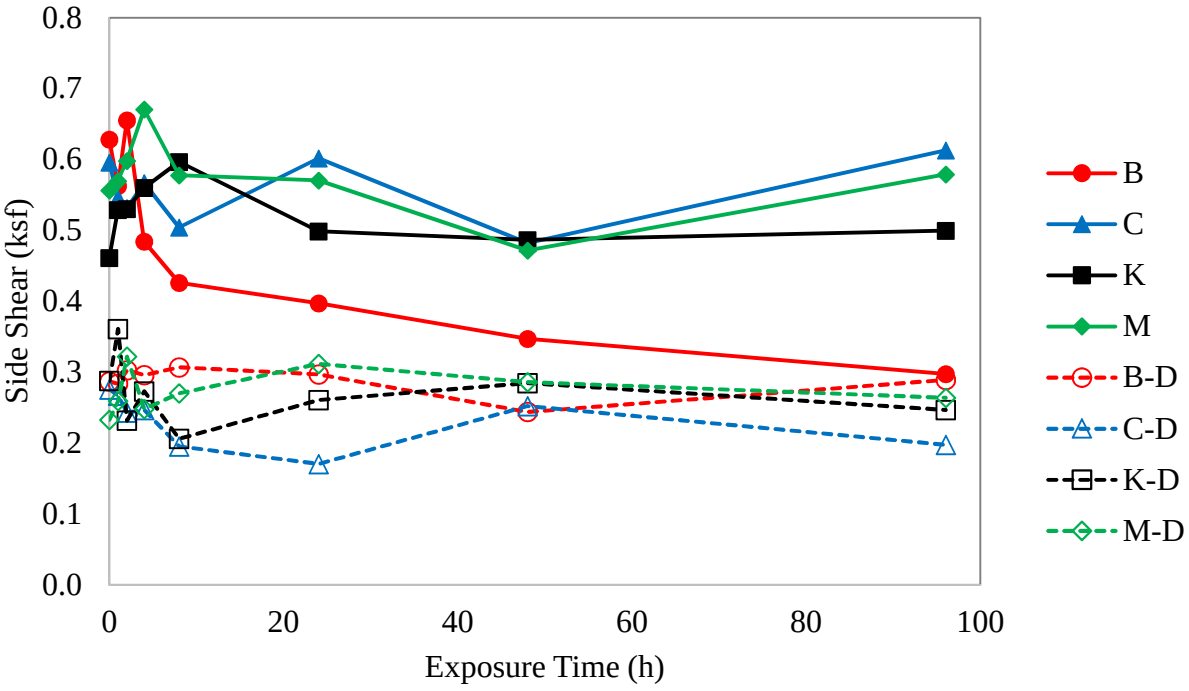

Figure 5.4. Measured vs design side shear (Brown et al. 2010).

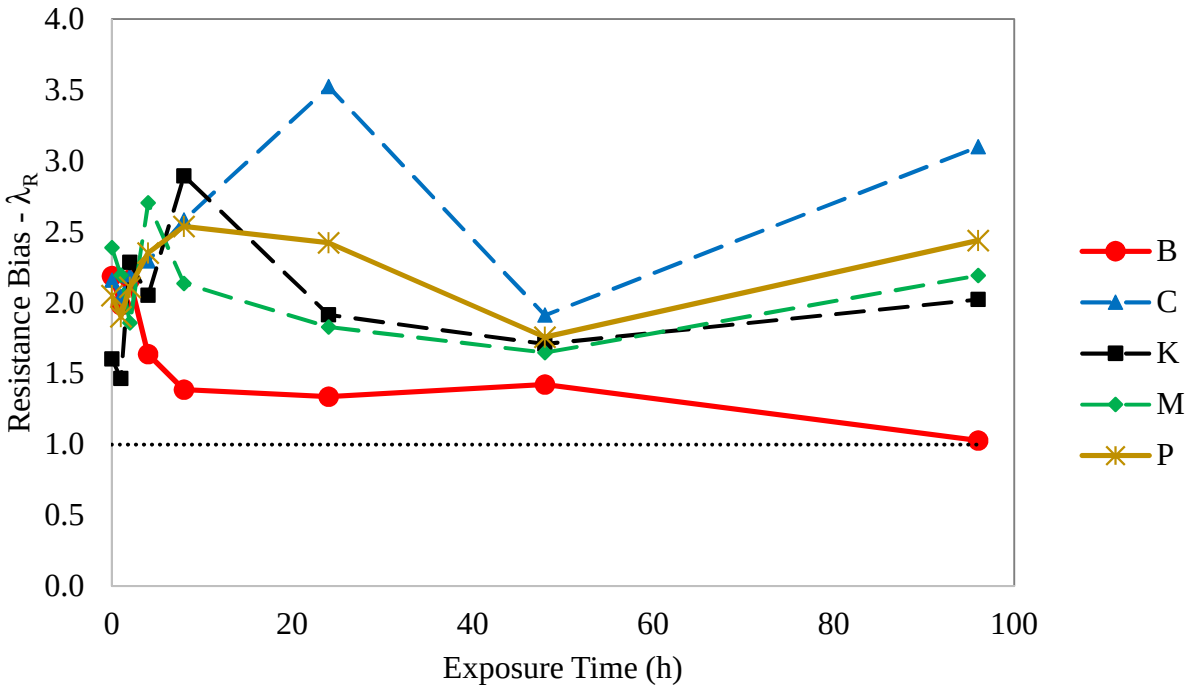

Figure 5.5. Resistance bias factor based on Brown et al. (2010).

While some reduction in pullout force was noted with time for the bentonite shafts (Figure 5.2 and 5.4), the local soil strength and predicted capacity coincidentally also decreased for one prediction method making the bias unaffected after 8h (Figure 5.3). Nevertheless, it should be noted that there was a loss in side shear for bentonite shafts before 8h of exposure (somewhere between 2h and 4h), whereas the polymer shafts did not experience notable changes in side shear over time. The variations observed on the polymer shafts over time may be attributed to the presence of roots in the excavation not detected during soil strength profiling and subtle differences on shaft geometry due to the manual excavation performed.

5.3 Temporary Casing Shafts

In this study, twenty nine small scale rock socketed drilled shafts were constructed in simulated limestone beds where the unconfined compressive strength of the beds ranged from 64.8 to 885psi. All sockets were pull-out tested for quantification of side shear resistance.

All construction and testing was performed at the outdoor Engineering Research Compound, at the University of South Florida. The range of unconfined compressive strengths of the simulated limestone beds targeted typical Florida limestone formations and the strength values that might be encountered in field where temporary casings are likely to be used. Figure 5.6 illustrates one of the beds curing in preparation for the pull-out tests.

Figure 5.6. Rock socketed specimens being prepared for pull-out tests.

Figure 5.7 shows a comparison between four design methods (discussed in Chapter 2) and the measured side shear resistance for the 29 specimens. The design methods include: (1) that recommended by FDOT (2017a), based on McVay et al. (1992), with recovery equal to 48.5% (admitted as representative based on an example shown on FDOT 2017a), (2 and 3) from Brown et al. (2010), with C coefficient of 0.63 (lower) and 1.00 (upper), and (4) from Horvath and Kenney

(1979), in which C = 0.65. Recovery refers to that proportion (length) of a small diameter cored limestone samples that was recovered relative to the total cored length.

The side shear values were divided by the unconfined compressive strength of each simulated limestone bed. A UCS strength threshold was also defined based on discussions with contractors that noted that limestone with SPT blow counts of 60 or higher form sufficient resistance to embedment and where casings are not likely to inadvertently penetrate too deeply. This threshold was translated to an UCS value of approximately 330psi. Figure 5.8 shows the resistance bias corresponding to the four methods used.

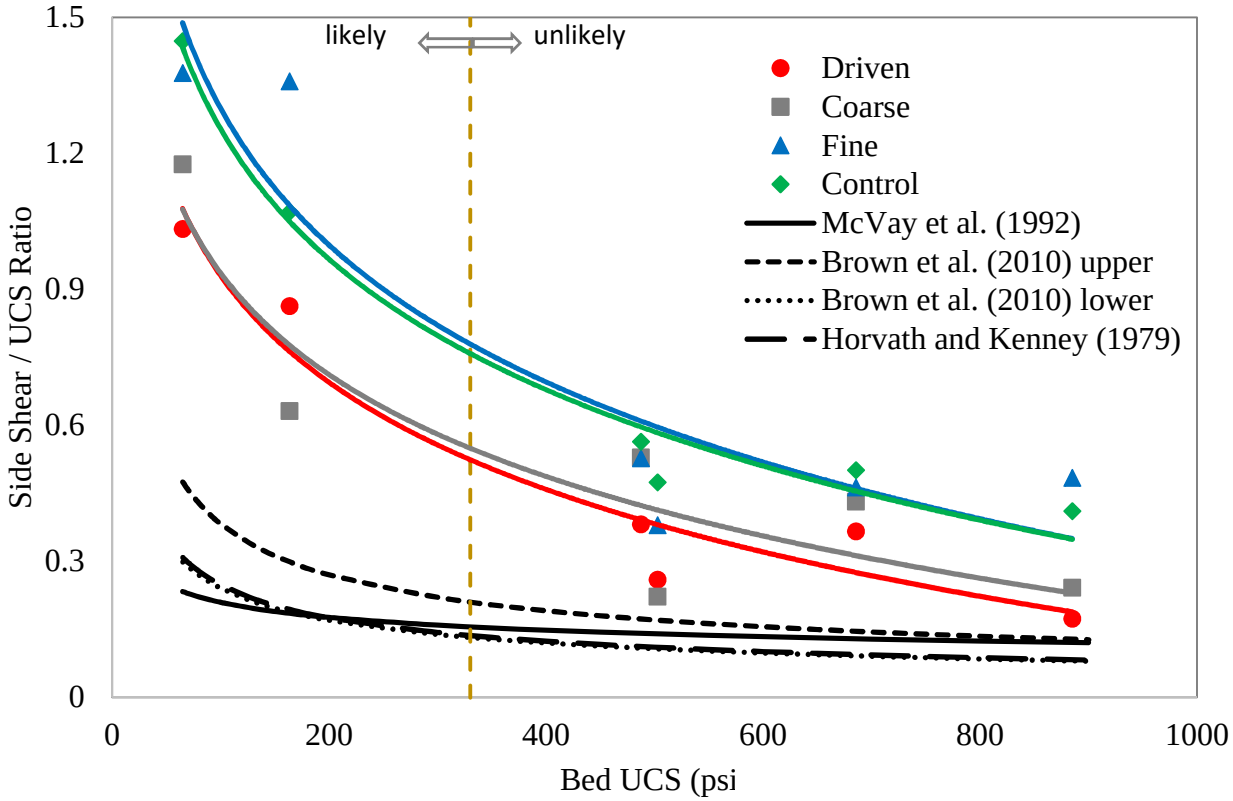

Figure 5.7. Design and measured side shear / UCS ratio vs simulated limestone beds UCS.

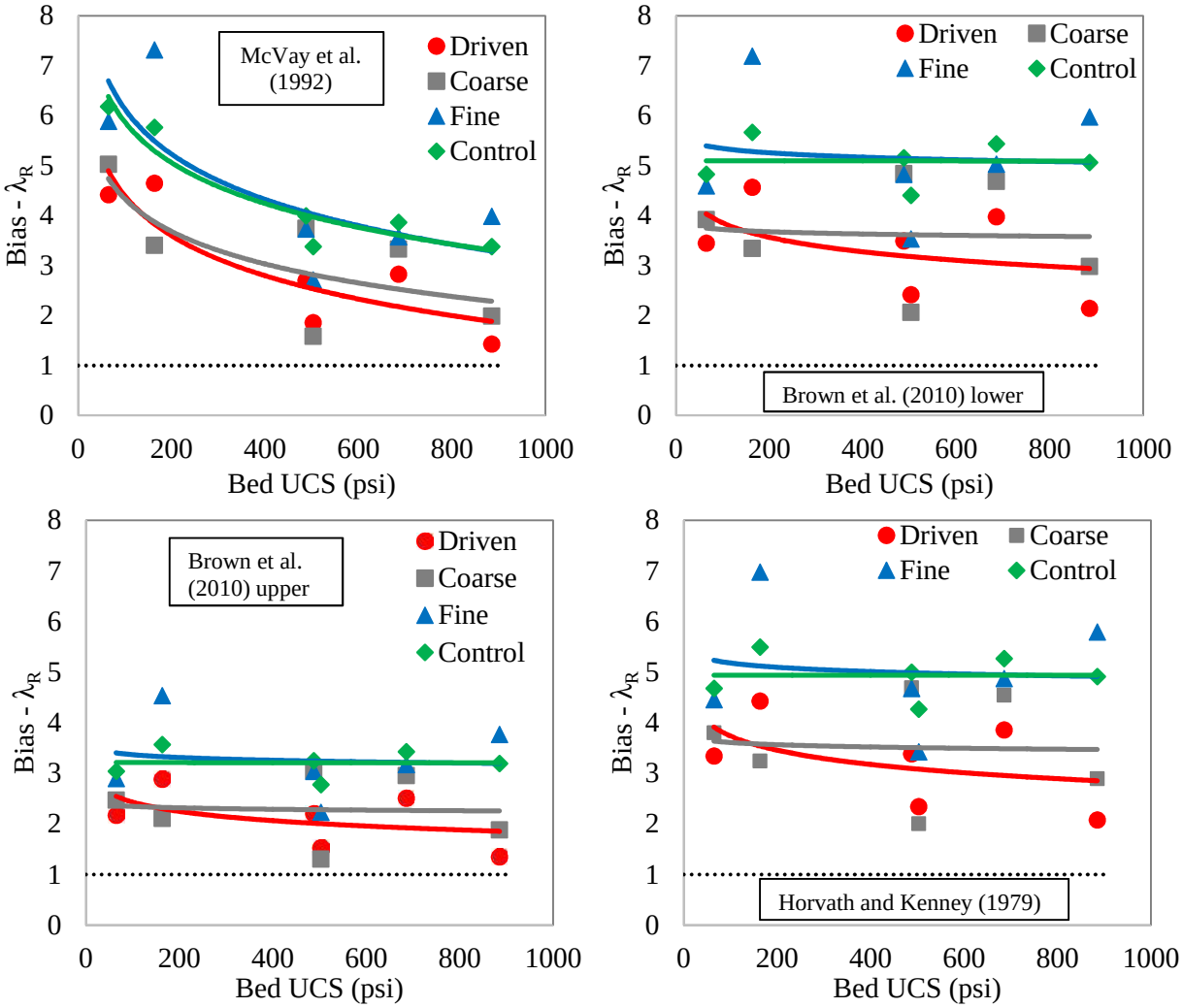

Figure 5.8. Resistance bias factor based on four methods – temporary casing sockets.

The resistance bias in the temporary casing (like slurry construction) also showed construction procedure dependency. All resistance bias were larger than 1.0 (as well as on the slurry shafts) indicating that all construction procedures exceeded the anticipated strength. One installation method, the fine-tooth rotated temporary casing sockets, exhibited side shear values that were comparable to the control sockets (i.e. no adverse effects). The driven temporary casing developed the lowest side shear values, but relatively close to the coarse-tooth rotated casing installation method. Because the fragments were not cleaned from the holes, the concrete could not bond as well to the parent simulated limestone.

5.4 Construction-Based Resistance Factors

After calculating a maximum design side shear capacity (R_n) of drilled shafts using the soil-type specific design equations (for clay, sand or rock), a resistance factor (ϕ) must be applied to that value so the resulting capacity accounts for variability and uncertainty (strength, ϕR_n, must exceed loads with an acceptable margin). In the LRFD arena, this means that the resistance factor must not exceed an acceptable probability of failure (AASHTO 2014):

$$\phi R_n \geq \sum \eta_i \gamma_i Q_i \qquad \text{eqn. 5.2}$$

In Equation 5.2, η_i is the load modifier, which accounts for ductility, redundancy and operational classification (importance); γ_i is the statistically determined load factors, applicable to different types of load (Q_i) such as temporary loads or permanent self-weight. For typical designs and conventional redundancy, and when the minimum values of the load factors are applied, AASHTO (2014) and Grubb et al. (2015) accept using $\eta_i = 1.0$. In this dissertation, this value was adopted for the calibrations.

AASHTO (2014) defines the resistance factor as a statistically-based multiplier that has to be applied to the nominal resistance (which comes from the design methods). The motivation for using this factor relies on the variability of material properties, structural dimensions, workmanship and uncertainties regarding prediction of strength. Tables 5.1 and 5.2 show recommended ϕ values for side shear resistance of drilled shafts in clay, sand, and rock (AASHTO 2014; FDOT 2017a, respectively). The resistance factors for uplift used in the calibrations performed by this study are shaded in both tables: 0.45 for the slurry shafts in sands; 0.40 (Horvath and Kenney 1979; Brown et al 2010 – lower and upper) and 0.50 (McVay et al. 1992) in rock.

Table 5.1. Resistance factors for side shear of drilled shafts (adapted from AASHTO 2014).

Geomaterial	Method	Resistance Factor, ϕ	
		Uplift	Compression
Clay	α-method (Brown et al. 2010)	0.35	0.45
Sand	β-method (Brown et al. 2010)	0.45	0.55
Rock	Kulhawy et al. (2005) Brown et al. (2010)	0.40	0.55

Table 5.2. Resistance factors for side shear of drilled shafts (adapted from FDOT 2017a).

Geomaterial	Method	Resistance Factor, ϕ			
		Uplift		Compression	
		Redundant	Non-redundant	Redundant	Non-redundant
Clay	α-method Brown et al. (2010)	0.35	0.25	0.60	0.50
Sand	β-method (Brown et al. 2010)	0.45	0.35	0.60	0.50
Rock	McVay et al. (1992) – neglecting end bearing	0.50	0.40	0.60	0.50
	McVay et al. (1992) – including 1/3 end bearing	Not applicable	Not applicable	0.55	0.45

Again, the resistance factors recommended in design manuals were statistically calculated based on case studies, which incorporate all types of construction procedures. This means that there was no attempt to individually consider the construction effects, although observations evidence otherwise.

The construction-based resistance factor may be calculated per Gunaratne (2014):

$$¤_R = \frac{ª_R[¥_D Q_D + ¥_L Q_L]\sqrt{\frac{(1+COV_{QD}^2+COV_{QL}^2)}{(1+COV_R^2)}}}{Q_m \exp\{\ _T\sqrt{\ln[(1+COV_{QD}^2+COV_{QL}^2)(1+COV_R^2)]}\}} \qquad \text{eqn. 5.3}$$

In equation 5.3, Q_D is the dead load, Q_L is the live load, R is the resistance, γ is the load factor applied to each type of load, λ is the bias and β_T is the target reliability, described below. When using equation 5.3 to compute the construction-based resistance factor, the only variables that change are the resistance bias (λ_R) and the resistance covariance (COV_R).

In this dissertation, the ratio between Q_D and Q_L, the load bias and its covariance, and the load factors used are shown on Table 5.3. The load parameters are the same as recently used by McVay and Wasman (2015), based on the work of Paikowsky et al. (2004), and are in accordance to those recommended in AASHTO (2014) for load cases, I, II, and IV, and in Grubb et al. (2015). In short, variability of loads is not considered in the determination of resistance factors.

The target reliability represents the desired (or required) probability of failure of a specific project. Typical recommended values of β_T used in drilled shaft design range between 2.33 and 3.00, which correspond to probability of failure of 1.0% (1/100) and 0.1% (1/1000), respectively (Paikowsky et al. 2004). In this study (and for FDOT calibrations), the target reliability was taken as 2.33.

Table 5.3. Load parameters used on this dissertation.

Load Parameter	Value
λ_D	1.05
λ_L	1.15
COV_{QD}	0.10
COV_{QL}	0.20
Q_D/Q_L	2.0
γ_D	1.25
γ_L	1.75

Figure 5.9 shows the construction-based resistance factors versus reliability index (with no adjustment) using the data from the pullout tests on the slurry-stabilized specimens, for two design methods for side shear resistance of drilled shafts: O'Neill and Reese (1999) and Brown et al.

(2010). Figure 5.10 presents the same type of plot for the temporary casing specimens (Horvath and Kenney 1979; Brown et al. 2010 – lower and upper; McVay et al. 1992).

In both Figures 5.9 and 5.10, all the specimens corresponding to its respective stabilization/construction method were used (32 for slurry and 29 for temporary casing). Tables 5.4 and 5.5 show the resistance factors obtained directly from the pull-out load test data considering a target reliability index of 2.33 for the slurry and temporary casing studies, respectively, using equation 5.3 and Table 5.3. In Table 5.4, A = all 32 slurry shafts, B = bentonite, C = Cetco polymer, K = KBI polymer, M = Matrix polymer, and P = all polymer shafts. In Table 5.5, A = all 29 sockets, DR = driven temporary casing, CT and FT = fine and coarse tooth rotated temporary casing (respectively), T = all temporary casing sockets (control excluded) and Ctrl = control sockets.

Table 5.4. Field resistance factor for target reliability index of 2.33 – slurry study.

Construction Method	Design	A	B	C	K	M	P
Field ϕ (O'Neill and Reese 1999)	0.45	1.26	0.96	1.72	1.29	1.46	1.47
Field ϕ (Brown et al. 2010)	0.45	1.23	0.97	1.55	1.25	1.49	1.39

Table 5.5. Field resistance factor for target reliability index of 2.33 – temporary casing study.

Construction Method	Design	A	DR	CT	FT	T	Ctrl
Field ϕ (Horvath and Kenney 1979)	0.40	2.48	1.85	1.96	3.07	2.04	3.59
Field ϕ (McVay et al. 1992)	0.50	1.80	1.21	1.43	2.10	1.48	2.50
Field ϕ (Brown et al. 2010 – lower)	0.40	2.56	1.91	2.02	3.17	2.10	3.71
Field ϕ (Brown et al. 2010 – upper)	0.40	1.61	1.20	1.27	1.99	2.04	2.33

The resistance factors obtained from the pull-out tests (Figures 5.9 and 5.10; Tables 5.4 and 5.5) are excessively large. The reduced scale of the test specimens in comparison with full-size drilled shafts and rock sockets (about $1/10^{th}$), and the limited amount of data (32 shafts in the slurry research and 29 sockets in the temporary casing study) may have caused the large bias and, consequently, the large resistance factors when using the field data with no adjustment.

Adjustments to the field resistance factor values were performed based on recommendations proposed by Paikowsky et al. (2004). An adjusting factor (ξ) was calculated using equation 5.4, where ϕ_d is the design resistance factor recommended in the manuals (either 0.45 for the slurry shafts or 0.50 for the casing sockets), and ϕ_p is the reference value, obtained from the data series that most closely relate to the mix of different construction procedures used on the development of the design methods (recall from Chapter 2).

$$\xi = \frac{\phi_d}{\phi_p} \qquad \text{eqn. 5.4}$$

This method of adjusting the resistance factors calibrates the differences noted from construction in this study to the statistically determined resistance factor values associated with accepted values for all shafts constructed elsewhere and used in present codes.

In the slurry research, the values of ϕ_p were obtained considering all 32 shafts (from near 0h to 96h exposure) and the corresponding statistical analysis (equation 5.3). Both design methods and resistance factors were calibrated using all construction procedures. Only mineral and synthetic polymer slurry were used in this study where present values in design codes most likely include dry construction or temporarily cased excavations in soil with no slurry. A closer to practice approach would be considering only the 8h to 96h shafts, because smaller exposure times are unlike to be achieved in field construction.

In the temporary casing research, ϕ_p was calculated based on all sockets (29) because, again, design methods and code resistance factors were calibrated considering all construction procedures in rock.

For both the slurry and casing studies it is not known the exact distribution of construction types used to formulate the existing code resistance values, so the ϕ_p reference value may or may

not be statistically similar to the distribution of construction types in code values. Figures 5.9 and 5.10 show the unadjusted resistance factors from this study.

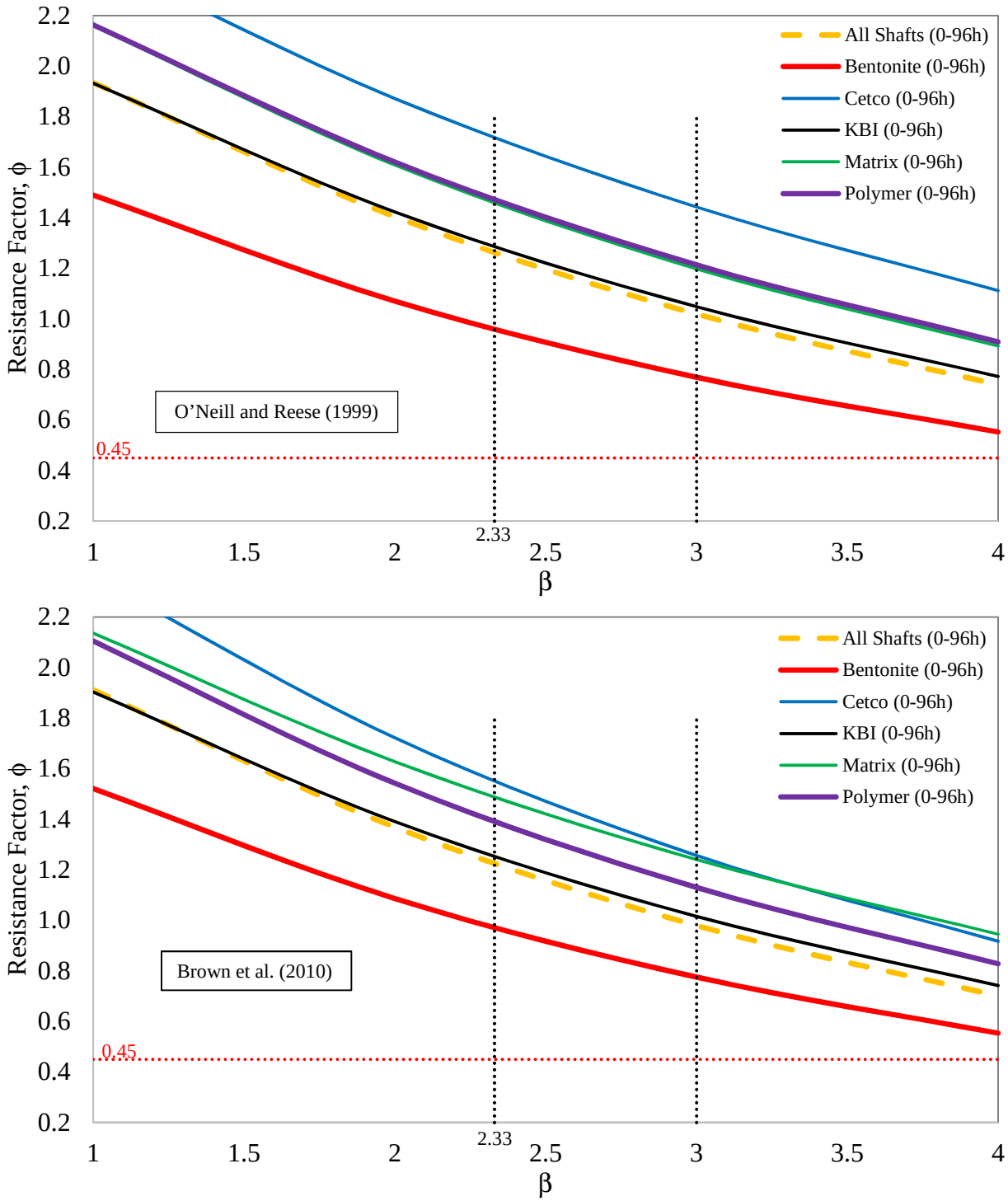

Figure 5.9. Resistance factor vs reliability index – slurry effects research (0h – 96h).

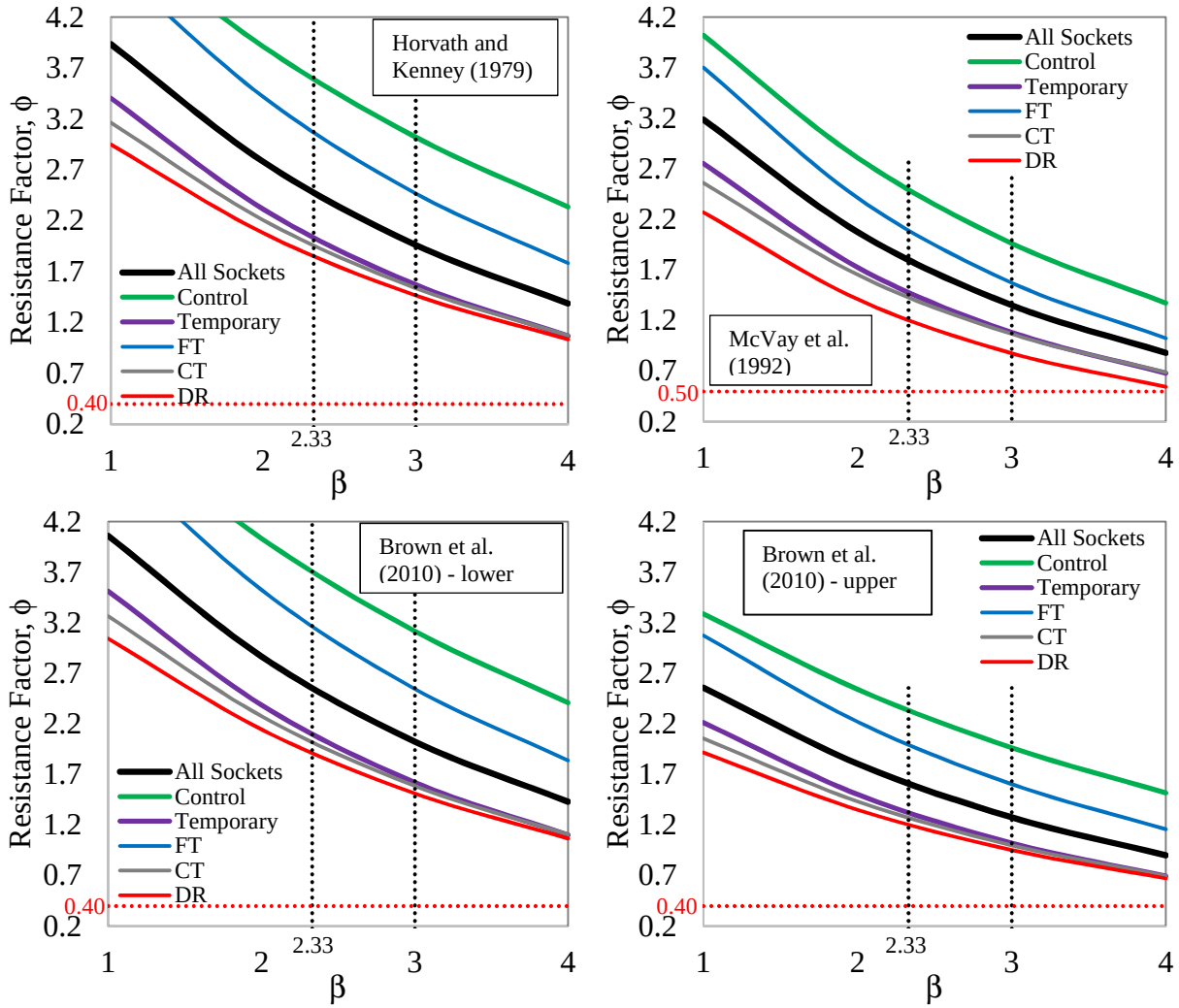

Figure 5.10. Resistance factor vs reliability index – temporary casing effects research.

Next, ξ was applied to the ϕ value of each individually analyzed data series (ϕ_s) using the equation as follows to obtain the adjusted resistance factor (ϕ_a) (which became specific for each data set).

$$\phi_a = \xi * \phi_s \qquad \text{eqn. 5.5}$$

The data sets considered in the slurry research were again: (1) bentonite slurry, (2) Cetco polymer, (3) KBI polymer, (4) Matrix polymer, (5) all polymer products and (6) all 32 shafts. Figure 5.11 shows the adjusted resistance factors (O'Neill and Reese 1999 – top; Brown et al. 2010 – bottom).

In the temporary casing research, the individually analyzed data sets were again: (1) driven temporary casing (DR), (2) coarse-tooth rotated temporary casing (CT), (3) fine-tooth rotated temporary casing (FT), (4) all temporary casing sockets, (5) all control specimens and (6) all 29 sockets. Figure 5.12 shows the adjusted resistance factors based on the design methods proposed by Horvath and Kenney (1979), Brown et al. (2010) – lower and upper (plot on top), and McVay et al. (1992) (plot on bottom). As expected, the adjusted resistance factors for the first three cited methods resulted in the same effect as these methods all use the same equation for computing the design side shear only changing "C".

Tables 5.6 and 5.7 show the adjusted resistance factors considering a target reliability index of 2.33, for the slurry and temporary casing studies, respectively.

Table 5.6. Adjusted resistance factor for target reliability index of 2.33 – slurry study.

Construction Method	Design	All	B	C	K	M	P
Adjusted ϕ (O'Neill and Reese 1999)	0.45	0.45	0.34	0.61	0.46	0.52	0.52
Adjusted ϕ (Brown et al. 2010)	0.45	0.45	0.35	0.57	0.46	0.54	0.51

Table 5.7. Adjusted resistance factor for target reliability index of 2.33 – temporary casing study.

Construction Method	Design	All	DR	CT	FT	T	Ctrl
Adjusted ϕ (Horvath and Kenney 1979)	0.40	0.40	0.30	0.31	0.49	0.33	0.58
Adjusted ϕ (McVay et al. 1992)	0.50	0.50	0.33	0.40	0.58	0.41	0.69
Adjusted ϕ (Brown et al. 2010 – lower)	0.40	0.40	0.30	0.31	0.49	0.33	0.58
Adjusted ϕ (Brown et al. 2010 – upper)	0.40	0.40	0.30	0.31	0.49	0.33	0.58

From the presented results, it is again evident that different construction methods may result in significantly varying adjusted resistance factors (this statement is also observable in the non-adjusted resistance factors). The resistance factor variations observed between design methods was less significant and relatively small.

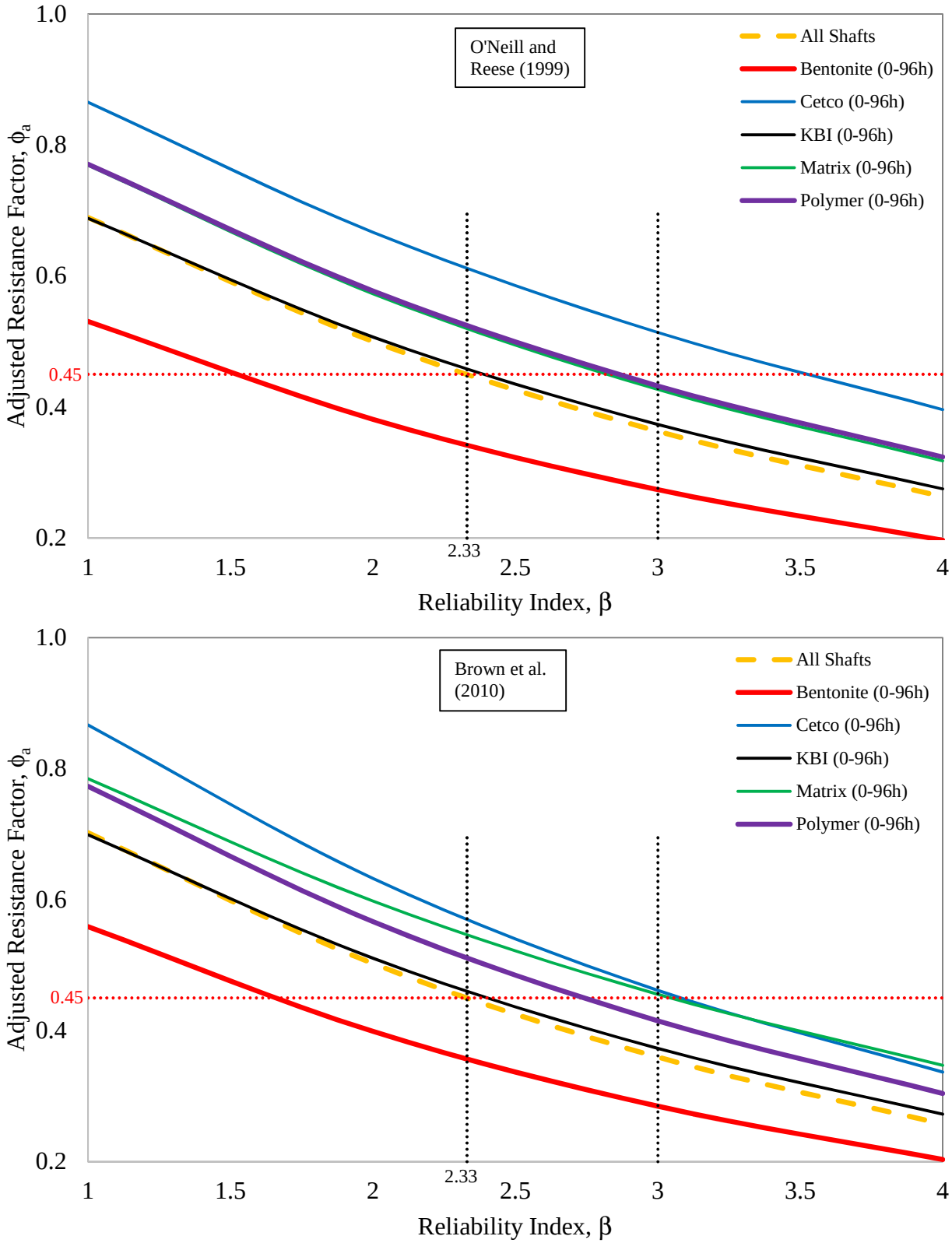

Figure 5.11. Adjusted resistance factors – slurry study.

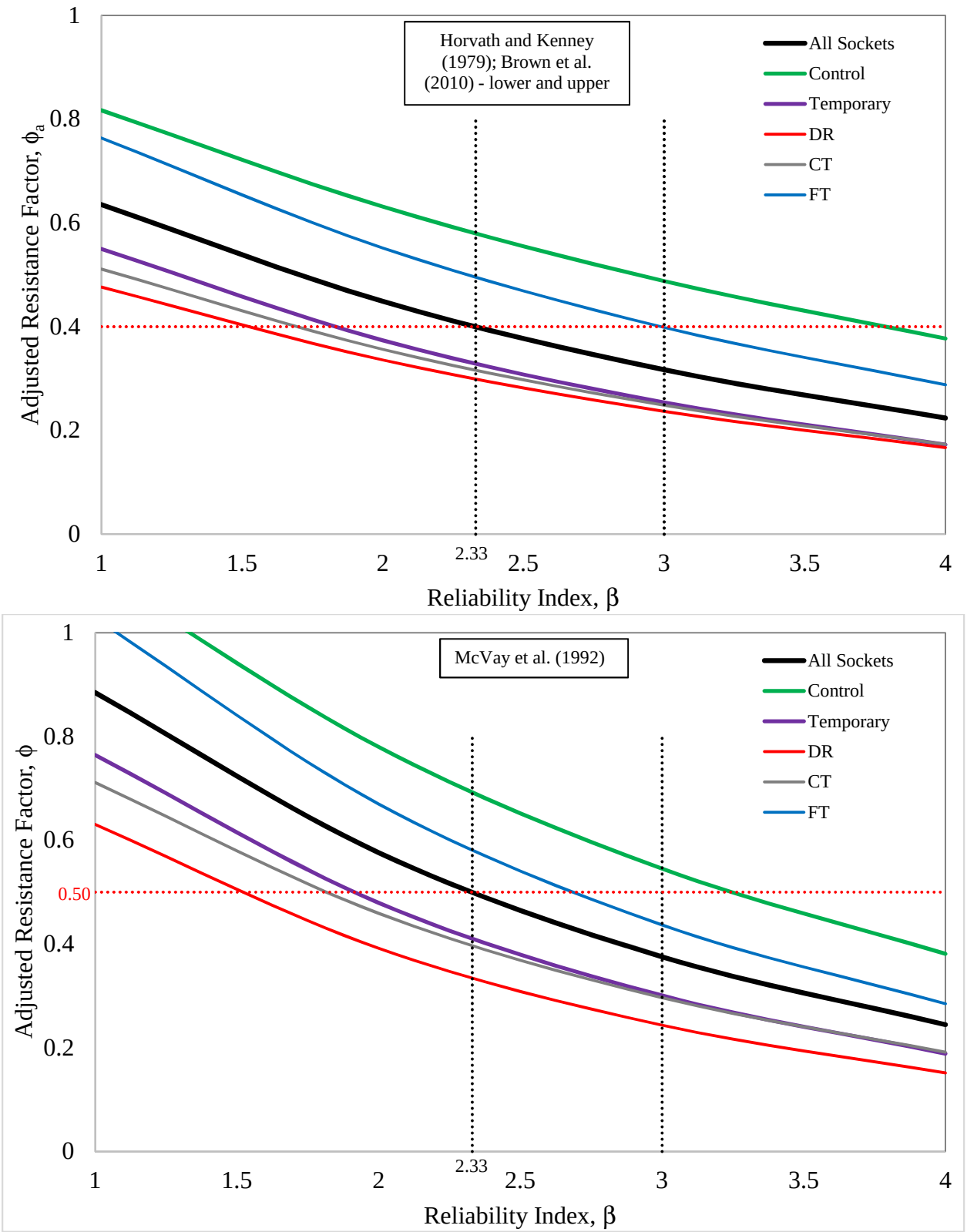

Figure 5.12. Adjusted resistance factors – temporary casing study.

Regarding slurry stabilization, the bentonite shafts exhibited an adjusted resistance factor 24.4% smaller that the recommended in design manuals when using the method developed by O'Neill and Reese (1999), and 22.2% smaller when using Brown et al. (2010) method.

Regardless of differences between one polymer slurry product and another, the conjunct of polymer shafts exhibited an adjusted resistance factor 15.5% higher than recommended in the manuals if using O'Neill and Reese (1999), and 13.3% higher if using Brown et al. (2010).

Other construction procedures, such as dry excavation and temporary casings in sandy soils were not addressed in this study, but it is not viewed to be a problem. Because of the limited amount of data for each analyzed exposure time (1 bentonite and 3 polymer shafts per each exposure), it is not appropriate to suggest variations on the resistance factor on the basis of open excavation time (soil remained in contact with the drilling slurry). However, the effects of prolonged exposure can clearly be seen and could be reflected in future specifications.

Similar observations may be made in the temporary casing study. The construction procedures used in this research (which are, typically, used in Florida limestone formations) have resulted in different resistance factors. The differences of adjusted resistance factors between the methods proposed by McVay et al. (1992) and those from Horvath et al. (1979), and Brown et al. (2010 – lower and upper) for a given excavation method were relatively small, but the differences due to construction procedures are evident.

The driven temporary casing sockets displayed an adjusted resistance factor 25.0% smaller than the recommended by FDOT (2017a) when using the design methods proposed by Horvath and Kenney (1979) and Brown et al. (2010). This difference increases to 34.0% when considering the method proposed by McVay et al. (1992). The conjunct of all temporarily cased sockets

showed adjusted resistance factors 17.5% and 18.0% smaller in comparison to AASHTO (2014) and FDOT (2017b), respectively.

The control sockets showed 45.0% and 38.0% larger adjusted resistance factors in comparison to the standards of AASHTO (2014) and FDOT (2017a). However, given that this type of socket is preferred in the field (e.g. below the temporary casing in the rock socket), the adjusted resistance factors would be further reduced for all temporary casing methods if the reference sample data set were the control sockets and not all 29 shaft specimens. This again highlights the importance of knowing the distribution of construction techniques used in the database formulating present FDOT and AASHTO code resistance values.

5.5 Conclusions

The use of a resistance factor equal to 0.45 for design side shear of drilled shafts subjected to uplift in sands may not be technically valid for all construction procedures, because each excavation method result in its particular side shear behavior. Furthermore, the design methods analyzed herein produced different resistance bias and covariance values, and based on statements presented in the 2010 FHWA Drilled Shafts Manual, the newer beta method (Brown et al. 2010) is being used presently without a thorough statistical validation.

The bentonite shafts performed similarly to the polymer shafts in terms of side shear up to 2h or 4h of exposure. After 2h, the filter cake seemed to have caused a drastic reduction in side shear capacity of the bentonite shafts. In field construction, the time that the excavation remains open before concreting can easily exceed 4h, and a large reduction in side shear when using bentonite slurry should be expected. In the polymer shafts, this phenomenon was not observed. A suggested change to the present specifications might remove limitations to open excavations times on the basis of filter cake formation as polymer slurry did not degrade side shear with time and

bentonite exposure effects ceased after 8hrs. Recall, the present specification restricts open excavation times to 36h per FDOT specifications and the last 5ft of the excavation can only be open for 12h.

The temporary casing study of rock socketed drilled shafts in simulated limestone showed that, again, construction procedures have led to different side shear and adjusted resistance factors. The recommendation of extending the socket depth by 50% of the extra length that the casing is driven into Florida limestone formations (FDOT 2017b) is reasonable based on the results of this study.

Regardless of the database that comprises each of the methods discussed herein, significant differences can be observed between construction procedures (e.g. excavation stabilization) and these particularities are not included on the design methods or in the suggested resistance factor.

As a suggestion for further research, it is recommended that a more in depth investigation of the data used to determine present code specified resistance factors be performed. This should define the distribution of construction methods used such that adjustment factors like that suggested in this study can be properly matched and not skewed to a preponderance of one construction technique. For example, the average bias for this study was skewed to include: ¾ polymer and ¼ mineral shafts; ¾ temporary casing and ¼ no casing. For the adjustments proposed in this study to be meaningful, both data sets should have a similar distribution of construction techniques.

REFERENCES

[1] AASHTO (2014). "AASHTO AASHTO LRFD Bridge Design Specifications 2014, 7th Edition, with 2015 and 2016 Interim Revisions", Customary U.S. Units. American Association of State Highway and Transportation Officials. ISBN number: 978-1-56051-952-0.

[2] AASHTO (2016). "AASHTO LRFD Bridge Construction Specifications", 3rd Edition, with 2010, 2011, 2012, 2014, 2015, and 2016 Interim Revisions. American Association of State Highway and Transportation Officials. ISBN number: 978-1-56051-452-7.

[3] Allen, W. R. (2016). "Time Dependent Effect of Drilling Slurries On Side Shear Resistance of Drilled Shafts". Master thesis, University of South Florida, Tampa FL.

[4] Bernal, J. B., and Reese, L. C. (1983). "Study of the Lateral Pressure of Fresh Concrete as Related to the Design of Drilled Shafts". Research Report No 308-1F, Center for Transportation Research, The University of Texas at Austin.

[5] Brown, D. (2002). "Effect of Construction on Axial Capacity of Drilled Foundations in Piedmont Soils." Journal of Geotechnical and Geoenvironmental Engineering, Vol. 128, No. 12, pp. 967-973, (doi: http://dx.doi.org/10.1061/(ASCE)1090-0241(2002)128:12(967)).

[6] Brown, D. A., and Vinson, J. (1998). ''Comparison of Strength and Stiffness Parameters for a Piedmont Residual Soil.'' Geotechnical site characterization, ISC'98, P. K. Robertson and P. W. Mayne, eds., Vol. 2, Balkema, Rotterdam, The Netherlands, 1229–1234.

[7] Brown, D. A., and Drew, C. (2000). ''Axial Capacity of Augered Displacement.'' New Technological and Design Developments in Deep Foundations, GSP 100, N. D. Dennis, R. Castelli, and M. W. O'Neill, eds., ASCE, New York, 397–403.

[8] Brown, D. A., Turner, J. P., Castelli, R. J. (2010). "Drilled Shafts: Construction Procedures and LRFD Design Methods," NHI Course No. 132014, FHWA-NHI-10-016, FHWA GEC 010, U.S. Department of Transportation, Federal Highway Administration.

[9] Caliari de Lima, L., Allen, W. R., and Mullins, A. G. (2016). "Effect of Polymer Slurry Stabilization on Drilled Shaft Side Shear Over Time". FDOT Project No. BDV25-977-19, Task 3 Deliverable – Laboratory Side Shear Testing.

[10] Caliari de Lima, L., Hagerman, D. J., and Mullins, A. G. (2017). "Evaluating the Effect of Temporary Casing on Drilled Shaft Rock Socket Friction." FDOT Project No. BDV25 TWO 977-18, Task 3 Deliverable – Small Scale Side Shear Testing.

[11] Camp, W.M., Brown, D.A., and Mayne, P.W. (2002). "Construction Methods Effects on Drilled Shaft Axial Performance." Deep Foundations 2002, Geotech Spec. Publ. 116, M.W. O'Neill and F. C. Townsend, eds., ASCE, Reston, VA, pp. 193-208.

[12] Castelli, R. J., and Fan, K. (2002). "O-Cell Test Results for Drilled Shafts in Marl and Limestone." Deep Foundations 2002: pp. 807-823. Doi: 10.1061/40601(256)57.

[13] CETCO (2017). "Shore Pac Calculator," Accessed August 3, 2017, http://www.cetco.com/en-us/Tools/Drilling-Products/SHORE-PAC-Calculator

[14] Clayton, C. R. I., and Milititsky, J. (1983). "Installation effects and the performance of bored piles in stiff clay". Ground Engineering, 16, (2), 17-22.

[15] Chang, M. and Zhu, H. (2004). "Construction Effect on Load Transfer along Bored Piles." Journal of Geotechnical and Geoenvironmental Engineering, 130(4), 426–437.

[16] Chen, YJ, and Kulhawy, F. H. (2002). "Evaluation of Drained Axial Capacity for Drilled Shafts". Deep Foundations 2002: pp. 1200-1214. Doi: 10.1061/40601(256)86.

[17] Das, B. M. (2008). "Advanced Soil Mechanics". Third Edition, Taylor & Francis, New York. ISBN 0-203-93584-5 Master e-book ISBN.

[18] Deese, G. G. (2004). "Slurry Sand Content and Concrete Interaction in Drilled Shaft Construction". Master thesis, University of South Florida, Tampa FL.

[19] FDOT (2017a). "Soils and Foundation Handbook." State Materials Office, Gainesville, Florida.

[20] FDOT (2017b). "Standard Specifications for Road and Bridge Construction". Florida Department of Transportation, 2014.

[21] FHWA (2010). "Drilled Shafts: Construction Procedures and LRFD Design Methods," NHI Course No. 132014, FHWA-NHI-10-016, FHWA GEC 010, U.S. Department of Transportation, Federal Highway Administration.

[22] Fleming, W. K., and Sliwinski, Z. J. (1977). "The use and influence of bentonite in bored pile 121onstruction." Report PG3, Construction Industry Research and Information Association, London, England.

[23] Frizzi, R. P., Meyer, M. E. and Zhou, L. (2004). "Full scale field performance of drilled shafts constructed utilizing bentonite and polymer slurries". Proceedings, GeoSupport Conference 2004, Orlando, FL, American Society of Civil Engineers, pp. 573-586.

[24] Grace, H. P. (1953) Resistance and compressibility of filter cakes: Chem. Engineering Prog. 49, 303-318,367-377.

[25] Grubb, M. A., Wilson, K. E., White, C. D., and Nickas, W. N. Load and Resistance Factor Design (LRFD) For Highway Bridge Superstructures – Reference Manual. NHI Course No. 130081, 130081A, and 130081B. Report Number FHWA-NHI-15-047, U.S. Department of Transportation, Federal Highway Administration.

[26] Gunaratne, M. (2014). "The Foundation Engineering Handbook." Second Edition, CRC Press, Taylor and Francys Group, Boca Raton, FL. ISN 978-1-4398-9278-7 (eBook – PDF).

[27] Hagerman (2017). "Evaluating the Effect of Temporary Casing on Drilled Shaft Rock Socket Capacity." Master thesis, University of South Florida, Tampa FL. 318pp.

[28] Hassan, K. and O'Neill, M. (1997). "Side Load-Transfer Mechanisms in Drilled Shafts in Soft Argillaceous Rock." Journal of Geotechnical and Geoenvironmental Eng., 123(2), 145–152.

[29] Horvath, R. G., and Kenney, T. C. (1979). "Shaft Resistance of Rock-Socketed Drilled Piers," in Proceedings, Symposium on Deep Foundations (Fuller, ed.), ASCE, Atlanta, October, pp. 182 – 214.

[30] Hudyma, N., and Hiltunen, D. R. (2014). "Variability of Weathered Limestone Properties In Light of Drilled Shaft Design in Florida." Geo-Congress 2014 Technical Papers: pp. 989-998. Doi: 10.1061/9780784413272.096.

[31] KB International (1991). "Slurry Pro CDP, Product Technical Sheet," Accessed August 1, 2017, http://www.kbtech.com/assets/slurrypro-cdp-product-data-sheet.pdf

[32] KB International (2015), Enhanced CDP SlurryPro System, KB International LLC, http://www. Kbtech .com/kb–enhanced-slurrypro –cdp-system.html.

[33] Kulhawy, F.H., Prakoso, W.A., and Akbas, S.O. (2005). "Evaluation of Capacity of Rock Foundation Sockets," Alaska Rocks 2005, Proceedings, 40th U.S. Symposium on Rock Mechanics, G. Chen, S. Huang, W. Zhou and J. Tinucci, Editors, American Rock Mechanics Association, Anchorage, AK, 8p.

[34] Lam, C. and Jefferis, S. (2015). "Performance of Bored Piles Constructed Using Polymer Fluids: Lessons from European Experience." J. Perform. Constr. Facil., 10.1061/(ASCE)CF.1943-5509.0000756 , 04015024.

[35] Law Engineering and Environmental Services, Inc. (2002). "Interoffice Memorandum: Side Shear Loss Attributed to Rock Coring During Drilled Shaft Construction." Jacksonville, Florida.

[36] Macey, H. H. (1942). “Clay-water relationship and the internal mechanisms of drying”. Trans. Br. Ceram. Soc. 41, 73-121.

[37] Majano, R. E. (1992). “Effect of mineral and polymer slurries on perimeter load transfer in drilled shafts.” Ph.D. dissertation, University of Houston, TX, 388p.

[38] Majano, R. E., and O’Neill, M. W. (1993). “Effect of mineral and polymer slurries on perimeter load transfer in drilled shafts”. Report to the ADSC: The International Association of Foundation Drilling, Houston, TX, 410p.

[39] Majano, R., O’Neill, M., and Hassan, K. (1994). “Perimeter Load Transfer in Model Drilled Shafts Formed under Slurry.” Journal of Geotechnical Engineering, 10.1061/(ASCE)0733-9410(1994)120:12(2136), pp. 2136-2154.

[40] Matrix (2016). “Bigfoot Polymer Slurry, Product Data Sheet,” Accessed August 1, 2017, http://www.matrixcp.com/big-foot/

[41] McVay, M. C., Townsend, F., and Williams, R. (1992). ”Design of Socketed Drilled Shafts in Limestone.” Journal of Geotechical Engineering., 118(10), 1626–1637.

[42] McVay, M. C., and Wasman, S. J. (2015). “Embedded Data Collector (EDC) Phase II Load and Resistance Factor Design (LRFD).” Final Report Submitted to Florida Department of Transportation, FDOT Contract No.: BDV31-977-13, Gainesville, FL.

[43] Mesri, G., and Olson, R. E. (1971). “Mechanisms Controlling the Permeability of Clays”. In: Clays and Clay Minerals, 1971,Vol. 19, pp. 151-158. Pergamon Press, England.

[44] Mullins, A. G., and Ashmawy, A. K. (2005). “Factors Affecting Anomaly Formation in Drilled Shafts – Final Report.” Final Report Submitted to the Florida Department of Transportation.

[45] Mullins, A. G. (2012). Load Testing of Drilled Shafts Constructed with CETCO Polymer Slurry, Final Report.

[46] Mullins, A. G. (2014a). Effect of Polymer Slurry Stabilization on Drilled Shaft Side Shear over Time. Exhibit A – Scope of Service, Research Project Proposal sent to the Florida Department of Transportation.

[47] Mullins, A. G. (2014b). “Chapter 7: Design of Drilled Shafts, in: The Foundation Engineering Handbook, Second Edition.” Edited by Manjriker Gunaratne, CRC Press, Taylor & Francis Group.

[48] Mullins, A. G. and Winters, D. (2014). “Defining the Upper Viscosity Limit for Mineral Slurries used in Drilled Shaft Construction.” FDOT Project No. BDK84-977-24, Final Report.

[49] NRC (1995). “Probabilistic Methods in Geotechnical Engineering.” National Research Council, Washington, D.C., 84p.

[50] O’Neill, M. W. (1981). “Drilled Piers and Caissons”. Proceedings of a session sponsored by the Geotechnical Engineering Division at the ASCE National Convention, St. Louis, Missouri. ISBN 0-87262-285-1.

[51] O’Neill, M. W., (2001). ”Side Resistance In Piles and Drilled Shafts.” Journal of Geotechnical and Geoenvironmental Engineering, 127(1), 3–16. 34th Terzaghi Lecture.

[52] O’Neill, M. W., and Hassan, K. M. (1994). “Drilled Shafts: Effects of Construction on Performance and Design Criteria.” Proceedings: International Conference on Design and Construction of Deep Foundations. Volume I, Keynote Papers. US Federal Highway Administration (FHWA), pp 137-187.

[53] O’Neill, M.W., and Reese, L. C. (1978). “Load Transfer in a Slender Drilled Pier in Sand”. Preprint 3141, ASCE Spring Convention and Exhibit, April 24-28, 1978, Pittsburgh, Pennsylvania.

[54] O’Neill, M. W., and Reese, L. C. (1999). Drilled Shafts: Construction Procedures and Design Methods. DTFH6 1-96-2-0005, Report Number FHWA-IF-99-025.

[55] Paikowsky, S. G., (2004). Load and resistance factor design (LRFD) for deep foundations.” NCHRP Report 507, Transportation Research Board, Washington D.C.

[56] Reese, L. C., and O’Neill, M. W. (1988a). “Drilled Shafts: Construction Procedures and Design Methods”. US Department of Transportation, FHWA, Office of Implementation, McLean, Virginia.

[57] Reese, L. C., and O'Neill, M. W. (1988b). "Field Load Tests of Drilled Shafis," in Proceedings, International Seminar on Deep Foundations on Bored and Auger Piles, Van Impe (ed.), Balkema, Rotterdam, June, pp. 145-192.

[58] Reese, L. C, O'Neill, M. W., and Touma, F. T. (1973). "Bored piles installed by slurry displacement." Proc, 8th International Conference on Soil Mechanics and Foundations Engineering, Moscow, U.S.S.R.

[59] Reese, L.C., Owens, M., Hoy, H. (1985) “Effects of Construction Methods on CIDH piles”. Proceedings of a session sponsored by the Geotechnical Engineering Division of the American Society of Civil Engineers in conjunction with the ASCE Convention, Denver, Colorado.

[60] Robertson, P. K. 1990. Soil classification using the cone penetration test. Canadian Geotechnical Journal 27 (1), pp. 151 – 158.

[61] Seavey, D. A., and Ashford, S. A. (2004). “Effects of Construction Methods on the Axial Capacity of Drilled Shafts.” Final Report Submitted to Caltrans, Contract No. 59A0337, Report No SSRP-04/17.

[62] Terzaghi, C. (1925). “Determination of the permeability of clay”. Engineering News Rec. 95, 832-836.

[63] Touma, F. T. (1972). “The Behavior of Axially Loaded Drilled Shafts in Sand”. Ph.D Dissertation, the University of Texas at Austin, December, 1972, Austin, Texas.

[64] Touma, F. T., and Reese, L. C. (1972). “The Behavior of Axially Loaded Drilled Shafts in Sand”. Research Report No 176-1 – The Behavior of Drilled Shafts, Center for Highway Research, the University of Texas at Austin.

[65] TRB (2005). “Calibration to Determine Load and Resistance Factors for Geotechnical and Structural Design.” Transportation Research Board, Circular No E-C079, September 2005, Washington, D.C., 93p.

[66] Turner, J. P. (1992). “Constructability for Drilled Shafts”. Journal of Construction Engineering and Management, American Society of Civil Engineers, 10.1061/(ASCE)0733-9364(1992)118:1(77), 77-93.

[67] Wheeler, P. (2003). “Piles Unlock Polymer Potential.” European Foundation, 8–9.

APPENDIX A: CPT RESULTS OF PHASE 2 SHAFTS

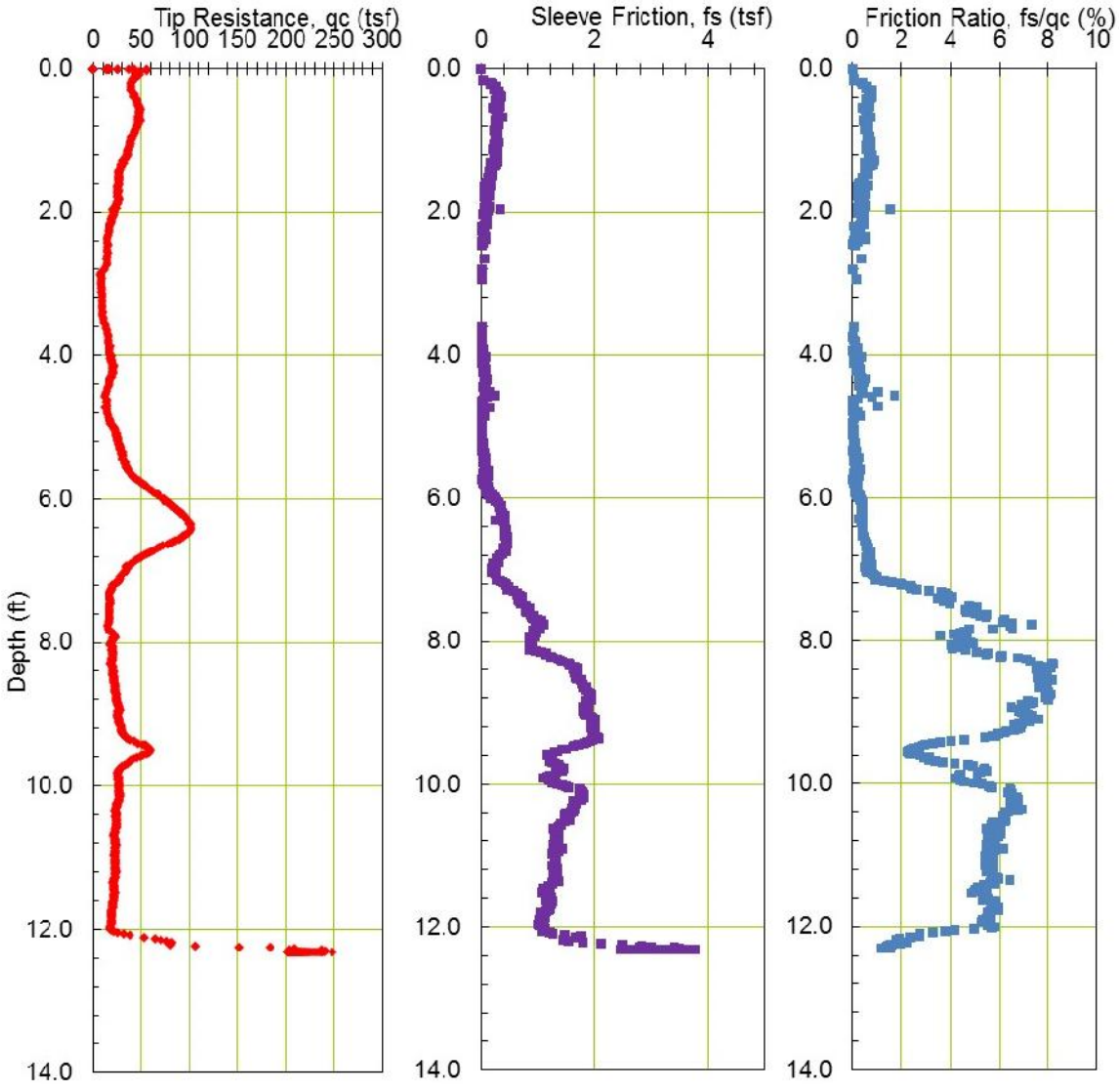

Figure A.1. CPT test results – shaft B48.

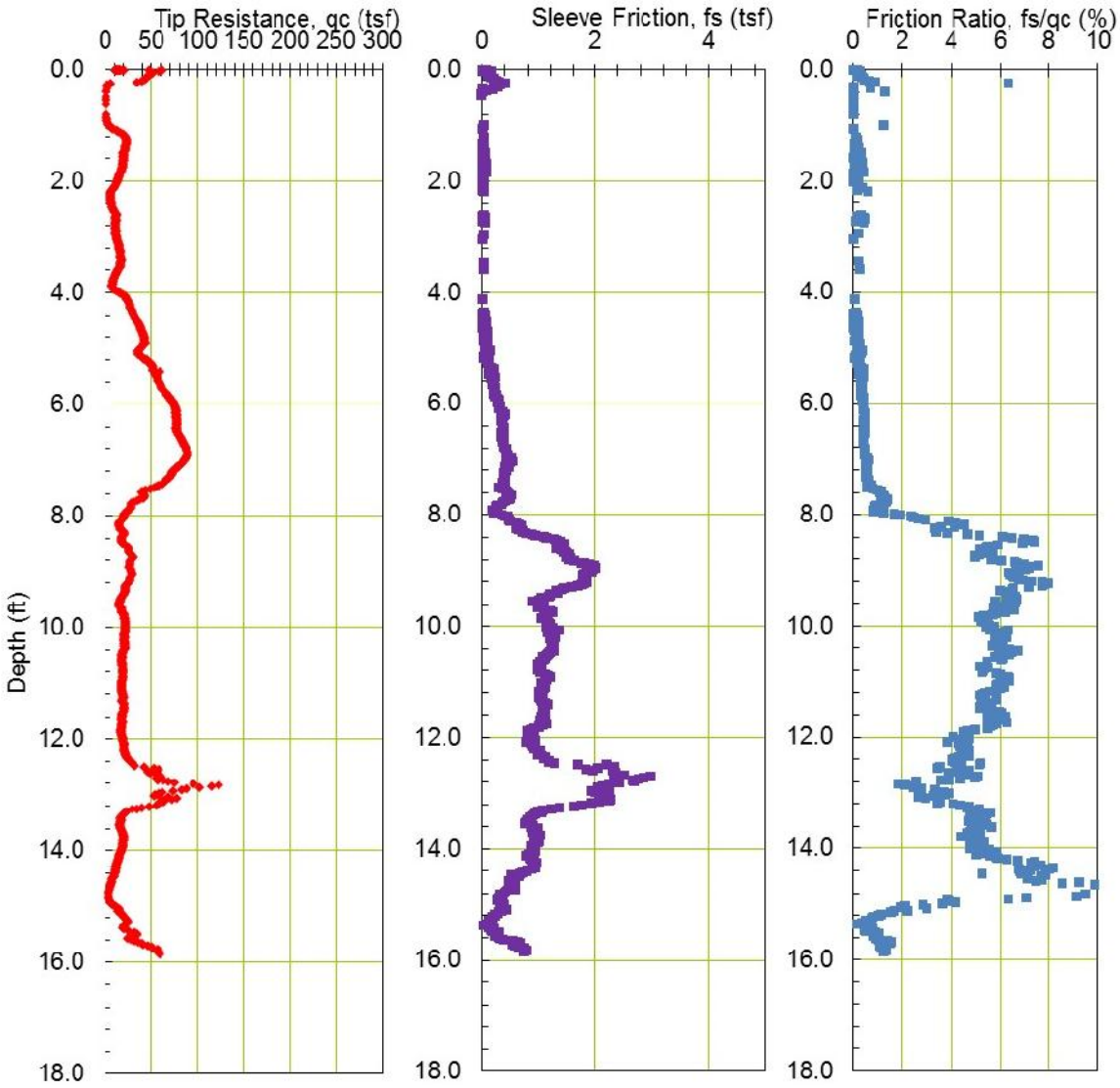

Figure A.2. CPT test results – shaft B96.

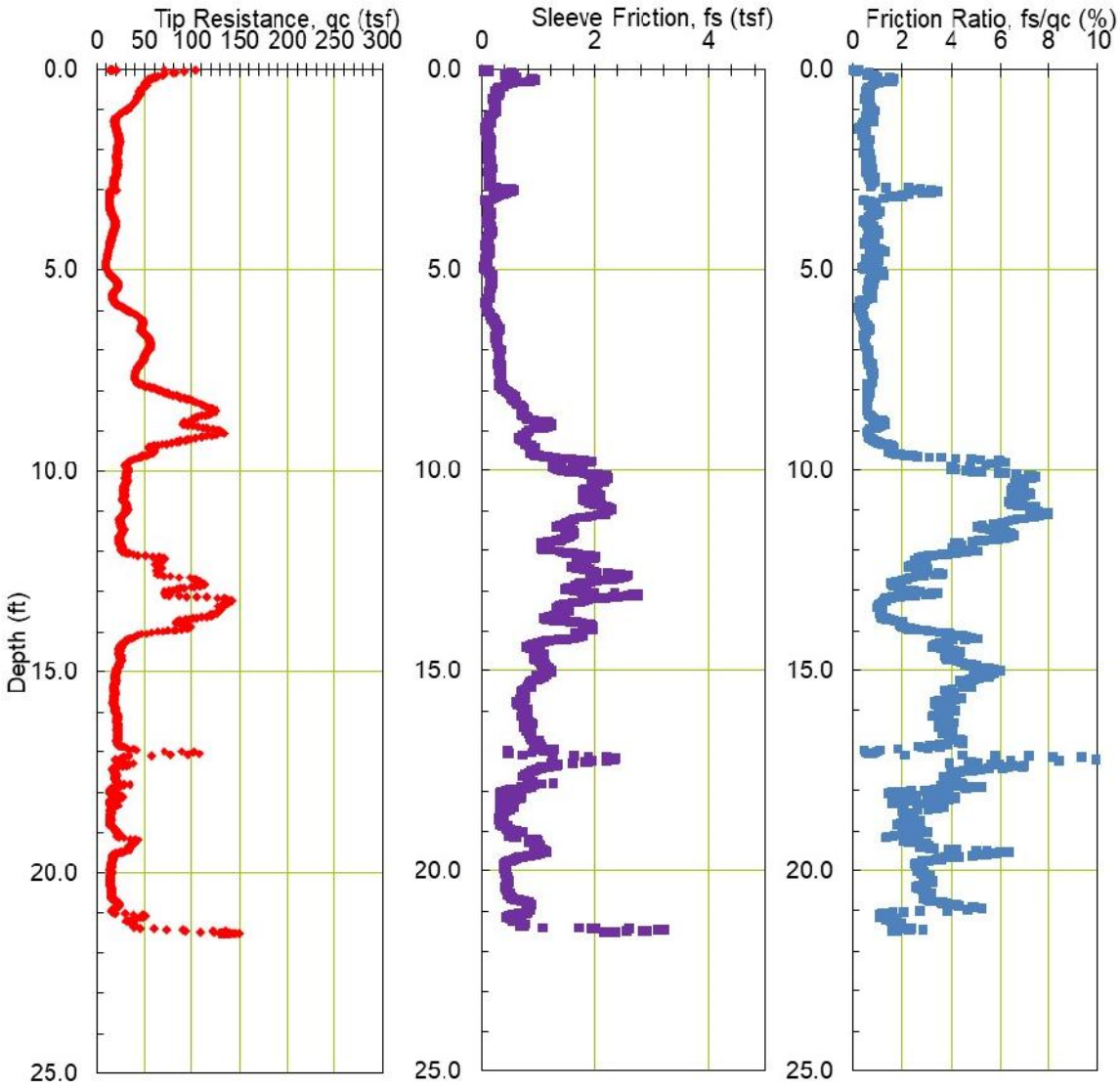

Figure A.3. CPT test results – shaft C48

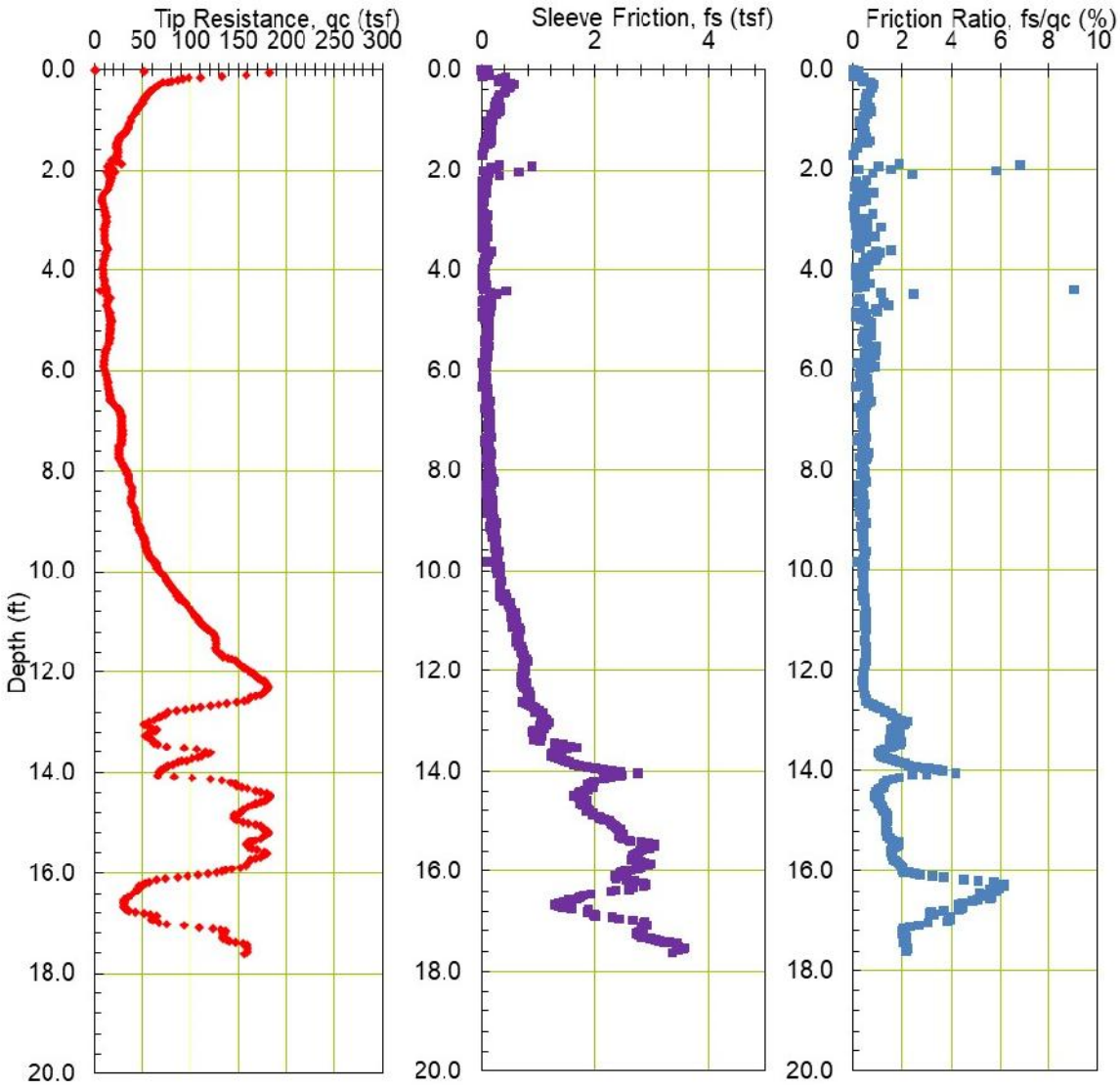

Figure A.4. CPT test results – shaft C96

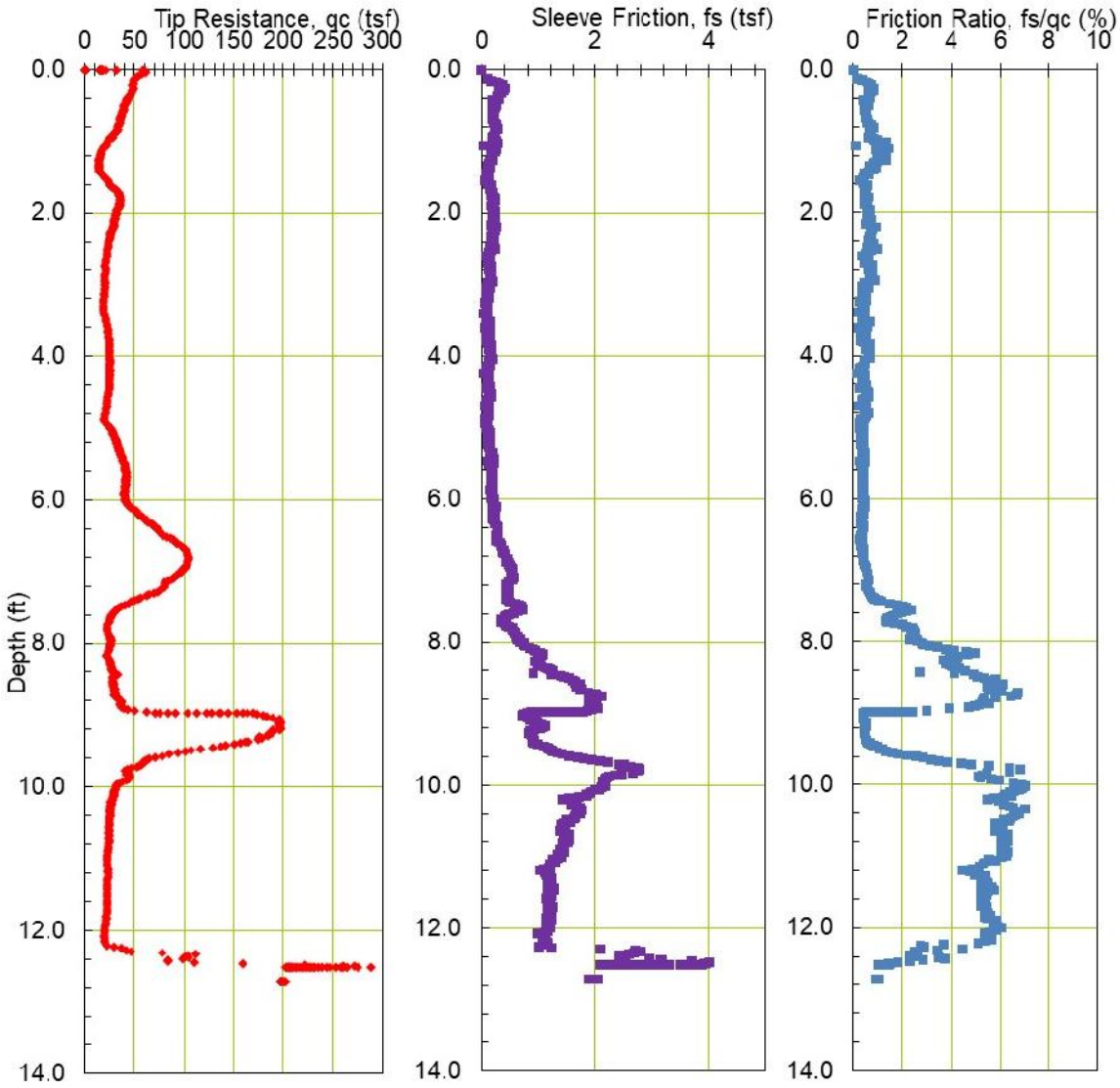

Figure A.5. CPT test results – shaft K48

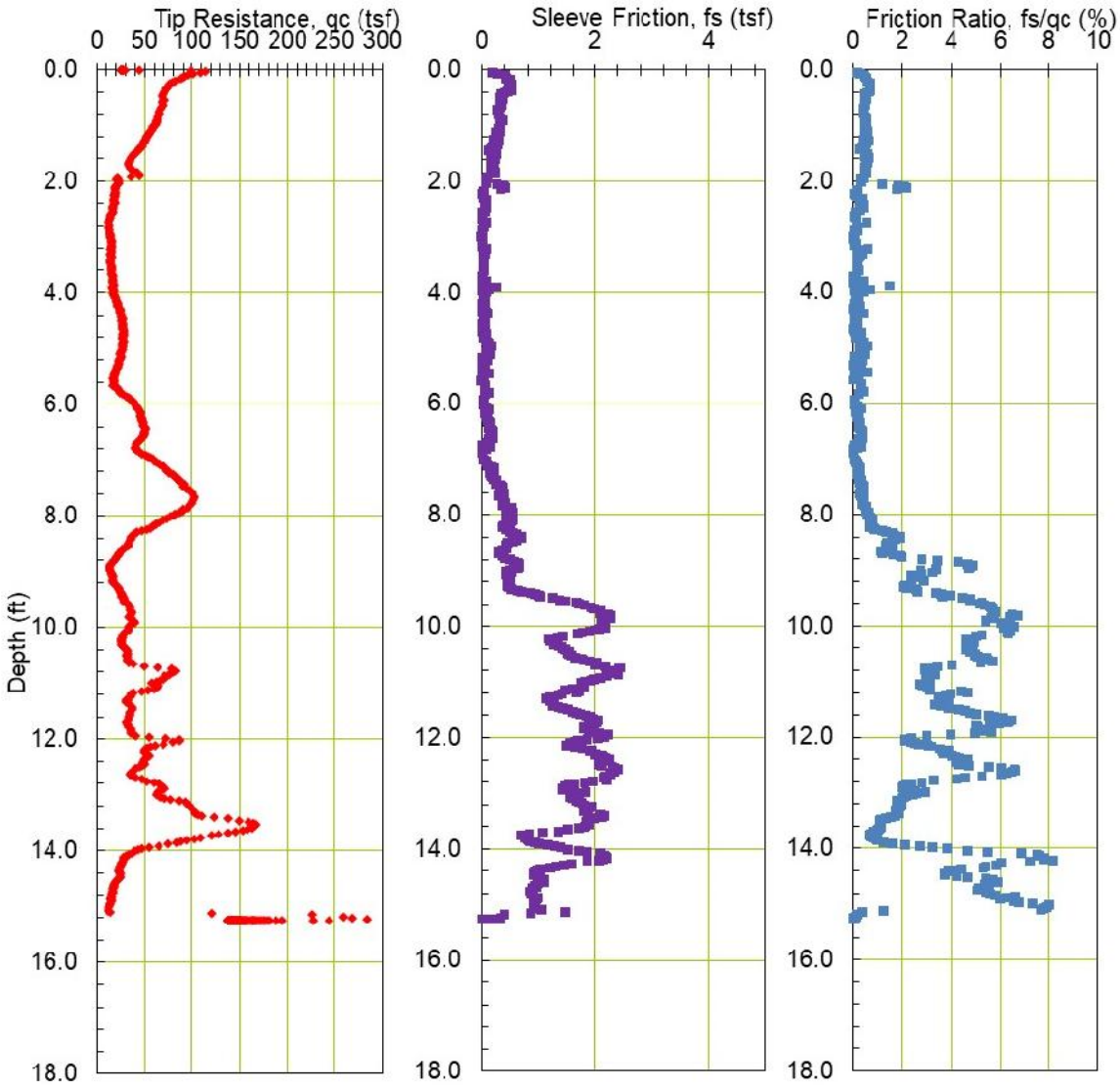

Figure A.6. CPT test results – shaft K96

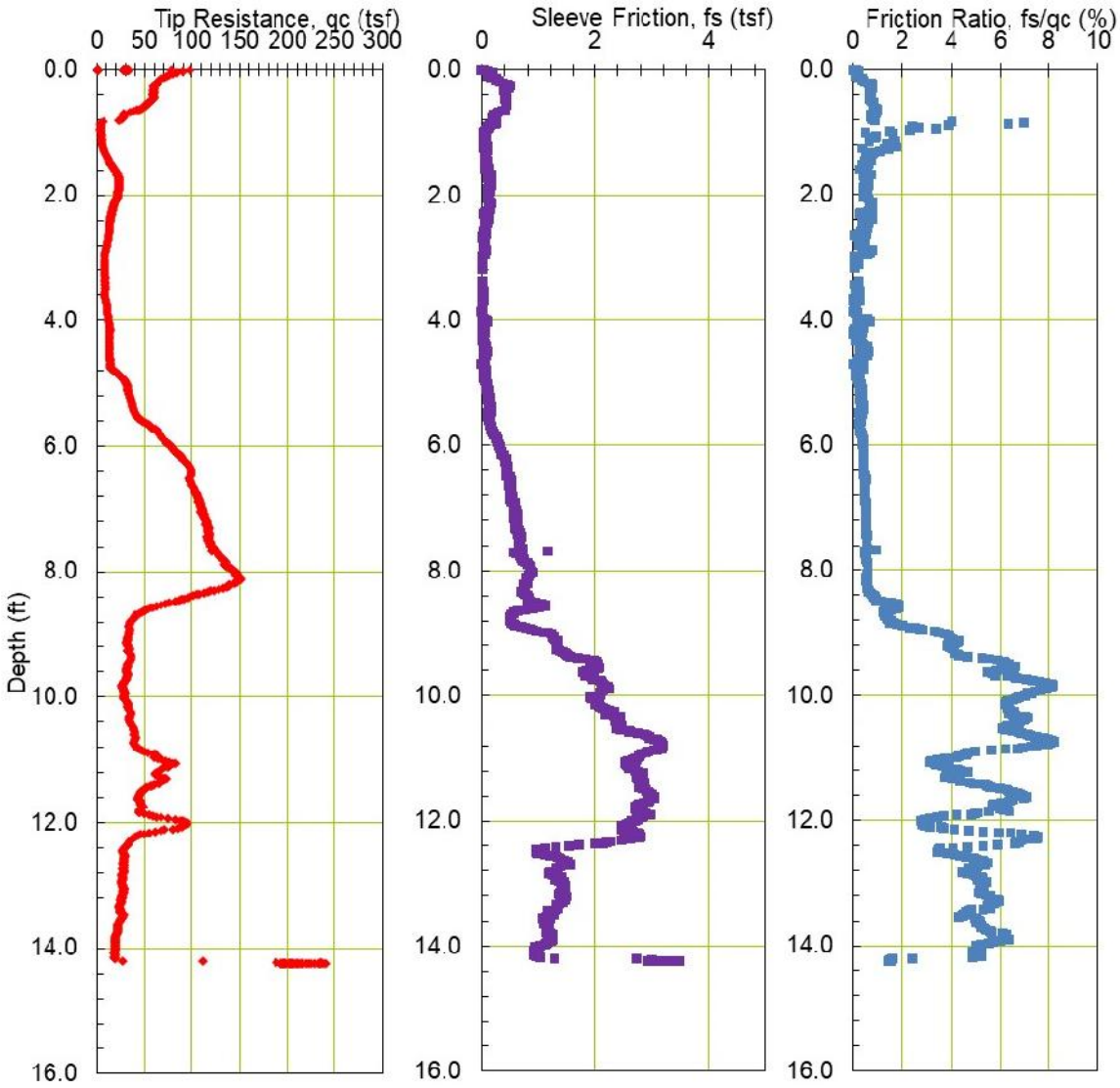

Figure A.7. CPT test results – shaft M48

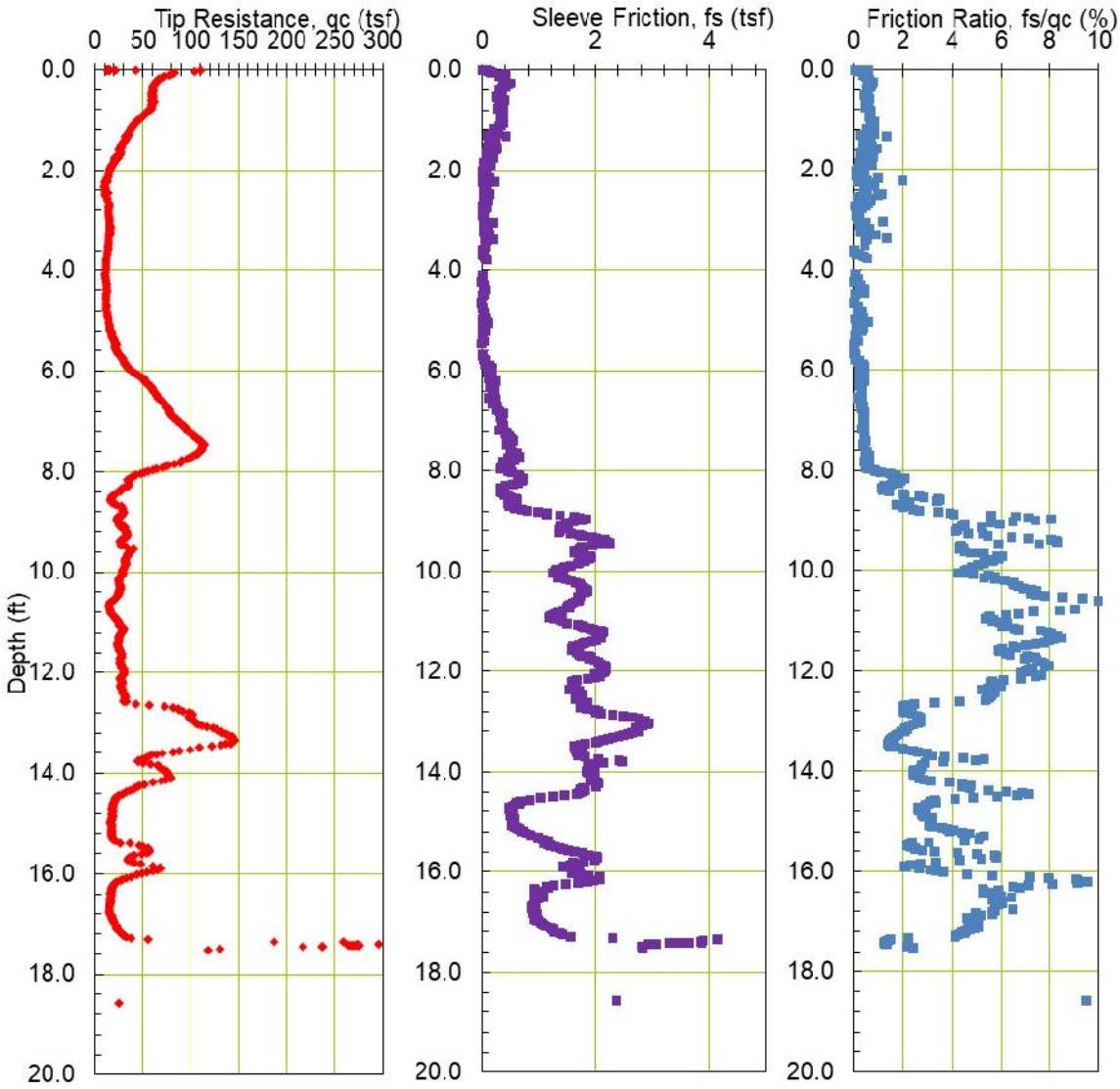

Figure A.8. CPT test results – shaft M96

APPENDIX B: COPYRIGHT PERMISSIONS

B.1 Permissions from Individuals in Photographs

Below are the permissions from individuals in photographs included in my dissertation. The individuals are: Daniel Hagerman, Warren Allen, Jeffrey Vomacka, Sarah Mobley, Miles Mullins, Joseph Scott and Kevin Johnson, in this order.

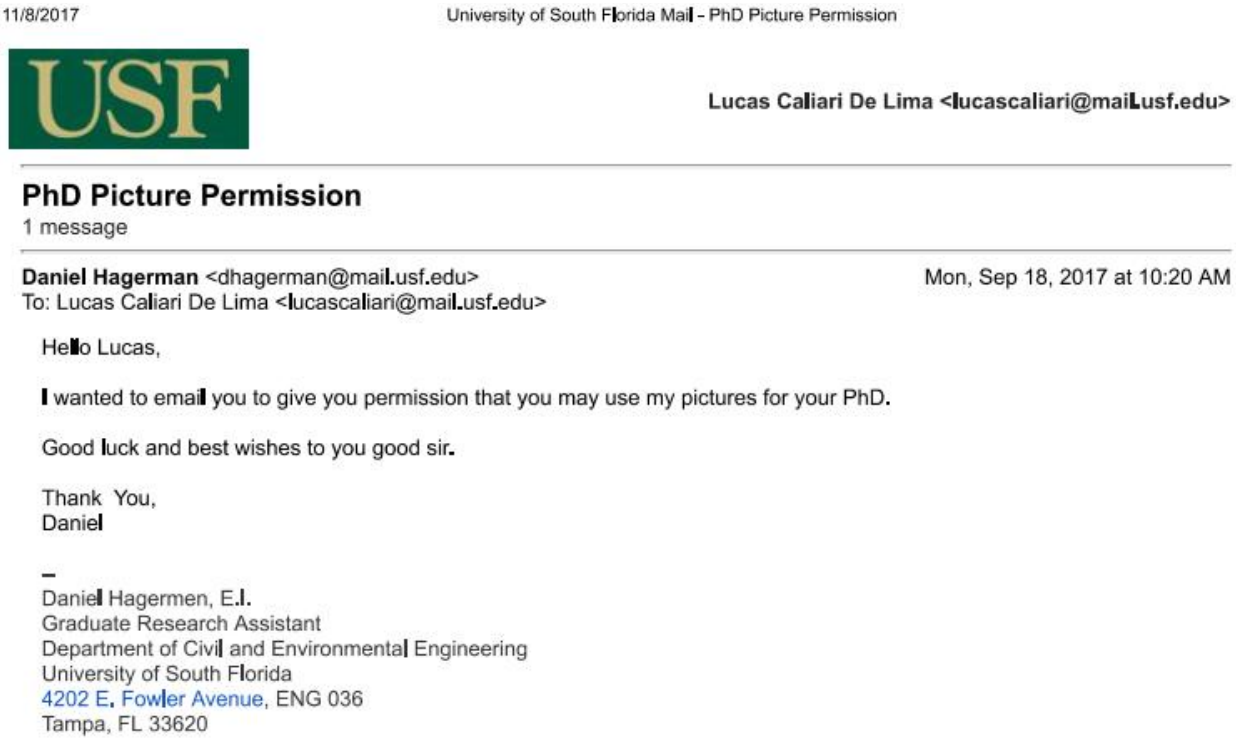

11/8/2017 University of South Florida Mail - PhD Picture Permission

USF

Lucas Caliari De Lima <lucascaliari@mail.usf.edu>

PhD Picture Permission

1 message

Daniel Hagerman <dhagerman@mail.usf.edu> Mon, Sep 18, 2017 at 10:20 AM
To: Lucas Caliari De Lima <lucascaliari@mail.usf.edu>

Hello Lucas,

I wanted to email you to give you permission that you may use my pictures for your PhD.

Good luck and best wishes to you good sir.

Thank You,
Daniel

–
Daniel Hagermen, E.I.
Graduate Research Assistant
Department of Civil and Environmental Engineering
University of South Florida
4202 E. Fowler Avenue, ENG 036
Tampa, FL 33620

Lucas Caliari De Lima <lucascaliari@mail.usf.edu>

Permission for Photograph Use

2 messages

Lucas Caliari De Lima <lucascaliari@mail.usf.edu> Thu, Nov 9, 2017 at 3:23 PM
To: Warren Allen <wrallen@mail.usf.edu>

Warren,

There are some pictures in which you can be recognized in my dissertation. Do I have your permission to use these photographs?

Thank you,

Lucas Caliari de Lima

Warren Allen <wrallen@mail.usf.edu> Thu, Nov 9, 2017 at 3:31 PM
To: Lucas Caliari De Lima <lucascaliari@mail.usf.edu>

Hi Lucas,

Yes, I give you permission to use all the photographs.

Warren Allen, E.I.
[Quoted text hidden]

Lucas Caliari De Lima <lucascaliari@mail.usf.edu>

Permission for Photograph Use

3 messages

Lucas Caliari De Lima <lucascaliari@mail.usf.edu> Thu, Nov 9, 2017 at 3:25 PM
To: Jeffrey Vomacka <vomacka@mail.usf.edu>

Jeff,

There are some pictures in which you can be recognized in my dissertation. Do I have your permission to use these photographs?

Thank you,

Lucas Caliari de Lima

Jeffrey Vomacka <vomacka@mail.usf.edu> Thu, Nov 9, 2017 at 3:29 PM
To: Lucas Caliari De Lima <lucascaliari@mail.usf.edu>

Yes, you have my permission.

Regards,

Jeffrey G. Vomacka
[Quoted text hidden]

Lucas Caliari De Lima <lucascaliari@mail.usf.edu> Fri, Nov 10, 2017 at 6:05 PM
To: "Mobley, Sarah" <sarahmobley@mail.usf.edu>

Sarah,

There is a picture in which you can be recognized in my dissertation. Do I have your permission to use the photograph below?

Thank you,

Lucas Caliari de Lima

Sarah Mobley <sarahmobley@mail.usf.edu> Fri, Nov 10, 2017 at 6:49 PM
To: Lucas Caliari De Lima <lucascaliari@mail.usf.edu>

Hello, Lucas.

Yes. You have my permission.

-Sarah

Sarah J. Mobley, MSCE, PE, M.ASCE
Instructor / Teaching Assistant / Research Assistant
University of South Florida
Civil and Environmental Engineering
sarahmobley@mail.usf.edu

[Quoted text hidden]

Lucas Caliari De Lima <lucascaliari@mail.usf.edu>

Permission for Photograph Use

3 messages

Lucas Caliari De Lima <lucascaliari@mail.usf.edu> Thu, Nov 9, 2017 at 3:30 PM
To: Miles Mullins <mpmullin@mail.usf.edu>

Miles,

There are some pictures in which you can be recognized in my dissertation. Do I have your permission to use these photographs?

Thank you,

Lucas Caliari de Lima

Miles Mullins <mpmullin@mail.usf.edu> Thu, Nov 9, 2017 at 3:38 PM
To: Lucas Caliari De Lima <lucascaliari@mail.usf.edu>

Lucas,

Yes, You have my permission to use photographs I am in.
[Quoted text hidden]

Lucas Caliari De Lima <lucascaliari@mail.usf.edu>

Permission for Photograph Use

3 messages

Lucas Caliari De Lima <lucascaliari@mail.usf.edu> Thu, Nov 9, 2017 at 3:47 PM
To: "Scott, Joseph" <josephscott@mail.usf.edu>

Joe (Joseph),

There are some pictures in which you can be recognized in my dissertation. Do I have your permission to use these photographs?

Thank you,

Lucas Caliari de Lima

USF <josephscott@mail.usf.edu> Thu, Nov 9, 2017 at 3:50 PM
To: Lucas Caliari De Lima <lucascaliari@mail.usf.edu>

Lucas,

Yes, you have my permission to use photographs in which I can be recognized in your dissertation.

Joe

Joseph Scott, EI
Graduate Research Assistant
Department of Civil and Environmental Engineering
University of South Florida
4202 E. Fowler Avenue
Tampa, FL 33620 ENG 038
Office: (813) 974-6147
Mobile: (813) 810-2994
Josephscott@mail.usf.edu
[Quoted text hidden]

Lucas Caliari De Lima <lucascaliari@mail.usf.edu>

Permission for Photograph Use

2 messages

Lucas Caliari De Lima <lucascaliari@mail.usf.edu> Thu, Nov 9, 2017 at 3:20 PM
To: Kevin Johnson <krjohns8@mail.usf.edu>

Kevin,

There are some pictures in which you can be recognized in my dissertation. Do I have your permission to use these photographs?

Thank you,

Lucas Caliari de Lima

Kevin Johnson <krjohns8@mail.usf.edu> Thu, Nov 9, 2017 at 5:43 PM
To: Lucas Caliari De Lima <lucascaliari@mail.usf.edu>

Permission granted.

Kevin R. Johnson, Ph.D, E.I.
University of South Florida
Civil Engineering Department
4202 E. Fowler Ave., ENB 118
Tampa, FL 33620
Office: (813) 974-5830
Cell: (813) 299-0969
krjohns8@mail.usf.edu
[Quoted text hidden]